UPPSALA
UNIVERSITET

Magnetic reconnection and separatrix regions

BY

Tomas Lindstedt

December 22, 2009

DEPARTMENT OF PHYSICS AND ASTRONOMY
UPPSALA UNIVERSITY
SE-75120 UPPSALA, SWEDEN

Submitted to the Faculty of Science and Technology, Uppsala University in partial fulfillment of the requirements for the degree of Licentiate of Philosophy in Physics with specialization in Space and Plasma Physics.

Abstract

Magnetic reconnection is a fundamental process in a magnetized plasma. It changes the topology of the magnetic fields and allows particles to move between different regions. Reconnection can occur at the magnetopause, the boundary between the solar wind and the magnetosphere, and allows entry of solar wind particles into the magnetosphere. In addition to mass, also energy and momentum is transferred to the magnetosphere as a result of reconnection. This transfer affects the whole magnetosphere and also the ionosphere. Thus, it is important to study the connection between the reconnection site and other regions of the magnetosphere.

An important tool for investigating reconnection at the magnetopause are the ESA Cluster spacecraft. They consist of four spacecraft flying in formation to give a three dimensional view of space.

Using data from the four Cluster spacecraft we study the separatrix regions of magnetic reconnection sites at the magnetopause under conditions when reconnection is occurring in the magnetopause current layer, which separates magnetosheath plasma from the hot magnetospheric plasma sheet. The time scale for the observations are from a few seconds up to several minutes, corresponding to distances of a few hundred km up to a few several thousand km. We define the separatrix region as the region between the separatrix, the first field line opened by reconnection, and the reconnection jet (outflow region). We analyze eight separatrix region crossings on the magnetospheric side of the magnetopause and present detailed data for two of the events. We show that characteristic widths of the separatrix regions are of the order of ten ion inertial lengths at the magnetopause. Narrow separatrix regions with widths comparable to a few ion inertial lengths are rare. We show that inside the separatrix region there is a density cavity which sometimes has complex internal structure with multiple density dips. Strong electric fields exist inside the separatrix regions and the electric potential drop across the regions can be up to several kV. On the magnetosheath side of the region there is a density gradient with strong field aligned currents. The observed strong currents inside the separatrix region can be important for magnetosphere-ionosphere coupling. We also provide evidence that the electric field in the separatrix region can energize oxygen ions to several keV.

List of papers

This thesis is based on the following papers.

I. **T. Lindstedt**, Yu.-V. Khotyaintsev, A. Vaivads, M. André, R.-C. Fear, B. Lavraud, S. Haaland, and C.-J. Owen *Separatrix regions of magnetic reconnection at the magnetopause*, Ann. Geophys., **27**, 4039–4056, 2009.

II. **T. Lindstedt**,Yu.-V. Khotyaintsev, A. Vaivads, M. André, H. Nilsson, M. Waara *Oxygen energization by localized perpendicular electric fields*, Manuscript

Contents

Chapter 1

Introduction

In this thesis we investigate how magnetic reconnection, one way to transfer mass, energy and momentum across the magnetopause, can interact with the space surrounding the Earth. Chapter 2 is an introduction to the Earth environment and plasma physics in general. The instruments to study this environment are briefly described. In chapter 3 we introduce magnetic reconnection – a fundamental process to convert magnetic energy to kinetic energy. It is also one of the most important processes allowing the solar wind to connect to the Earth. Chapter 4 discuss more details of the regions that provide the coupling between the reconnection site and different parts of the Earth environment. One consequence of reconnection is that inside these regions heavy ions can be energized which is discussed in chapter 5. In chapter 6 we suggest some future work.

Chapter 2

The magnetosphere and the CLUSTER mission

In the visible universe the most common state of matter is the *plasma* state. Plasma can be described as a gas of charged particles. A charged particle in motion is a source of electric and magnetic fields. The electromagnetic fields from one particle affect all other particles and the plasma shows a collective behavior. Plasma is neutral on large scales (Chen, 1984; Kivelson and Russell, 1995). In an astronomical perspective stars, stellar winds and cometary tails are made of plasma. In our solar system plasma is found in the solar atmosphere and in the magnetospheres and ionospheres of the planets and their moons. On Earth plasma is used in laboratories and in fusion reactors. Industry uses plasma for waste burning, surface treatment and in plasma displays in television sets. We will investigate plasma around planet Earth, but the conclusions are of importance also for other plasma environments.

Plasma behavior can to some extent be described by considering the motion of a single charged particle (Chen, 1984). A charged particle moving perpendicularly to a magnetic field senses a force perpendicular to its velocity and the magnetic field. This magnetic force gives rise to a gyro motion (see Figure 2.1) with a frequency (ω) depending on the charge (q) and mass (m) of the particle and also the magnitude of the magnetic field (B) where $\omega = qB/m$. The center of the motion is called the gyro center from which the distance to the particle is the gyro radius or the *Larmor radius*, r_L in Figure 2.1. If the plasma is collisionless, the particles can freely move along the magnetic field lines, but perpendicular to the magnetic field the gyro center of the particle and the field move in approximately the same way. This behavior is called the *frozen-in* condition and is common in the space environment (Bellan, 2006). We consider the interesting case when the frozen-in condition is not valid. Breaking of the frozen-in condition in a small region has large impact on the surroundings, e.g. that different plasma populations can mix.

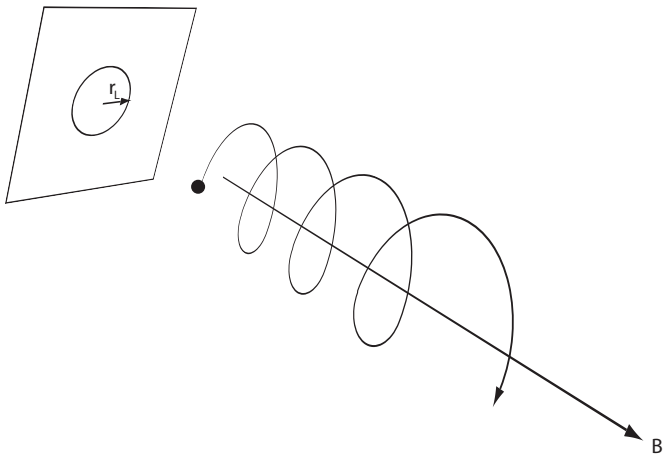

Figure 2.1: Illustration of the gyro or Larmor radius r_L. In an ideal plasma where the magnetic field is frozen-in to the plasma, particles are tied to a certain field line, but free to move along it.

In interplanetary space there is a flow of plasma away from the Sun called the *solar wind*. The solar wind consists of plasma from the Sun accelerated to super-Alvénic speeds. The magnetic field in this region is called the *interplanetary magnetic field (IMF)* and also originates from the Sun. The solar wind is highly collisionless and the magnetic field is frozen-in to the plasma (Kivelson and Russell, 1995). Due to the frozen-in condition, the IMF is carried away from the Sun by the solar wind. The solar wind motion together with the rotation of the Sun causes the magnetic field on a large scale to be shaped as spirals. At the Earth the IMF direction can vary greatly due to frequently occurring solar eruptions and variations of the solar wind velocity. Close to the Earth the solar wind speed slows down to sub-Alfvénic speeds and the particles are heated at the bow shock (Baumjohann and Treumann, 1996). The region behind the bow shock where the plasma flows around the Earth is the *magnetosheath*. It is a turbulent region with heated solar wind plasma (the dark blue region in Figure 2.2).

The plasma around the Earth is encapsulated by a magnetic field created by currents inside the planet. The region with magnetic fields originating from the Earth is called the *magnetosphere*. To a first approximation these magnetic fields are dipolar and are deformed by the pressure from the *solar wind* (the outer blue parts in Figure 2.2) (Kivelson and Russell, 1995). In the magnetosphere there is plasma from the ionosphere and the solar wind. In the *plasma sheet* (red in Figure 2.2) the plasma is relatively hot and dense compared to other parts of the magnetosphere. The plasma sheet is on closed magnetic field lines, i.e. both ends are connected to the Earth. The *lobes* are almost empty of plasma. The magnetic field lines in the lobes are open, that is one end is connected to the Earth and the other to the solar wind. The *cusps* are very turbulent regions that allow entry of the solar wind into the magnetosphere. The cusps are like funnels separating the dayside

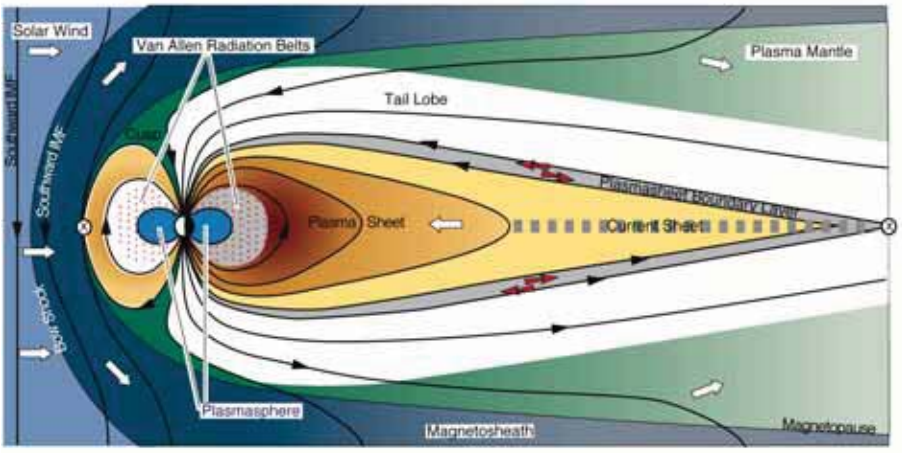

Figure 2.2: Illustration of regions in the solar wind and in the magnetosphere. The magnetopause is located where the pressure balance of the solar wind and the magnetosphere balance. The figure is adopted from (?).

and the nightside of the magnetosphere and their position depends on the IMF (Russell, 2000).

The plasma in the solar wind cannot easily flow into the magnetosphere due to the frozen-in condition. This makes the magnetosphere a cavity in the solar wind. Instead, the solar wind dynamic pressure compresses the dayside of the magnetopause and extends the nightside as in Figure 2.2. The pressure balance between the magnetosphere and the solar wind on the dayside occurs at approximately ~ 10 earth radii (R_E) (depending on the solar wind pressure) and is called the *magnetopause* (Kivelson and Russell, 1995); it is the outer boundary of the magnetosphere. The magnetopause is a discontinuity between different plasmas and magnetic fields. Due to the different magnetic fields on each side, the magnetopause is also a current sheet. The typical thickness of the magnetopause current layer is several ion gyro radii (Cravens, 2004). In the following we investigate the magnetopause when the frozen-in condition is not valid, and particles, momentum and energy can be transported across the magnetopause.

2.1 The CLUSTER mission

The CLUSTER mission consists of four spacecraft and was launched by ESA in 2000 (Escoubet et al., 1997). The main objective of the CLUSTER mission is to study the interaction of the solar wind with the magnetosphere on different length scales. The four spacecraft fly in pre-decided formations with a separation of about 100 km to 18,000 km. These constellations allows one to make a three dimensional mapping of space and distinguish between temporal and spatial structures. Instruments on the spacecraft detect waves, fields and particles. The instruments have different modes with different

resolutions to optimize studies of various regions and length scales. The spacecraft are spin stabilized with a spin period of about 4 s. The spin axes point approximately toward the south ecliptic pole. The instruments used in this study are briefly introduced here.

Magnetic fields are measured by the Fluxgate Magnetometer (FGM) (Balogh et al., 2001). It measures the full magnetic field vector at the location of every spacecraft. For the events in this report, the sampling rate is 22.4 Hz in normal mode and 67.3 Hz in burst mode. The Electric Field and Wave experiment (EFW) measures the electric field with wire booms in the satellite spin plane (Gustafsson et al., 2001). The third electric field component can be calculated assuming that the electric field is perpendicular to the magnetic field ($\mathbf{E} \cdot \mathbf{B} = 0$). This estimation of the third electric field component is unreliable unless the magnetic field is nearly perpendicular to the satellite spin axis. The third electric field component is calculated for relative angles $> 15°$ between the spin axis and the magnetic field. The electric field is sampled at 25 Hz and low-pass filtered at 10 Hz in normal mode. In burst mode the electric field is sampled at 450 Hz and low-pass filtered at 180 Hz. The potential difference between the spacecraft and the probes at the end of the wire booms is sampled at 5 Hz and can be used as an estimate of the spacecraft potential and can also be used to estimate the plasma density.

Three dimensional ion distributions are measured with the Cluster Ion Spectrometry (CIS) instrument (Rème et al., 2001). The Hot Ion Analyzer (CIS-HIA) samples ions in the energy range ∼5 eV/e – 32 keV/e. The energy sweep period is 62.5 ms (1/64 of one spin) and the angular resolution is $\sim 6° \times 6°$(see (Rème et al., 2001) for details). CIS-HIA does not differentiate between ion species. By using a time-of-flight technique the Composition and Distribution Function analyzer (CIS-CODIF) can differentiate between the ion species in the energy range ∼15 eV/e-38 keV/e, however with a lower time resolution than the CIS-HIA. The accumulation period is 125 ms (1/32 of one spin) and the angular resolution is $\sim 11° \times 23°$ (see (Rème et al., 2001) for details). To sample a 3D distribution both CIS-HIA and CIS-CODIF need a full spacecraft spin of about 4 s. Electron distributions are measured with the Plasma Electron And Current Experiment (PEACE) (Johnstone et al., 1997; Owen et al., 2001). PEACE has two detectors but we only use the High Energy Electron Analyzer (HEEA) to detect electrons in the energy range 30 eV – 26 keV. The PEACE-HEEA has a sweep time of 125 ms and an angular resolution of $\sim 11° \times 15°$ (see Johnstone et al. (1997) for details).

Chapter 3

Magnetic reconnection

Magnetic reconnection is a process that restructures magnetic fields. Due to reconnection, initially separated plasma regions can become magnetically connected and plasma and energy can flow between the earlier separated magnetic field lines (Priest and Forbes, 2000). Reconnection also enables release of energy stored in magnetic field stresses. This energy is transferred to acceleration and heating of plasma. Magnetic reconnection can occur in different plasma environments, such as accretion discs (Rastaetter and Neukirch, 1997), cometary tails (Jovanović et al., 2005), solar flares (Lin et al., 2005), the Earth's magnetosphere (Phan et al., 2005) and the magnetotail (Walker et al., 1999) and in laboratory plasmas (Yamada et al., 1997).

Onset of magnetic reconnection requires a shear between two magnetic fields, which implies the existence of a thin current layer. If the plasma is collisionless on each side of the current layer the magnetic fields are "frozen-in" to the plasma, and plasmas from the two regions cannot mix. Inside the current layer the frozen-in condition breaks down. This breakdown can be due to an increasing anomalous resistivity that enables magnetic field diffusion across the plasma. On the microscopic scale ($\sim c/\omega_{ci}$) the magnetic field lines diffuse across the plasma and reconnect in small regions called *diffusion regions*. From the diffusion region *separatrices* extend. A separatrix is the most recent reconnected field line that separates regions with magnetic fields of different topology; these magnetic fields may be anti-parallel, while the reconnected fields are found where the oppositely directed fields have been interconnected. The separatrices meet at the *X-line*. The X-line is surrounded by the diffusion region. The frozen-in condition is broken not only in the diffusion region, but also around the separatrices. However, the magnetic fields are not reconnecting there, but the particles are heated and accelerated. In this new field topology where the oppositely directed fields have been connected, plasma can flow along the field lines across the current layer and mix with plasma in the opposite region.

Magnetic reconnection can be defined as a process with the following

properties (Priest and Forbes, 2000):

1. Reconnection occurs in the diffusion region where the frozen-in condition breaks down. During the process of magnetic reconnection magnetic field lines are brought together and in the diffusion region they are "broken" and interconnected causing a magnetic topology change.

2. There is an electric field perpendicular to the reconnection plane (inflow plane) causing an inflow of plasma toward the diffusion region.

3. The frozen-in condition breaks down around the separatrices and there is a flow of plasma across the separatrices.

4. Energy stored in the magnetic field configuration, can be transferred to the particles in the diffusion region and along the separatrices.

3.1 Reconnection models

3.1.1 Sweet-Parker model

The first reconnection model was developed by Sweet (1958) and Parker (1957). Anti-parallel magnetic fields are separated by a current layer (with current density J) as in Figure 3.1. In the center of the current layer the magnetic fields vanish. The current layer has a length of $2L$ and a thickness of $2l$. Plasma and magnetic fields are flowing in towards the current layer at the velocity $v_i = \eta/l$, where η is the magnetic diffusivity (Priest and Forbes, 2000). The velocity v_i is the diffusion velocity in the current layer – the current layer is therefore also called the diffusion region, marked with grey in Figure 3.1. In the Sweet-Parker model plasma is accelerated inside the diffusion region. The length of the diffusion region is of macroscopic scale

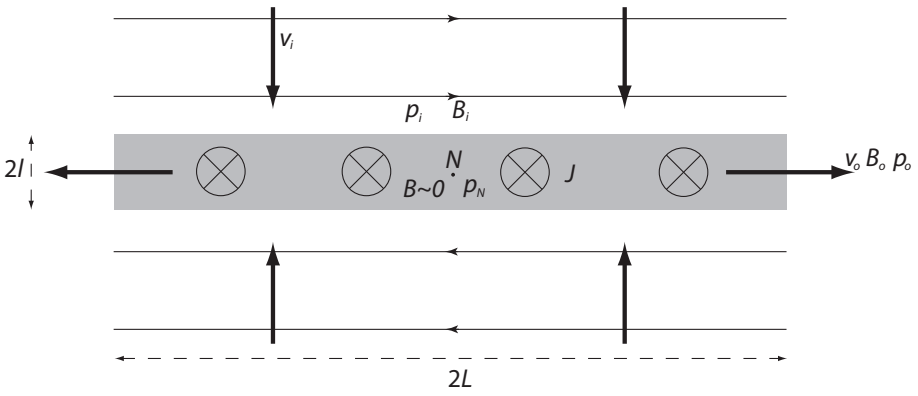

Figure 3.1: Illustration of the Sweet-Parker reconnection model. Adopted from Priest and Forbes (2000).

in the Sweet-Parker model with the consequence that there is no X-line.

From the inflow velocity we can calculate the dimensionless number called the reconnection rate:

$$M_i = \frac{v_i}{v_{Ai}} = \frac{1}{\sqrt{R_{mi}}}$$

where $R_{mi} = v_{Ai}L/\eta$ is the magnetic Reynolds number – the ratio between the Alfvén velocity (v_{Ai}) in the inflow region and η/L, which is the diffusion velocity out from the diffusion region. Inside the diffusion region near to the neutral point (N) the magnetic field vanishes and a pressure gradient $\sim (p_N - p_o)/L$ accelerates the plasma outward (Biskamp, 2000). Farther out towards the sides of the diffusion region the magnetic field increases and the magnetic force $\mathbf{J} \times \mathbf{B}$ becomes important and further accelerates the plasma (Priest and Forbes, 2000). In total the plasma is accelerated to the velocity v_o in the outflow region, which equals the (inflow region) Alfvén velocity,

$$v_o = v_{Ai}.$$

The conservation of mass ($v_i L = v_o l$) and the fact that the diffusion velocity is much smaller than the Alfvén velocity ($v_i \ll v_{Ai} = v_o$) shows that the thickness of the diffusion region is much smaller than the length $l \ll L$. This also means that the reconnection rate $M_i \ll 1$. The Sweet-Parker reconnection rate for observed solar parameters is $\sim 10^{-9}$ (see e.g. Li and Zhang (2009)). The observed reconnection rate in solar flares is ~ 0.01 and cannot be explained by the Sweet-Parker model. The kinetic energy (KE) in the inflowing plasma is negligible compared to the inflowing magnetic energy (EM),

$$\frac{\text{inflow KE}}{\text{inflow EM}} = \frac{\frac{1}{2}\rho v_i^2}{B_i^2/\mu} = \frac{v_i^2}{2v_{Ai}^2} \ll 1$$

Due to the conservation of magnetic flux ($v_i B_i = v_o B_o$) the magnetic field in the outflow region B_o is reduced ($B_o \ll B_i$) and, hence, magnetic energy is converted to kinetic energy and heat in the outflowing plasma. It can be shown (see Priest and Forbes (2000)) that about half of the inflowing magnetic energy is converted to kinetic energy,

$$\frac{\text{outflow KE}}{\text{inflow EM}} = \frac{\frac{1}{2}\rho v_o^2 (v_o l)}{v_i B_i^2 L/\mu} = \frac{\frac{1}{2}v_o^2}{v_{Ai}^2} = \frac{1}{2}.$$

3.1.2 Petschek model

The Sweet-Parker model was further developed by Petschek (1964). In the more realistic Petschek model the undisturbed external anti-parallel magnetic field lines (B_e, in Figure 3.2) becomes slightly curved closer to the current layer with a decreasing magnitude down to the strength B_i of the inflowing magnetic field. The velocity toward the current sheet increases from the undisturbed external velocity (v_e) to the inflowing velocity (v_i). The external length scale $2L_e$ in Figure 3.2 is the typical scale of the magnetic field far from the diffusion region. The diffusion region has length $2L$ and thickness $2l$. In the Sweet-Parker model the external length scale L_e

is also the half-length (L) in Figure 3.1. The half-length of the diffusion region (L) in the Petschek model is reduced compared to the Sweet-Parker model, but plasma acceleration occurs not only in the diffusion region. Only a small fraction of the plasma is accelerated in the diffusion region in the Petschek model. Most of the plasma is accelerated as it crosses the *slow shocks* extending from the diffusion region. At the shock front an electric field accelerates the plasma. The slow shocks are standing in the inflow region because plasma inflow and the shock propagation speed are the same. The slow shocks provide another way to efficiently transfer energy from the magnetic field to the particles. Thus, the plasma is not required to pass through the diffusion region to get energized like in the Sweet-Parker model. Since the magnetic flux is conserved from the external to the inflow region it

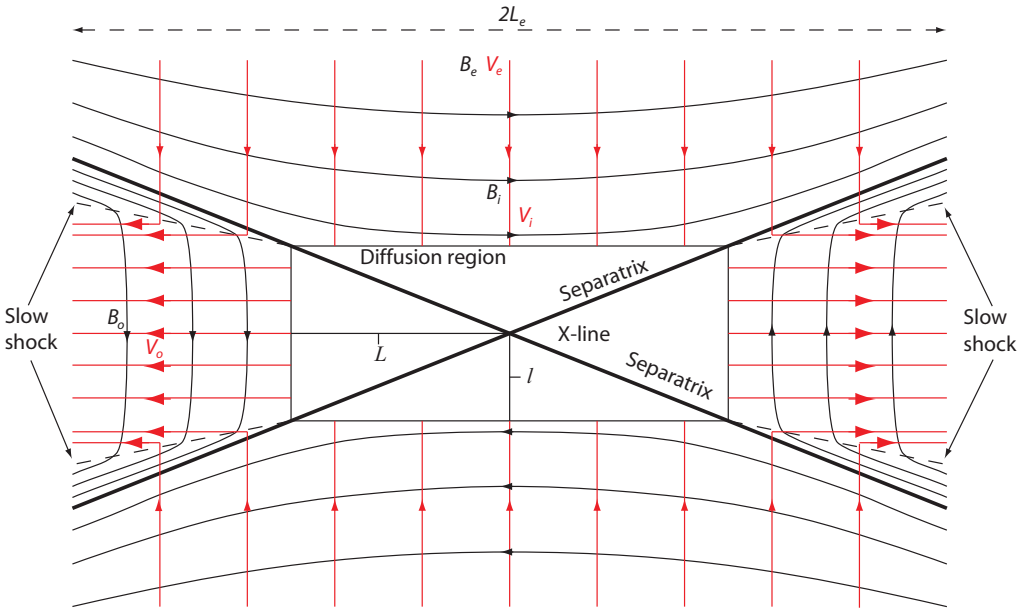

Figure 3.2: The Petschek reconnection model.

can be shown that the external length scale is much larger than the length of the diffusion region ($L_e \gg L$) in the Petschek model. The reduction in the half-length (L) also leads to a thinning of the current sheet (reduction of l) and, thus, a shorter diffusion time. Close to the small diffusion region in Figure 3.2 the process described by the Sweet-Parker model is the dominating source for accelerated plasma. On the external length scale (L_e) the diffusion region is often referred to as the X-line, where the separatrices meet.

The reconnection rate in the Petschek model is, like in the Sweet-Parker model, measured in the global external variables far from the diffusion region

$$M_e = \frac{v_e}{v_{Ae}} \approx \frac{\pi}{8 \log R_{me}}.$$

The reconnection rate for the Petschek model is much faster than for the

Sweet-Parker model.

3.1.3 Numerical simulations

Numerical simulations are important for understanding magnetic reconnection. MHD simulations are sufficient in a collisional plasma where a Sweet-Parker layer forms and limits the reconnection rate. For collisionless plasmas Hall-MHD must be used to describe reconnection. In Hall-MHD the Hall term ($\mathbf{J} \times \mathbf{B}$) and the electron pressure (∇P_e) is included in the MHD equations. Similar to Hall-MHD is the hybrid model with the difference that ions are treated as particles, whereas electrons are treated as a fluid like in MHD. In a particle-in-cell (PIC) simulation both ions and electrons are

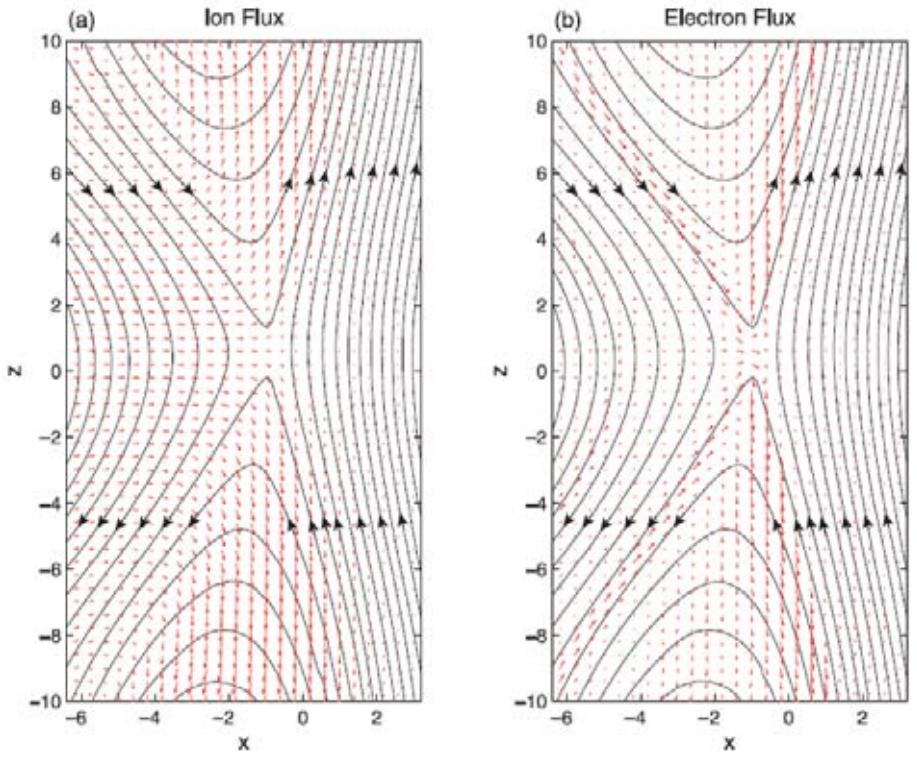

Figure 3.3: Structure of magnetic fields and electron and ion flow in a PIC simulation of magnetic reconnection. The left side corresponds the magnetosheath with a density n_0 and magnetic field strength $B_0/2$. The right side corresponds to the magnetosphere with density $n_0/3$ and magnetic field strength $3B_0/2$. The magnetopause current layer is located where the magnetic field rotates. Adopted from Pritchett (2008).

treated as particles (Shay et al., 2001). In collisionless simulations the acceleration of the ions mainly occurs in a region along the separatrices. The size of the diffusion region is small compared to the external length scale. The Petschek model considers symmetric reconnection, Figure 3.3 on the other hand, shows a PIC simulation (Pritchett, 2008) done for magnetopause-like

conditions with asymmetric density and magnetic field strength. The difference from the Petschek model is that the slow shocks are difficult to identify (Nakamura and Scholer, 2000; Shay et al., 2001; Pritchett, 2008). Instead, the magnetic field rotates continuously over the reconnection layer, like in Figure 3.3. Electrons are flowing in towards the diffusion region along the separatrices on the high density/magnetosheath side and flowing out along the separatrices on the low density/magnetospheric side. The ions in the outflow region consist mainly of ions from the magnetosheath. Near the separatrices there is a density depletion observed in the simulations (not shown).

3.1.4 Time dependent reconnection

The reconnection rate is in reality varying and time dependent. Semenov et al. (1992) and Biernat et al. (1998) have solved the time dependent MHD equations for different reconnection problems analytically to investigate the time dependence when reconnection turns on and then off. Reconnection that turns on and off is called *transient reconnection*. A varying reconnection

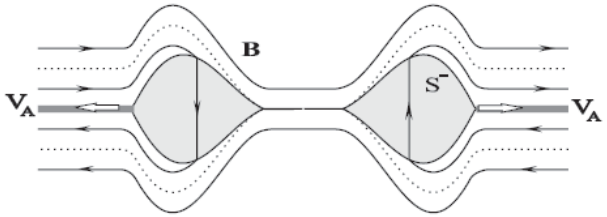

Figure 3.4: FTEs created during transient reconnection. Adopted from Semenov et al. (2005).

rate at the magnetopause causes magnetic "bulges". The bulges are called *flux transfer events (FTEs)* and travel along the magnetopause (Russell and Elphic, 1978). In the model used in e.g. Semenov et al. (1992) the reconnection rate is controlled by a time varying electric field. The electric field is set up in a small region around the diffusion region. In this model, slow shocks (S^-, bounding surface to the grey regions in Figure 3.4) are created and propagate out from the diffusion region at the Alfvén velocity. The slow shocks enclose the outflow region with heated and accelerated plasma. When reconnection turns off, the slow shocks detach from the diffusion region. This situation is depicted in Figure 3.4. The dotted lines in Figure 3.4 are separatrices between different magnetic topologies. The FTEs propagate along the magnetopause away from the diffusion region, leaving the undisturbed field lines behind.

3.2 Kinetic model of the reconnection layer

Instead of describing reconnection in the fluid formulation with slow shocks one can use a kinetic model, that focuses on particles and small scale signatures, since this is a better description of detailed observations of reconnection events (Gosling et al., 1990; Mozer et al., 2002; Vaivads et al., 2004; Lindstedt et al., 2009) and use the magnetopause as an example. When reconnection is ongoing at the magnetopause there are three different types of magnetic field lines – the magnetospheric field lines are so called "closed" field lines that start and end on the Eartha and the IMF represents field lines outside the magnetosphere. There are also "opened" field lines that magnetically connect the magnetosphere to the solar wind. During ongoing reconnection at the magnetopause, the magnetosphere and the magnetosheath are separated by the reconnection layer in Figure 3.5 (Gosling et al., 1990). The reconnection layer consists of the opened field lines and is bounded by the separatrices (Lockwood et al., 1996) that separate regions of different magnetic topology. In the magnetosheath and magnetosphere convection drives the plasma towards the X-line and the separatrices. As described in section 3.1, reconnection can heat and accelerate electrons to the electron Alfvén velocity (v_{Ae}), that is much larger than the ion Alfvén velocity ($v_{Ai} \ll v_{Ae}$) because of the small mass of the electrons. Outside the diffusion region the electrons follow the magnetic field and travel faster than the ions along a field line due to their higher velocity. The fastest moving electrons that have crossed the magnetopause current layer can be observed just inside the separatrix, the outer edge of the reconnection layer. This boundary is called the *electron edge* and is a good approximation of the location of the separatrix. The outer edges of the reconnection jet are also referred to as the *ion edges* since this is where the fastest ions accelerated by reconnection are observed. The reconnection/ion jet is the accelerated plasma flow caused by reconnection. The jet fills the entire *outflow region*. Between the separatrix and the outflow region we find the *separatrix region* where only the electrons from different origin mix. Ions mix in the outflow region. Inside the outflow region the magnetic field makes its main rotation and we refer to this as the *field reversal region*; this is the location of the magnetopause current layer. Sometimes this current layer is narrower than the outflow region. The part of the reconnection layer with magnetospheric orientation of the field lines is called the low latitude boundary layer (LLBL).

The kinetic model can be compared to the Petschek model. The separatrices in the Petschek model are closely related to the electron edges in the kinetic model due to the small inertia of the electrons. The ion edges are defined to be where the accelerated ion flow in the outflow region is observed. In the Petschek model, ion acceleration occurs at slow shocks extending from the diffusion regions. These slow shocks are hard to identify using spacecraft data. In principal, the slow shocks would be located at the ion edges. In the kinetic model, ion acceleration occurs in potential drops over the separatrix region. Several of these potential drops are analyzed

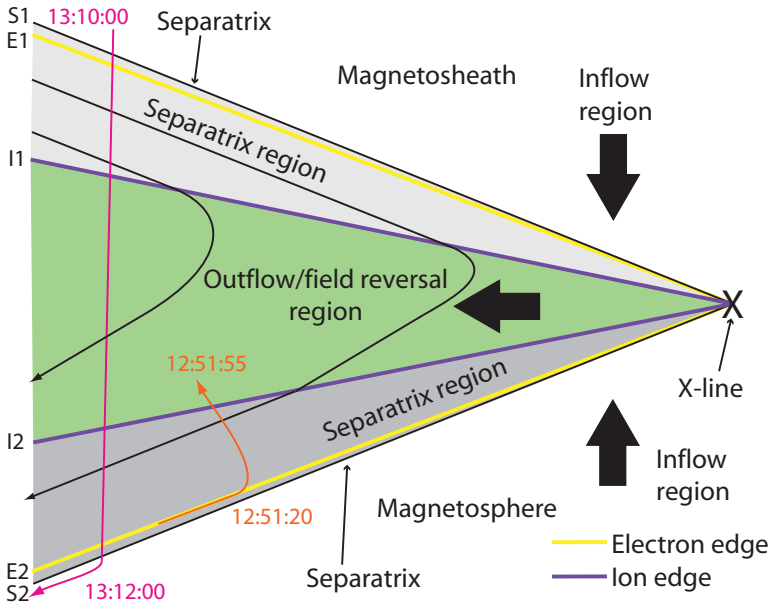

Figure 3.5: The regions of the magnetopause reconnection layer.

in this thesis. The rotational discontinuity (Alfvén wave) in the Petschek model is located along the slow shocks. This is not necessarily the case in the kinetic model where the main rotation occurs in the outflow region, also called the field reversal region.

Chapter 4

Separatrix regions of magnetic reconnection at the magnetopause

The magnetopause is the outer boundary of the magnetosphere. The magnetic fields are frozen-in to the plasma in the magnetosphere and the solar wind respectively, and plasma in the two regions normally do not mix. The regions are separated by a current layer at the magnetopause (Kivelson and Russell, 1995).

Magnetic reconnection can, however, transfer mass, momentum and energy across the magnetopause. In this chapter we will first discuss the location of magnetic reconnection on a large scale at the magnetopause in section 4.1. Spacecraft observations of reconnection evidence is discussed in section 4.2. Finally in section 4.3 we show an example of a spacecraft crossing of the magnetopause.

4.1 Magnetic reconnection at the magnetopause

Magnetic reconnection frequently occurs at the magnetopause where the geomagnetic field and the magnetosheath interact. The location of the X-line is directly related to the direction of the IMF since the geomagnetic field is relatively constant. The magnetic field in the more turbulent magnetosheath directly adjacent to the magnetopause can vary more than the IMF in the solar wind, but on average the direction of the magnetic field is the same in the two regions (Coleman, 2005). Reconnection occurs where the shear between the magnetic fields (IMF and geomagnetic field) is large (Luhmann et al., 1984; Trattner et al., 2005, 2007).

Figure 4.1 shows the shear angle between the IMF and the geomagnetic field during southward IMF (Trattner et al., 2007). Inside the magnetopause the Tsyganenko 96 (Tsyganenko, 1995) model is used to approximate the geomagnetic field. An estimation of the magnetic field outside the magnetopause in the magnetosheath is obtained by using solar wind data from the WIND spacecraft and assuming the field is draped around the magnetopause

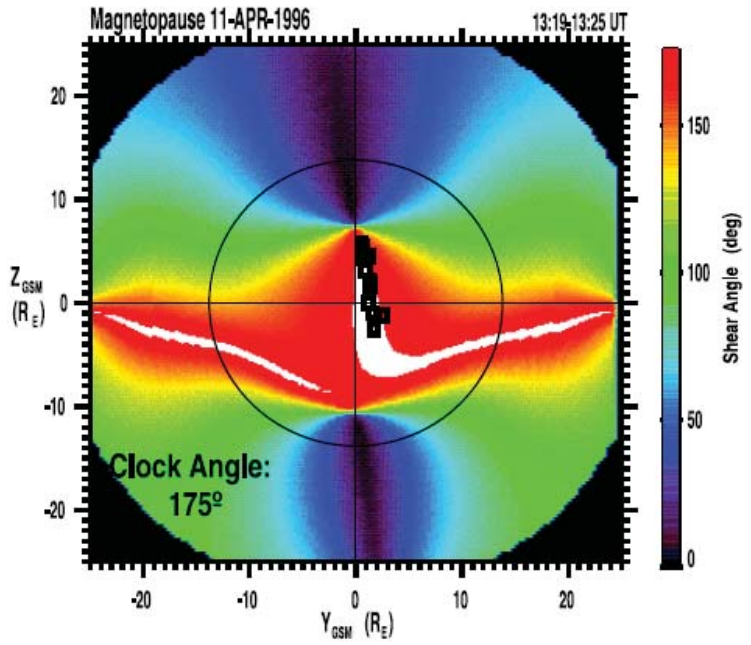

Figure 4.1: The colored surface shows the magnetic shear angle between the geomagnetic field and the IMF during southward IMF (clock angle 175°), seen from the sun looking toward the Earth. The white regions mark positions where the fields are antiparallel within 3°. Adopted from Trattner et al. (2007).

using the Cooling et al. (2001) model. When IMF is southward (IMF$B_z < 0$ and IMF$B_y \sim 0$) it is antiparallel to the geomagnetic field near the sub-solar point. In the example in Figure 4.1 the clock angle indicating the IMF direction in the GSM $y - z$ plane is 175° (where 0° and 180° corresponds to strictly northward ($B_z > 0$) and southward ($B_z < 0$) IMF respectively, while 90° and 270° corresponds to $B_y > 0$ and $B_y < 0$ with $B_z = 0$). In red areas the magnetic fields are antiparallel within 150° to 180°. The white regions mark positions where the fields are antiparallel within 3°. This means that during southward IMF the X-lines are located near the equatorial plane. If the magnitude of IMFB_y increases, the high magnetic shear is located at the separated red areas as in Figure 4.2 (Trattner et al., 2007). For IMF with clock angle 117° the high shear region stretches to the southern cusp in the dawn sector and to the northern cusp in the dusk sector. The white line in Figure 4.2 represents the location of the X-line indicating the maximal reconnection component B_N at the magnetopause (Moore et al., 2002). The black line represents the position of maximum magnetic shear across the magnetopause. For northward IMF (clock angle 39°), as in Figure 4.3, the magnetic shear has its maximum at high latitudes. Thus, reconnection

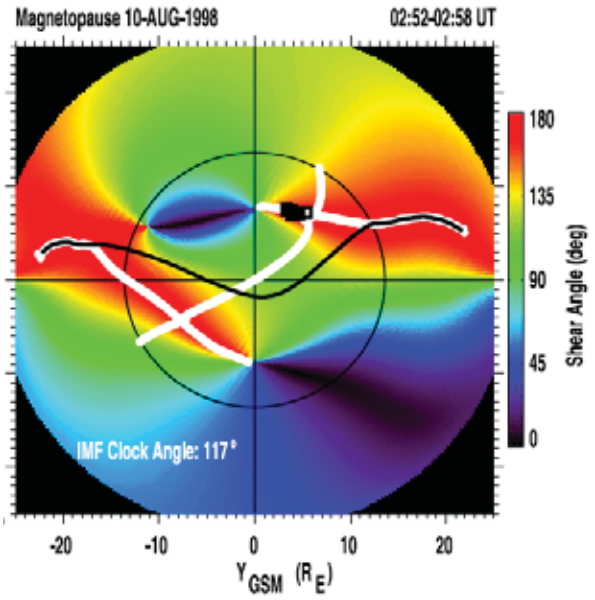

Figure 4.2: Shear angle between the geomagnetic field and the IMF when there is a strong IMF B_y component (clock angle 117°). The white line represents the location of the tilted X-line (Moore et al., 2002) and the black line represents the position of maximum magnetic shear across the magnetopause. Adopted from Trattner et al. (2007).

can be expected to occur tailward of the cusp (Trattner et al., 2004).

4.2 Signatures of reconnection at the magnetopause

Reconnection occurs at the magnetopause in the diffusion regions. The diffusion regions are of the order of a few ion inertial lengths $c/\omega_{pi} \sim 100\,\mathrm{km}$. The diffusion regions are in general too small to be observed by spacecraft and only a few observations exist (Mozer et al., 2002). In practice, spacecraft can only detect the consequences of reconnection. This is for example a magnetic field component normal to the magnetopause, ion jets, flux transfer events and particle energy dispersion.

The *Walén test* (Sonnerup et al., 1981) gives strong evidence of ongoing reconnection (Phan et al., 2004; Retinò et al., 2006). If reconnection is ongoing the geomagnetic field and the IMF are magnetically connected via a magnetic field component normal to the magnetopause and, thus, the magnetic field rotates across the magnetopause. This connection implies that the magnetic field lines on different sides of the magnetopause current layer move together. When this is the case it is possible to find a reference frame moving with velocity $\mathbf{V}_{HT}$ in which the plasma flow is parallel to the magnetic field and the convection electric field is zero $\mathbf{E}' = (\mathbf{v} - \mathbf{V_{HT}}) \times \mathbf{B} = 0$. This reference frame is called the *de Hoffmann-Teller frame*. In the de Hoffmann-Teller frame plasma is accelerated to the Alfvén velocity as it

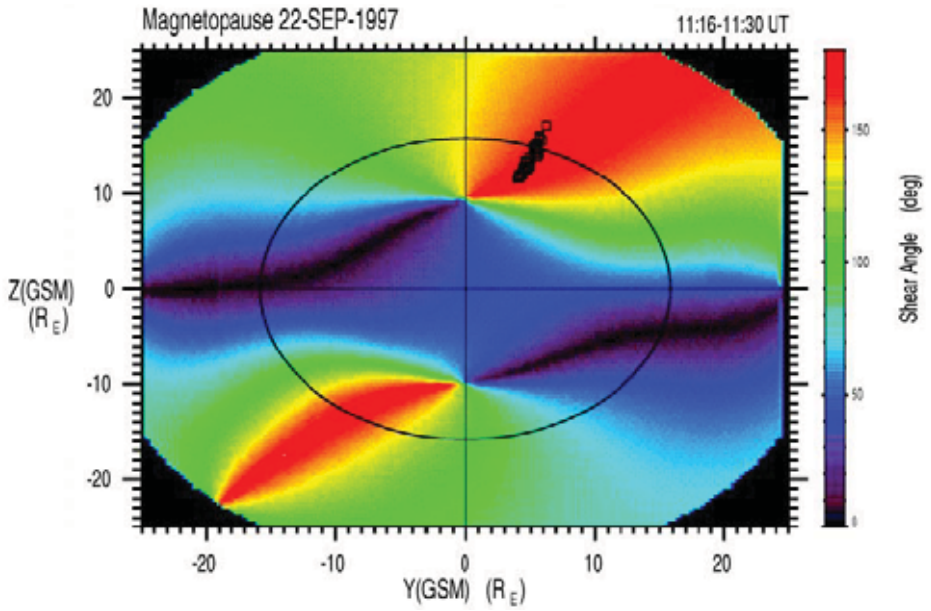

Figure 4.3: Magnetic shear during northward IMF and clock angle 39°. *Red areas correspond to high magnetic shear and black to low shear. Adopted from Trattner et al. (2004).*

crosses the discontinuity,

$$\mathbf{v}_2 - \mathbf{V}_{HT} = \pm(1-\alpha_2)\mathbf{B}_2[\mu_0\rho_1(1-\alpha_1)]^{-1/2}$$

where $\alpha = \mu_0(p_{||} - p_\perp)/B^2$ is the pressure anisotropy and subscript 1 and 2 refer to the magnetosheath and the outflow region, respectively. In a good Walén test when reconnection is ongoing, both the direction and magnitude of the velocity $\mathbf{v} - \mathbf{V}_{HT}$ is comparable to the Alfvén velocity in the outflow region. In Paper 1 in this thesis an alternative version of the Walén test is used. From the jump conditions of a rotational discontinuity we calculate the the expected velocity change in the tangential direction to the discontinuity according to (Retinò et al., 2005)

$$\mathbf{v}_{2t} - \mathbf{v}_{1t} = \pm[(1-\alpha_1)\mu_0\rho_1]^{1/2} \cdot [\mathbf{B}_{2t}(1-\alpha_2) - \mathbf{B}_{1t}(1-\alpha_1)].$$

The expected velocity change is then compared to the observed velocity change in the tangential direction to the discontinuity.

Another typical signature of reconnection is the existence of flux transfer events (FTEs) (Russell and Elphic, 1978). An FTE is created during changing reconnection rate (Southwood et al., 1988) like in transient reconnection, discussed in section 3.1.4. As the reconnection rate increases, more plasma is transported into the outflow region and creates a bulge on the magnetopause. Neighboring unreconnected field lines are pushed to the sides as the FTE travels along the magnetopause. A spacecraft that is located just inside or outside the magnetopause observes a bipolar signature in the magnetic field component normal to the magnetopause, B_N in Figure 4.4, as the

FTE passes. Note that the normal direction $\hat{\mathbf{N}}$ in this case is normal to the large scale magnetopasue. If the IMF is directed southward and reconnec-

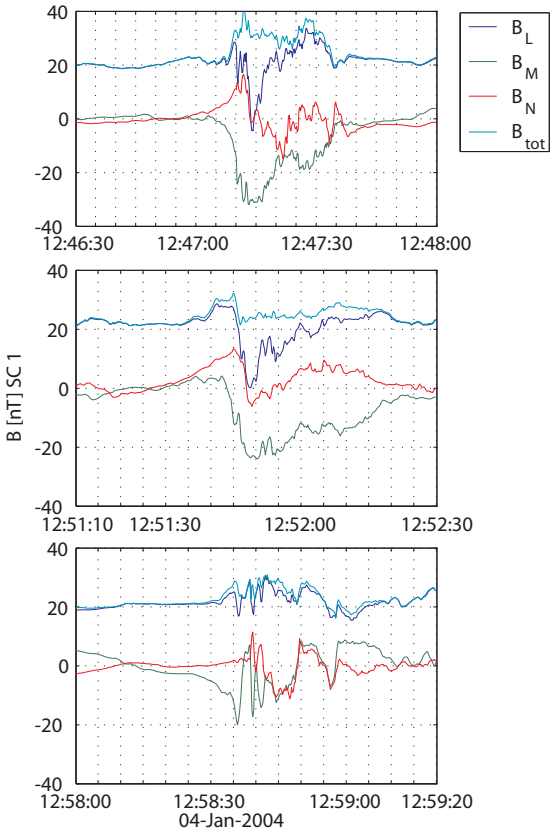

Figure 4.4: Observations of a bipolar normal magnetic field B_N due to FTEs by Cluster 1 at the magnetopause. From Paper 1 in this thesis.

tion takes place sunward of the cusps, the polarity of the signature depends on whether the spacecraft is on the north or south side of the X-line. With the normal component directed roughly toward the Sun, the bipolar signature is positive/negative if the spacecraft is northward of the X-line, and the signature is negative/positive if the spacecraft is southward of the X-line.

4.3 Separatrix regions

The separatrix region is located between the separatrix and the ion edge (see Figure 3.5) and has been extensively studied at low (Sandholt et al., 2002; Lockwood et al., 1996) and mid altitudes (Topliss et al., 2001; Bogdanova et al., 2004, 2006) and also to some extent at the magnetopause (Khotyaintsev et al., 2006; Retinò et al., 2006). The separatrix is identified from the electrons since the separation of the separatrix and the electron edge (the fastest electrons that travel along a field line when it is opened by reconnection) is very small. The ion edge is defined from ions and is located where

the ion jet is observed. The separatrix region is also called the electron edge of the LLBL in the literature (Bogdanova et al., 2006).

An example of a spacecraft crossing of the reconnection layer (Figure 3.5) at the magnetopause is shown in Figure 4.5. This event was analyzed in detail in Paper 1 together with seven other events. This event is a full crossing of the magnetopause reconnection layer, while some crossings in Paper 1 are partial. During these events the IMF was southward. Cluster crossed the magnetopause in the northern hemisphere sunward of the cusp. Both the Walén test and FTE observations indicate ongoing reconnection.

The observations in Figure 4.5 are presented in the local LMN-coordinate system of the magnetopause obtained from minimum variance analysis (MVA). The local LMN-coordinate system is obtained for single crossings of the magnetopause reconnection layer. The L-coordinate is along the magnetopause toward the positive GSE z component. The N-coordinate is normal to the magnetopause toward the sun and M = N $\times$ L. The N direction given by MVA is consistent with normal direction obtained from timing analysis of the magnetopause crossing using all four Cluster satellites (both density and magnetic field).

In Figure 4.5 data from Cluster 1, 2, 3 and 4 are shown in black, red, green and blue respectively. The spacecraft separations are $\sim$300 km. The data is also time-shifted to show similarities between the spacecraft. The time shift for spacecraft 1–4 is 1.0, 0, 0.5 and -0.3 s. Panels (a–d) show the magnetic field B_L, B_M, B_N components and the total magnetic field B_{TOT} from FGM. Panel (e) shows the density derived from the spacecraft potential measured by EFW. Panel (f) shows an ion spectrogram from CIS-HIA on C1. Panel (g) shows the ion velocity along the magnetopause current layer from CIS on C1 and EFW on C2. In panel (h) the current parallel to the magnetic field obtained from a single spacecraft method and in (i) the normal component of the electric field. In panel (j) we show the electric potential derived from the integrated normal electric field. Panel (k–m) show electron spectrograms from C2 in the perpendicular, parallel and the antiparallel direction to the magnetic field. Due to the rotation of the spacecraft the covered pitch angles change so that the parallel and anti-parallel directions are only observed during limited times. Panel (n) shows the distance to the magnetopause.

At the start of the interval Cluster is located in the cold and dense magnetosheath with southward IMF (negative B_L component). The magnetopause current layer is located where B_L changes sign from negative to positive (marked by the green bar in Figure 4.5).

The outflow region is where there is accelerated plasma flow. The magnetospheric edge is observed at the boundary between magnetosheath-like plasma and magnetospheric plasma at 13:11:06 UT in Figure 4.5. At this time there is also a sharp density gradient and this is defined to be the ion edge, marked with a purple bar. The magnetosheath ion edge is not clearly observed in the ion spectrogram, but an increasing ion velocity defines this boundary. In this event the outflow region totally coincides with

the magnetopause current layer.

In the magnetosheath, at 13:10:20 UT Cluster detects a sharp increase in anti-parallel (away from the magnetopause) electron flux at energies above 400 eV, i.e. electrons of magnetospheric origin. This is the outer separatrix or the magnetosheath electron edge, indicated with a yellow line in Figure 4.5. On the magnetospheric side of the magnetopause, 13:11:06 – 13:11:28 UT, there is a mixture of magnetosheath-like electrons and electrons with energies 1 – 10 keV, similar to the magnetospheric electron population both in the parallel and antiparallel direction. After 13:11:28 UT there is only a pure magnetospheric electron population. We identify this point as the inner separatrix or magnetospheric electron edge.

The separatrix regions are defined to be located between the ion and the electron edges. On the magnetospheric side, the separatrix region is observed between 13:11:06 – 13:11:28 UT. Inside the separatrix region we observe a density cavity. This density cavity might even coincide with the separatrix region. It is believed that the density cavity is created when the magnetic field line is opened by reconnection and the electrons escape. To keep the plasma quasi-neutral, an electric field normal to the region is set up that removes the ions (Khotyaintsev et al., 2006). One can indeed observe a normal electric field up to 30 mV/m inside the separatrix region. This normal electric field gives rise to a potential jump of about 4 kV.

On the density gradient (ion edge) that bound the outflow region on the magnetospheric side, a strong current of $0.2\,\mu\mathrm{A/m^2}$ parallel to the magnetic field is located. This current coincides with the outer edge of the bipolar Hall B_M signature, produced by Hall currents flowing towards and away from the X-line. In this case the strongest parallel current is flowing towards the X-line. Mapping the parallel current to the ionosphere we find that it corresponds to a current of $400\,\mu\mathrm{A/m^2}$, which is of the same magnitude as the several hundreds $\mu\mathrm{A/m^2}$ that has been observed (Stasiewicz et al., 1998; Ivchenko and Marklund, 2002).

The observations in Figure 4.5 agree well with the kinetic model in Figure 3.5 and add important information to the model. If we compare these two figures several features of the model can be identified in the data. The separatrix regions are identified in the data between the electron edges/separatrices, the outermost boundary of the magnetopause reconnection layer, and the outflow region. The observed magnetopause current layer that coincides with the outflow region also agrees well with the kinetic model. In addition to the kinetic model, the data also shows that the magnetospheric-side separatrix region coincides with a density cavity. Also along the magnetospheric-side ion edge there is a strong field aligned current.

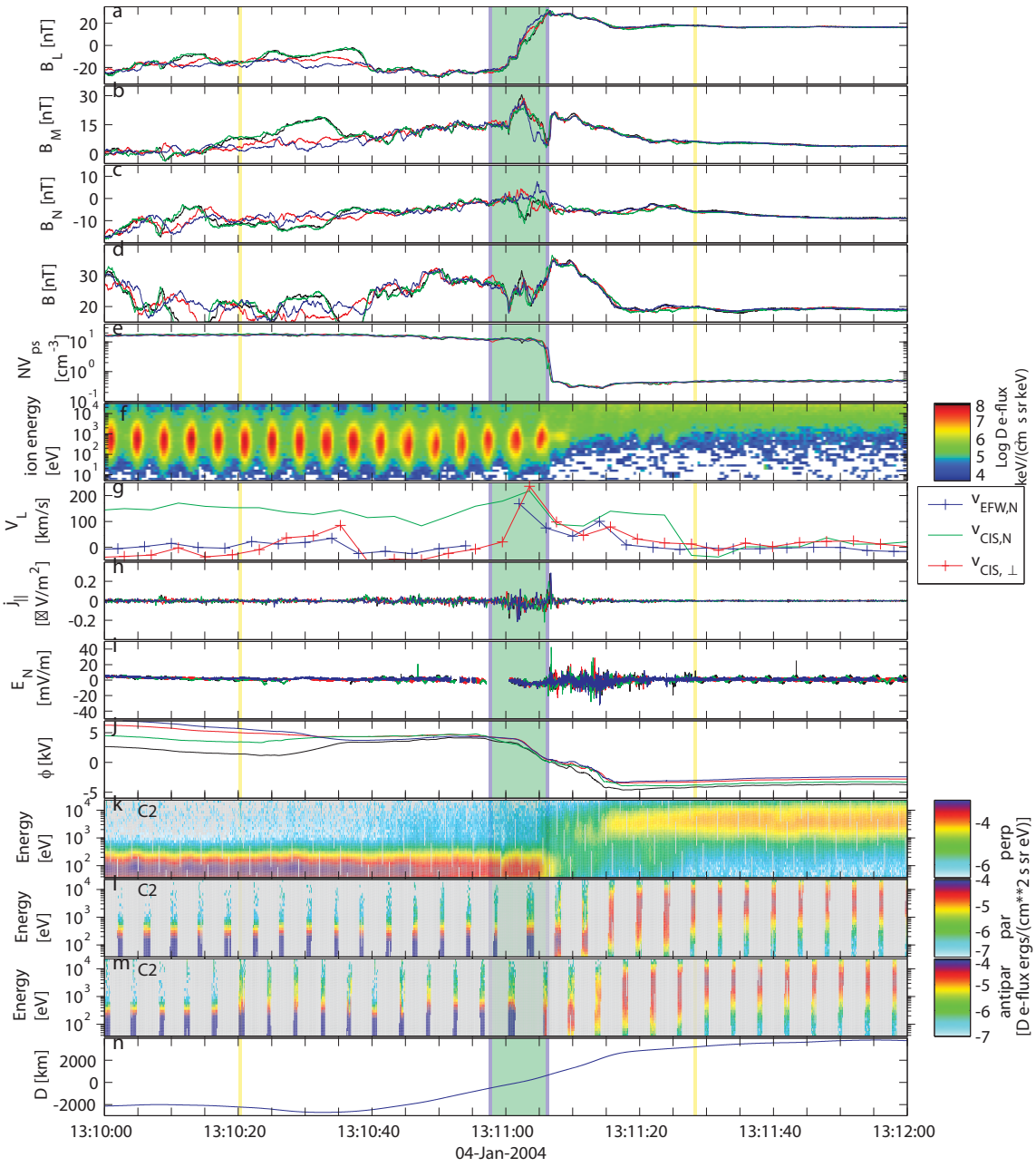

Figure 4.5: Observation of a magnetopause reconnection layer by the Cluster spacecraft at the magnetopause, see the text for details.

Chapter 5

Ion energization

Ion heating in the magnetosphere is an important process that has great impact on the dynamics of the magnetosphere. The plasma in the magnetosphere comes from the ionosphere and the solar wind. Ions in the ionosphere can be energized to overcome the gravitational energy and escape into the magnetosphere (Chappell, 1988). A significant part of the ionospheric ions is made up by oxygen ions. Because of their large mass, oxygen ions can affect the magnetosphere to a large extent (Winglee et al., 2002). The ions flowing out from the ionosphere can be further energized in the magnetosphere. These acceleration mechanisms contribute to loss of the Earth's atmosphere (Seki et al., 2001). The ions can be accelerated both parallel and perpendicular to the magnetic field. As an example, ions can be accelerated by parallel electric fields in the auroral region. In this thesis, energization perpendicular to the magnetic field by a transverse electric field, called *transverse ion heating*, will be discussed.

5.1 Transverse ion heating in the magnetosphere

In the lower magnetosphere (up to $\sim 1R_E$) transverse wave heating is an important process to energize oxygen ions (André et al., 1998; Norqvist et al., 1998). In broad-band electric field fluctuations the left-hand polarized waves around the local ion cyclotron frequency energize the ions by resonance heating (Chang et al., 1986). Left-hand waves rotate in the same sense as ions around the magnetic fields. Once the ions are heated in the perpendicular direction, the mirror force from the diverging dipole magnetic field converts the perpendicular velocity into parallel velocity. Thus, the heated ion velocity distribution has velocity components both perpendicular and parallel to the magnetic field. Since wave heating occurs in localized regions, the further away from the heating region the ions are observed, the more parallel the velocity. Distributions with velocity perpendicular to the magnetic field, possibly also with a parallel velocity component, are called *ion conics* (André and Yau, 1997; Moore et al., 1999).

Another mechanism for transverse heating by a static electric field is described by Cole (1976). The wave frequency is not in resonance with the ion cyclotron frequency, but a static electric field is observed in a region smaller than the gyro radius. This occurs when the electric field gradient is large enough, $\nabla E > \omega_c^2 m/q$. The particle cyclotron motion is then destroyed (Stasiewicz et al., 2000) and the result is that the ions are not $\mathbf{E} \times \mathbf{B}$-drifting over the region, but are instead accelerated along the electric field. Spatial and temporal variations of the electric field have the same effect on a charged particle in motion. This has been studied by Lundin and Hultqvist (1989) and Hultqvist (1996), who also concluded that oxygen ions are accelerated more effectively than protons.

In the higher altitude magnetosphere ($> 4R_E$) heated ions have been observed in the separatrix region (see Figure 3.5). The observations of heated ions have been correlated with low frequency waves (Topliss et al., 2001; Bogdanova et al., 2004). However, Bouhram et al. (2004) explained that wave heating is less important above $4.5R_E$. Still, locally heated ions are observed at higher altitudes (Arvelius et al., 2005; Nilsson et al., 2006; Waara, 2009). Also in the magnetosheath heated oxygen ions are observed (Eklund et al., 1997). According to Nilsson et al. (2004) acceleration mechanisms at these high altitudes favor heavy ions over light ions. Part of the high energy oxygen in the magnetosheath was explained by oxygen ions in a reconnection jet.

During reconnection at the magnetopause it is known that separatrix regions extend far from the reconnection site. Inside the separatrix regions there are localized strong normal electric fields (André et al., 2004; Khotyaintsev et al., 2006; Lindstedt et al., 2009). The width of the separatrix region is of the order of a proton gyro radius. This suggests the possibility that heavy ions with large gyro radius are accelerated as they enter and cross the separatrix region.

5.2 Observation of ion heating at high altitude

In this section we give an overview of an event on 13 March 2002 when Cluster was located in the southern hemisphere at an altitude of $\sim 10R_E$. The spacecraft separations were about 100 km. Cluster crossed from the magnetosheath, passing the cusp, into the lobe. At these high altitudes the spacecraft velocity is usually small compared to the convection velocity that makes the boundary between the cusp and the lobe move back and forth. This is the reason that, in this case, the spacecraft return back to the cusp and again finally enter the lobe, as shown in Figure 5.1. In Figure 5.2 the data is from the time interval when the spacecraft travel from the cusp, into the lobe and back to the cusp.

In Figure 5.2a the IMF data is from ACE spacecraft (Smith et al., 1998) located at the Lagrangian point (L1). The IMF data is time-shifted with $\sim$50 min to adjust for the propagation of the solar wind from the location

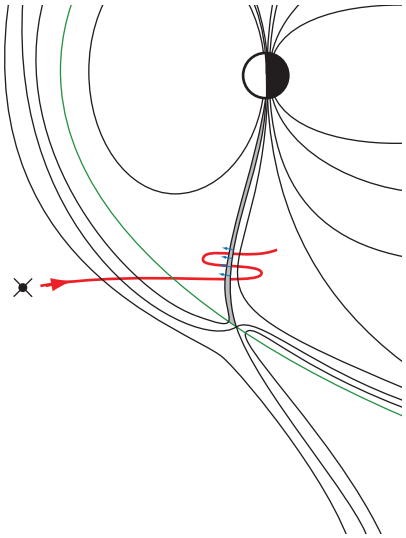

Figure 5.1: Illustration of regions observed by Cluster. The spacecraft are moving with a velocity of less than 3 km/s while plasma structures are moving much faster across the satellites.

of ACE to Cluster. The IMF B_y-component dominates the magnetic field. This suggests that if reconnection is ongoing the reconnection site is not located at the subsolar point. Figure 5.2b and Figure 5.2d show the magnetic field and the ion velocity from Cluster, respectively. Ion jets are observed parallel to the magnetic field, directed mostly in the positive z-direction. Thus, the reconnection X-line must be located tailward of the cusp. Further evidence of this picture is that when Cluster passed the magnetopause at 10:11 UT the IMF is similar to what is shown in Figure 5.2a. For this magnetopause crossing the Walén test is successfully performed and confirm the result. In the ion spectrogram in Figure 5.2e we also note velocity dispersion as the spacecraft enter the lobe (10:25–10:27 UT, protons with high energy are observed closer to the lobe). This is also an indication of ongoing reconnection (Escoubet et al., 2008). Thus, there are good reasons to believe that reconnection is ongoing tailward of the cusp.

Apart from the dispersion observed on the boundary between the cusp and the lobe in Figure 5.2e, the lobe (10:29–10:31 UT) is almost empty of protons. Figure 5.2c shows the low density in the lobe (10:29–10:31 UT). The oxygen in Figure 5.2f has a different behavior from the proton spectrogram. The dispersion 10:25–10:27 UT is absent and in the lobe there are still oxygen ions present with energy ∼100 eV. In some boundary layer between the lobe and the cusp (10:31–10:32:30 UT) the oxygen ions are heated to 200 eV–2 keV. Inside the cusp after 10:32:30 UT the oxygen energy is 1–20 keV. Figures 5.2g–i show the pitch angle of the observed oxygen ions for energies up to 500 eV, 500 eV–3 keV and 3 keV–6 keV, respectively. Inside the lobe (10:29–10:31 UT) there are only low energy (<500 eV) oxygen ions observed with a pitch angle of $\sim 90°$. In the boundary layer (10:31–10:32:30 UT) ions

are still observed with a pitch angle of $\sim 90°$, but with higher energy, 0.5–3 keV. Finally, when the spacecraft enter the cusp (after 10:32:30 UT) oxygen energies above 3 keV are observed. In the earlier crossing from the cusp to the lobe at 10:26–10:30 UT, the same characteristics as presented above are observed. However, it is not possible to determine the normal direction in the early event and detailed analysis is only possible for the event 10:31–10:32:30 UT. The high energy ions with a pitch angle $\sim 90°$ that are observed near the cusp–lobe boundary, marked with blue boxes in Figure 5.2h–i, correspond to transversally accelerated ions that are sometimes called ion conics.

We now consider the electric field at the boundary between the lobe and the cusp. In Figure 5.3 we plot the electric field normal to the magnetic field and the potential jump across the boundary. The normal direction is determined by timing analysis using four spacecraft. The normal direction is $\mathbf{N} \approx$[0.92 -0.34 -0.18] GSE, but is not constant during the crossing and changes by $\sim 20°$. The electric field is particularly strong in the normal direction between 10:32:40–10:32:42 UT where it is up to 60 mV/m. This electric field is balanced by the Hall-term ($\mathbf{J} \times \mathbf{B}$), which means that the frozen-in condition is broken in this region. This is a property typical of the separatrix region (Khotyaintsev et al., 2006). The normal velocity also changes from 35 km/s to 80 km/s. The line in Figure 5.3b corresponds to the approximate motion of the boundary from the $\mathbf{E} \times \mathbf{B}$-drift velocity. Together with the evidence for ongoing reconnection presented above, we interpret the potential jump in Figure 5.3b to be located in a separatrix region. Since the velocity changes, the upper dashed line corresponds to the lower velocity ($\sim$35 km/s) and the lower dashed line to the higher velocity ($\sim$80 km/s). The gyroradius of a 1 keV oxygen ion is about 400 km, corresponding to $\sim$8 s in the figure. During 8 s the electric potential changes by $\sim$4 kV (3–6 kV), corresponding to an energy increment of the oxygen ions of $\sim$4 keV.

Since the electric field is observed within a region that is comparable to the oxygen gyroradius, the results of Cole (1976) can be applied: if the region with the electric field is smaller than the gyroradius, the particle is accelerated along the electric field and does not $\mathbf{E} \times \mathbf{B}$-drift across the region. Since heavy ions have larger gyroradius, the mechanism preferentially heat heavy ions. This is consistent with the observations by Nilsson et al. (2004), who found that heating of oxygen ions was more efficient than heating of protons. In this case, the mechanism accelerates oxygen ions from the lobe to considerably higher energies in the cusp. The mirror force can then convert the transversal velocity into parallel velocity, allowing the ions escape to the magnetosheath. This agrees with the fact that high energy oxygen is observed in the magnetosheath (Eklund et al., 1997). We must however note that oxygen ion conics at these altitudes have been observed where no strong electric field has been seen (Waara, 2009). The conclusion is that the potential jump perpendicular to the magnetic field in the thin boundary can accelerate ions with large enough gyroradius from the lobe to

several keV in the cusp, as seen in Figure 5.2i.

In the alternative wave heating mechanism the resulting energy is dependent on the spectral density of the waves and the duration of the interaction between the ions and waves. Furthermore, only the left-hand polarized part energizes the ions. In this event, the spectral density is higher in the cusp than in the lobe regions (see Figure 5.4). A calculation based on the model by Chang et al. (1986), where the ions are allowed to be heated from lower altitudes up to the present altitudes and assuming a dipolar magnetic field, gives a maximum heating of less than 1 keV. For this calculation we use a pitch angle of 80° at C4 which means that most of the heating has taken place within ∼600 km below the point of observation, and 20% of the highest observed spectral density of $\sim 10\,(\mathrm{mV/m})^2/\mathrm{Hz}$. At lower altitudes ≤10% of the spectral density is needed to explain transversal heating of ions (André et al., 1998). In this event heating of the ions with energy <500 eV observed in Figure 5.2g to energies 500 eV–3 keV in Figure 5.2h can be explained by waves. Furthermore, the potential jump explains the oxygen ion energy in the range 3–6 keV in Figure 5.2i.

The event presented here shows that local oxygen ion energization to several keV can occur at high altitudes, and that the energization mechanism can be investigated. In the event studied here and in Paper 2, resonant heating by waves can give a significant contribution but most of the energization comes from a narrow potential drop in a magnetic reconnection separatrix region. However, note that this description only gives an estimate of ion heating, but also an intuitive picture of the process. A detailed description with the analysis in detail following Cole (1976) is presented in Paper 2.

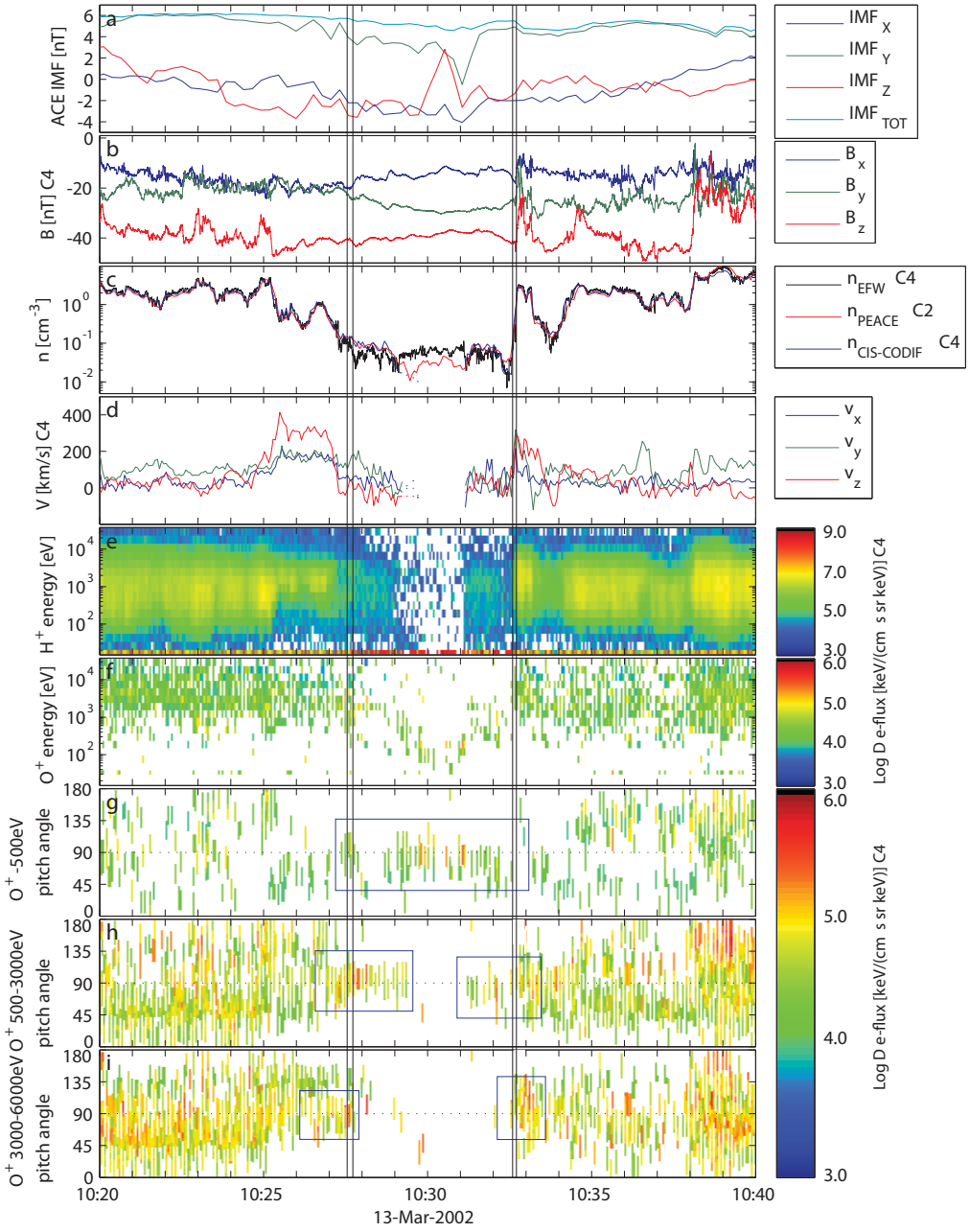

Figure 5.2: Oxygen acceleration at high altitudes by static electric fields. Panel (a) shows the IMF from ACE time-shifted by ∼50 min, (b) the magnetic field from FGM on Cluster 4 (C4) in GSE coordinates, (c) the density from EFW and CIS-CODIF on C4 and from PEACE on C2. Panel (d) shows the proton velocity from CIS-CODIF on C4. The data gap is due to the lack of protons in the lobe. Panel (e) shows the proton spectrogram and (f) the oxygen spectrogram from CIS-CODIF on C4. In panels (f)–(i) there can be some cross-talk from proton to oxygen CODIF channels, but the regions indicated by blue boxes in panels (g)–(i) have been carefully checked and contain essentially only oxygen ions. The pitch angles of the observed oxygen ions are shown in panel (g)–(i) for ions with energies up to 500 eV, 500 eV–3 keV and 3–6 keV respectively. During the time 10:20–10:27:30 UT and 10:32:30–10:40 UT the spacecraft are in the cusp. Between 10:29–10:31 UT the spacecraft are in the lobe. The narrow regions indicated around 10:27:40 UT and 10:32:40 UT include strong electric fields; see also Figure 5.3.

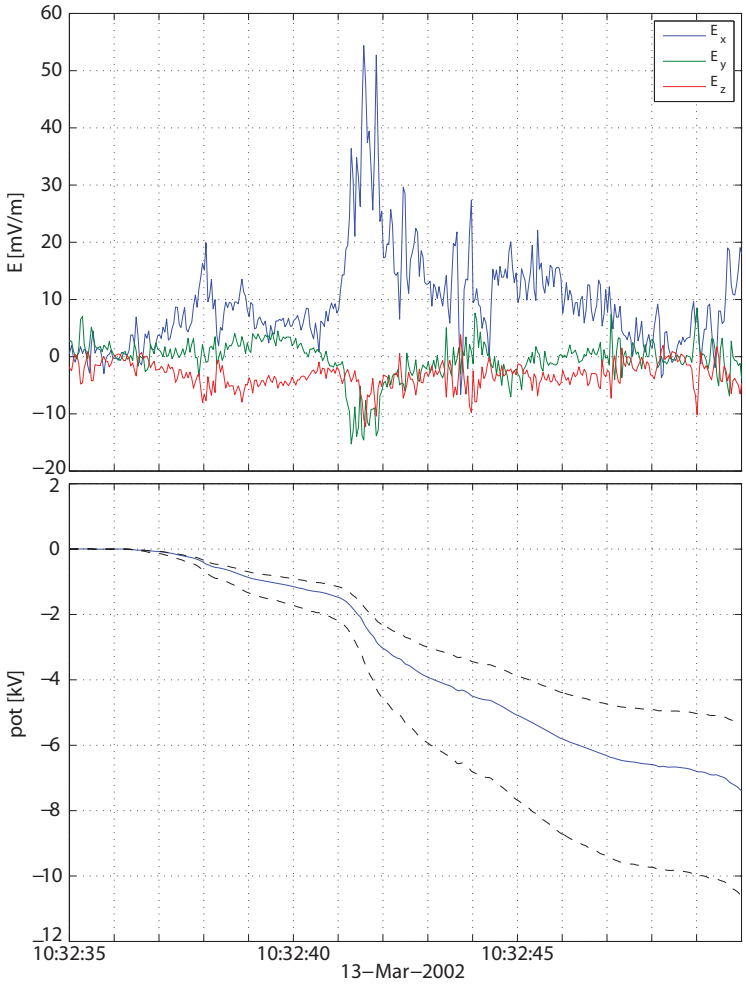

Figure 5.3: The electric field in GSE coordinates from C4 and the jump in the electric potential over the boundary between the lobe and the cusp. The solid line in the lower panel corresponds to the best estimate of the boundary motion from $\mathbf{E} \times \mathbf{B}$ *observations. The dashed lines give the upper and lower limits from the potential jump based on the lower and upper limits for the boundary velocity.*

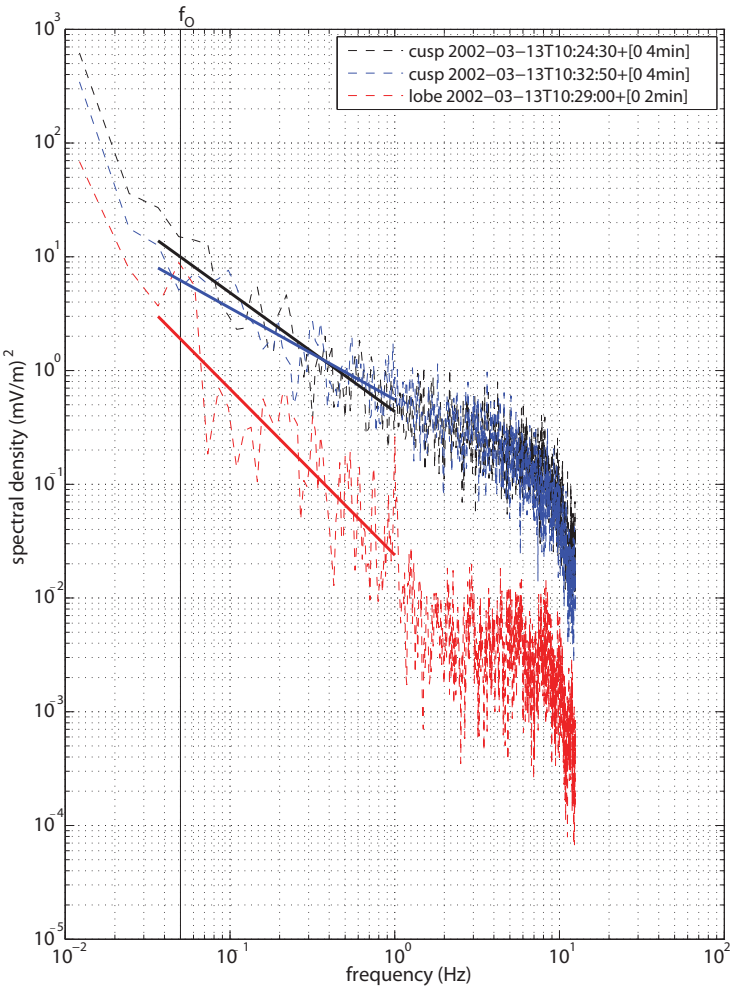

Figure 5.4: The spectral density calculated during 2 minutes in the lobe (red dashed line) and during 4 minutes in the cusp for two different time intervals (black and blue line). The thicker lines are linear fittings to the spectral density. The lines at 0.05 Hz indicates the oxygen ion gyro frequency.

Chapter 6

Future work

The structure and location of the separatrix region needs to be further studied to reveal its characteristics and effects on the magnetosphere. Possibly, the ion energization that occur on small scales in the separatrix region could have large impact on the dynamics of the magnetosphere and the ion outflow from the ionosphere. The separatrix region also holds the key to how the X-line affects the particles on small scales. These particles may then transport mass and energy over large distances, e.g. in ion jets, and affect the whole magnetosphere. It is important to study these effects and to determine which physical processes are most important.

The importance of the ion energization mechanism in the separatrix region needs to be further evaluated. To do this, it is necessary to find additional events and events where a larger amount of oxygen is present. The ion velocity distribution at different positions relative to the separatrix region needs to be studied. Such a study would give information about the development of the ion energization mechanism. Examples with clear electron and ion edges observed together with oxygen ions would also improve the understanding of the process.

To further study effects of separatrix regions it is necessary to use spacecraft observations from different altitudes. In the ideal case one would study conjunctions of several spacecraft (located on the same magnetic field line at the same time). Several interesting features can then be determined.

- The evolution of the width of the separatrix region.
- Where can the density cavity be found? And how is it created?
- Are the separatrix regions and the observed parallel currents found all the way down to the ionosphere?
- Does the electric field change with the distance from the X-line and the altitude? How does it affect the ions at different altitudes?
- Does the ion energization change with the distance from the X-line?

- Can the ions that are energized by potential jumps at low altitudes be observed at higher altitudes? Does the potential jump change with the distance from the X-line?

- How does the ion velocity distribution change with altitude, and what can it tell us about the heating mechanism?

- Can we determine the evolution of the electron and ion edges? How do the electron and ion edges correlate to the energized oxygen ions?

- How is plasma transported in the separatrix region?

The answer to these questions tell us how the separatrix region changes with distance from the X-line and with altitude. Observations at different altitudes can also give information to compare the characteristics of the separatrix region to the diffusion region close to the X-line.

In 2014, the NASA Magnetospheric Multi Scale (MMS) mission will be launched. Similar to Cluster, it will consist of four spacecraft but the spacecraft separation is planned to be smaller, down to $\sim$10 km. This will provide measurements with higher resolution and precision and the separatrix region can be studied in more detail. The Cross-Scale mission is another spacecraft mission being planned within the ESA cosmic vision. It would consist of up to 12 spacecraft with a separation from $\sim$10 km to more than an Earth radius. This would be an ideal mission to study separatrix regions that have different scale-lengths in different directions (stretched in one direction and narrow in another).

To further develop the understanding of the magnetosphere and the separatrix regions, one should also observe separatrix regions under different plasma conditions. In this thesis, we have studied separatrix regions at the magnetopause with dense and cold magnetosheath-like plasma on one side, while on the other side, we found in one case, hot and diluted magnetospheric plasma in one case; in the other case, almost no plasma at all. The separatrix region at the magnetopause on the magnetosheath side or a separatrix region in the magnetotail would provide different plasma conditions. A few studies of these regions exists (Lavraud et al., 2005; Wygant et al., 2005), but they need to be complemented by electric field and electron data and, if possible, observations of heavy ions. Comparing similarities and differences would provide important understanding of the processes in and around the separatrix region.

As an extension of these studies the loss of ionospheric plasma due to the separatrix region should be estimated. This would provides one measure of the importance of the separatrix region.

Finally, to get a full understanding of how the density cavity and electric field is created in the separatrix region, numerical simulations should be performed under realistic conditions. Most of the numerical simulations use an unrealistically large electron mass. This does not affect the reconnection rate, but it does affect the electron dynamics. A detailed investigation of the

separatrix regions including their width, the size of the density cavity and the location of the normal electric field should be done. A further discussion of the origin of the normal electric field and the density cavity would also be necessary.

The overall goal for space observations and numerical simulations, as discussed in this thesis, is to understand how magnetic reconnection works and how it affects plasmas in planetary magnetospheres, the solar wind, the solar corona and other astroplasmas.

Acknowledgements

I would like to thank my supervisors Andris Vaivads and Yuri Khotyaintsev for all their help and work. I also want to show my appreciation to Mats André for good discussions and great help with writing this thesis.

Bibliography

André, M. and Yau, A.: Theories and Observations of Ion Energization and Outflow in the High Latitude Magnetosphere, Space Science Reviews, 80, 27–48, doi:10.1023/A:1004921619885, 1997.

André, M., Norqvist, P., Andersson, L., Eliasson, L., Eriksson, A. I., Blomberg, L., Erlandson, R. E., and Waldemark, J.: Ion energization mechanisms at 1700 km in the auroral region, J. Geophys. Res., 103, 4199–4222, doi:10.1029/97JA00855, 1998.

André, M., Vaivads, A., Buchert, S. C., Fazakerley, A. N., and Lahiff, A.: Thin electron-scale layers at the magnetopause, Geophysical Research Letters, 31, 3803–+, doi:10.1029/2003GL018137, 2004.

Arvelius, S., Yamauchi, M., Nilsson, H., Lundin, R., Hobara, Y., Rème, H., Bavassano-Cattaneo, M. B., Paschmann, G., Korth, A., Kistler, L. M., and Parks, G. K.: Statistics of high-altitude and high-latitude O^+ ion outflows observed by Cluster/CIS, Annales Geophysicae, 23, 1909–1916, 2005.

Balogh, A., Carr, C. M., Acuña, M. H., Dunlop, M. W., Beek, T. J., Brown, P., Fornaçon, K.-H., Georgescu, E., Glassmeier, K.-H., Harris, J., Musmann, G., Oddy, T., and Schwingenschuh, K.: The Cluster Magnetic Field Investigation: overview of in-flight performance and initial results, Annales Geophysicae, 19, 1207–1217, 2001.

Baumjohann, W. and Treumann, R. A.: Basic space plasma physics, Imperial College Press, 1996.

Bellan, P. M.: Fundamentals of plasma physics, Cambridge University Press, iSBN: 0-521-82116-9, 2006.

Biernat, H. K., Semenov, V. S., and Rijnbeek, R. P.: Time-dependent three-dimensional Petschek-type reconnection: A case study for magnetopause conditions, J. Geophys. Res., 103, 4693–4706, doi:10.1029/97JA02965, 1998.

Biskamp, D.: Magnetic Reconnection in Plasmas, Magnetic reconnection in plasmas, Cambridge, UK: Cambridge University Press, 2000 xiv, 387 p. Cambridge monographs on plasma physics, vol. 3, ISBN 0521582881, 2000.

Bogdanova, Y. V., Fazakerley, A. N., Owen, C. J., Klecker, B., Cornilleau-Wehrlin, N., Grison, B., André, M., Cargill, P., Rème, H., Bosqued, J. M., Kistler, L. M., and Balogh, A.: Correlation between suprathermal electron bursts, broadband extremely low frequency waves, and local ion heating in the midaltitude cleft/low-latitude boundary layer observed by Cluster, Journal of Geophysical Research (Space Physics), 109, 12 226–+, doi: 10.1029/2004JA010554, 2004.

Bogdanova, Y. V., Owen, C. J., Fazakerley, A. N., Klecker, B., V., Y., and Rème, H.: Statistical study of the location and size of the electron edge of the Low-Latitude Boundary Layer as observed by Cluster at mid-altitudes, Annales Geophysicae, 24, 2645–2665, 2006.

Bouhram, M., Klecker, B., Miyake, W., Rème, H., Sauvaud, J., Malingre, M., Kistler, L., and Blagau, A.: On the altitude dependence of transversely heated O distributions in the cusp/cleft, Annales Geophysicae, 22, 1787–1798, 2004.

Chang, T., Crew, G. B., Hershkowitz, N., Jasperse, J. R., and Retterer, J. M.: Transverse acceleration of oxygen ions by electromagnetic ion cyclotron resonance with broad band left-hand polarized waves, Geophys. Res. Lett., 13, 636–639, doi:10.1029/GL013i007p00636, 1986.

Chappell, C. R.: The terrestrial plasma source - A new perspective in solar-terrestrial processes from Dynamics Explorer, Reviews of Geophysics, 26, 229–248, doi:10.1029/RG026i002p00229, 1988.

Chen, F. F.: Introduction to plasma physica and controlled fusion, Plenum Press, second edition edn., iSBN: 0-306-41332-9, 1984.

Cole, K. D.: Effects of crossed magnetic and /spatially dependent/ electric fields on charged particle motion, Planet. Space Sci., 24, 515–518, doi: 10.1016/0032-0633(76)90096-9, 1976.

Coleman, I. J.: A multi-spacecraft survey of magnetic field line draping in the dayside magnetosheath, Annales Geophysicae, 23, 885–900, 2005.

Cooling, B. M. A., Owen, C. J., and Schwartz, S. J.: Role of the magnetosheath flow in determining the motion of open flux tubes, J. Geophys. Res., 106, 18 763–18 776, doi:10.1029/2000JA000455, 2001.

Cravens, T. E.: Physics of Solar System Plasmas, Cambridge University Press, 2004.

Eklund, U., Lundin, R., and Sandahl, I.: Measurements of O+ in the high latitude magnetosheath, Physics and Chemistry of the Earth, 22, 639–644, doi:10.1016/S0079-1946(97)00189-4, 1997.

Escoubet, C. P., Schmidt, R., and Goldstein, M. L.: Cluster - Science and Mission Overview, Space Science Reviews, 79, 11–32, 1997.

Escoubet, C. P., Berchem, J., Bosqued, J. M., Trattner, K. J., Taylor, M. G. G. T., Pitout, F., Laakso, H., Masson, A., Dunlop, M., Dandouras, I., Reme, H., Fazakerley, A. N., and Daly, P.: Effect of a northward turning of the interplanetary magnetic field on cusp precipitation as observed by Cluster, Journal of Geophysical Research (Space Physics), 113, 7–+, doi:10.1029/2007JA012771, 2008.

Gosling, J. T., Thomsen, M. F., Bame, S. J., Onsager, T. G., and Russell, C. T.: The electron edge of the low latitude boundary layer during accelerated flow events, Geophysical Research Letters, 17, 1833–1836, 1990.

Gustafsson, G., André, M., Carozzi, T., Eriksson, A. I., Fälthammar, C.-G., Grard, R., Holmgren, G., Holtet, J. A., Ivchenko, N., Karlsson, T., Khotyaintsev, Y., Klimov, S., Laakso, H., Lindqvist, P.-A., Lybekk, B., Marklund, G., Mozer, F., Mursula, K., Pedersen, A., Popielawska, B., Savin, S., Stasiewicz, K., Tanskanen, P., Vaivads, A., and Wahlund, J.-E.: First results of electric field and density observations by Cluster EFW based on initial months of operation, Annales Geophysicae, 19, 1219–1240, 2001.

Hultqvist, B.: On the acceleration of positive ions by high-latitude, large-amplitude electric field fluctuations, J. Geophys. Res., 101, 27 111–27 122, doi:10.1029/96JA02435, 1996.

Ivchenko, N. and Marklund, G.: "Current singularities" observed on Astrid-2, Advances in Space Research, 30, 1779–1782, 2002.

Johnstone, A. D., Alsop, C., Burge, S., Carter, P. J., Coates, A. J., Coker, A. J., Fazakerley, A. N., Grande, M., Gowen, R. A., Gurgiolo, C., Hancock, B. K., Narheim, B., Preece, A., Sheather, P. H., Winningham, J. D., and Woodliffe, R. D.: Peace: a Plasma Electron and Current Experiment, Space Science Reviews, 79, 351–398, doi:10.1023/A:1004938001388, 1997.

Jovanović, D., Shukla, P. K., and Morfill, G.: Magnetic reconnection on the ion-skin-depth scale in the dusty magnetotail of a comet, Physics of Plasmas, 12, 042 904–+, doi:10.1063/1.1883184, 2005.

Khotyaintsev, Y. V., Vaivads, A., Retinò, A., André, M., Owen, C. J., and Nilsson, H.: Formation of Inner Structure of a Reconnection Separatrix Region, Physical Review Letters, 97, 205 003–+, doi:10.1103/PhysRevLett.97.205003, 2006.

Kivelson, M. G. and Russell, C. T.: Introduction to Space Physics, Cambridge University Press, 1995.

Lavraud, B., Thomsen, M. F., Taylor, M. G. G. T., Wang, Y. L., Phan, T. D., Schwartz, S. J., Elphic, R. C., Fazakerley, A., Rème, H., and Balogh, A.: Characteristics of the magnetosheath electron boundary layer under northward interplanetary magnetic field: Implications for high-latitude reconnection, Journal of Geophysical Research (Space Physics), 110, 6209–+, doi:10.1029/2004JA010808, 2005.

Li, L. and Zhang, J.: Observations of the Magnetic Reconnection Signature of an M2 Flare on 2000 March 23, ApJ, 703, 877–882, doi:10.1088/0004-637X/703/1/877, 2009.

Lin, J., Ko, Y.-K., Sui, L., Raymond, J. C., Stenborg, G. A., Jiang, Y., Zhao, S., and Mancuso, S.: Direct Observations of the Magnetic Reconnection Site of an Eruption on 2003 November 18, ApJ, 622, 1251–1264, doi:10.1086/428110, 2005.

Lindstedt, T., Khotyaintsev, Y. V., Vaivads, A., André, M., Fear, R. C., Lavraud, B., Haaland, S., and Owen, C. J.: Separatrix regions of magnetic reconnection at the magnetopause, Annales Geophysicae, 27, 4039–4056, 2009.

Lockwood, M., Cowley, S. W. H., and Onsager, T. G.: Ion acceleration at both the interior and exterior Alfvén waves associated with the magnetopause reconnection site: Signatures in cusp precipitation, J. Geophys. Res., 101, 21 501–21 514, doi:10.1029/96JA01948, 1996.

Luhmann, J. G., Walker, R. J., Russell, C. T., Crooker, N. U., Spreiter, J. R., and Stahara, S. S.: Patterns of potential magnetic field merging sites on the dayside magnetopause, Journal of Geophysical Research, 89, 1741–1744, doi:10.1029/0JGREA0000890000A3001741000001, 1984.

Lundin, R. and Hultqvist, B.: Ionospheric plasma escape by high-altitude electric fields - Magnetic moment 'pumping', J. Geophys. Res., 94, 6665–6680, doi:10.1029/JA094iA06p06665, 1989.

Moore, T. E., Lundin, R., Alcayde, D., André, M., Ganguli, S. B., Temerin, M., and Yau, A.: Chapter 2-Source Processes in the High-Latitude Ionosphere, Space Science Reviews, 88, 7–84, doi:10.1023/A:1005299616446, 1999.

Moore, T. E., Fok, M., and Chandler, M. O.: The dayside reconnection X line, Journal of Geophysical Research (Space Physics), 107, 1332–+, doi:10.1029/2002JA009381, 2002.

Mozer, F. S., Bale, S. D., and Phan, T. D.: Evidence of Diffusion Regions at a Subsolar Magnetopause Crossing, Physical Review Letters, 89, 015 002–+, doi:10.1103/PhysRevLett.89.015002, 2002.

Nakamura, M. and Scholer, M.: Structure of the magnetopause reconnection layer and of flux transfer events: Ion kinetic effects, J. Geophys. Res., 105, 23 179–23 192, doi:10.1029/2000JA900101, 2000.

Nilsson, H., Joko, S., Lundin, R., Rème, H., Sauvaud, J., Dandouras, I., Balogh, A., Carr, C., Kistler, L., Klecker, B., Carlson, C., Bavassano-Cattaneo, M., and Korth, A.: The structure of high altitude O+ energization and outflow: a case study, Annales Geophysicae, 22, 2497–2506, 2004.

Nilsson, H., Waara, M., Arvelius, S., Marghitu, O., Bouhram, M., Hobara, Y., Yamauchi, M., Lundin, R., Rème, H., Sauvaud, J., Dandouras, I., Balogh, A., Kistler, L. M., Klecker, B., Carlson, C. W., Bavassano-Cattaneo, M. B., and Korth, A.: Characteristics of high altitude oxygen ion energization and outflow as observed by Cluster: a statistical study, Annales Geophysicae, 24, 1099–1112, 2006.

Norqvist, P., André, M., and Tyrland, M.: A statistical study of ion energization mechanisms in the auroral region, J. Geophys. Res., 103, 23 459–23 474, doi:10.1029/98JA02076, 1998.

Owen, C. J., Fazakerley, A. N., Carter, P. J., Coates, A. J., Krauklis, I. C., Szita, S., Taylor, M. G. G. T., Travnicek, P., Watson, G., Wilson, R. J., Balogh, A., and Dunlop, M. W.: Cluster PEACE observations of electrons during magnetospheric flux transfer events, Annales Geophysicae, 19, 1509–1522, 2001.

Parker, E. N.: Sweet's Mechanism for Merging Magnetic Fields in Conducting Fluids, J. Geophys. Res., 62, 509–520, doi:10.1029/JZ062i004p00509, 1957.

Petschek, H. E.: Magnetic Field Annihilation, NASA Special Publication, 50, 425–+, 1964.

Phan, T., Dunlop, M., Paschmann, G., Klecker, B., Bosqued, J., Rème, H., Balogh, A., Twitty, C., Mozer, F., Carlson, C., Mouikis, C., and Kistler, L.: Cluster observations of continuous reconnection at the magnetopause under steady interplanetary magnetic field conditions, Annales Geophysicae, 22, 2355–2367, 2004.

Phan, T. D., Escoubet, C. P., Rezeau, L., Treumann, R. A., Vaivads, A., Paschmann, G., Fuselier, S. A., Attié, D., Rogers, B., and Sonnerup, B. U. Ö.: Magnetopause Processes, Space Science Reviews, 118, 367–424, doi:10.1007/s11214-005-3836-z, 2005.

Priest, E. and Forbes, T.: Magnetic Reconnection, Magnetic Reconnection, by Eric Priest and Terry Forbes, pp. 612. ISBN 0521481791. Cambridge, UK: Cambridge University Press, June 2000., 2000.

Pritchett, P. L.: Collisionless magnetic reconnection in an asymmetric current sheet, Journal of Geophysical Research (Space Physics), 113, 6210–+, doi:10.1029/2007JA012930, 2008.

Rastaetter, L. and Neukirch, T.: Magnetic reconnection in a magnetosphere-accretion-disk system. Axisymmetric stationary states and two-dimensional reconnection simulations., A&A, 323, 923–930, 1997.

Rème, H., Aoustin, C., Bosqued, J. M., Dandouras, I., Lavraud, B., Sauvaud, J. A., Barthe, A., Bouyssou, J., Camus, T., Coeur-Joly, O., Cros, A., Cuvilo, J., Ducay, F., Garbarowitz, Y., Medale, J. L., Penou, E., Perrier, H., Romefort, D., Rouzaud, J., Vallat, C., Alcaydé, D., Jacquey, C., Mazelle, C., D'Uston, C., Möbius, E., Kistler, L. M., Crocker, K., Granoff, M., Mouikis, C., Popecki, M., Vosbury, M., Klecker, B., Hovestadt, D., Kucharek, H., Kuenneth, E., Paschmann, G., Scholer, M., Sckopke, N., Seidenschwang, E., Carlson, C. W., Curtis, D. W., Ingraham, C., Lin, R. P., McFadden, J. P., Parks, G. K., Phan, T., Formisano, V., Amata, E., Bavassano-Cattaneo, M. B., Baldetti, P., Bruno, R., Chionchio, G., di Lellis, A., Marcucci, M. F., Pallocchia, G., Korth, A., Daly, P. W., Graeve, B., Rosenbauer, H., Vasyliunas, V., McCarthy, M., Wilber, M., Eliasson, L., Lundin, R., Olsen, S., Shelley, E. G., Fuselier, S., Ghielmetti, A. G., Lennartsson, W., Escoubet, C. P., Balsiger, H., Friedel, R., Cao, J.-B., Kovrazhkin, R. A., Papamastorakis, I., Pellat, R., Scudder, J., and Sonnerup, B.: First multispacecraft ion measurements in and near the Earth's magnetosphere with the identical Cluster ion spectrometry (CIS) experiment, Annales Geophysicae, 19, 1303–1354, 2001.

Retinò, A., Bavassano Cattaneo, M. B., Marcucci, M. F., Vaivads, A., André, M., Khotyaintsev, Y., Phan, T., Pallocchia, G., Rème, H., Möbius, E., Klecker, B., Carlson, C. W., McCarthy, M., Korth, A., Lundin, R., and Balogh, A.: Cluster multispacecraft observations at the high-latitude duskside magnetopause: implications for continuous and component magnetic reconnection, Annales Geophysicae, 23, 461–473, 2005.

Retinò, A., Vaivads, A., André, M., Sahraoui, F., Khotyaintsev, Y., Pickett, J. S., Bavassano Cattaneo, M. B., Marcucci, M. F., Morooka, M., Owen, C. J., Buchert, S. C., and Cornilleau-Wehrlin, N.: Structure of the separatrix region close to a magnetic reconnection X-line: Cluster observations, Geophysical Research Letters, 33, 6101–+, doi:10.1029/2005GL024650, 2006.

Russell, C. T.: The Polar Cusp, Advances in Space Research, 25, 1413–1424, doi:10.1016/S0273-1177(99)00653-5, 2000.

Russell, C. T. and Elphic, R. C.: Initial ISEE magnetometer results - Magnetopause observations, Space Science Reviews, 22, 681–715, 1978.

Sandholt, P. E., Denig, W. F., Farrugia, C. J., Lybekk, B., and Trondsen, E.: Auroral structure at the cusp equatorward boundary: Rela-

tionship with the electron edge of low-latitude boundary layer precipitation, Journal of Geophysical Research (Space Physics), 107, 1235–+, doi:10.1029/2001JA005081, 2002.

Seki, K., Elphic, R. C., Hirahara, M., Terasawa, T., and Mukai, T.: On Atmospheric Loss of Oxygen Ions from Earth Through Magnetospheric Processes, Science, 291, 1939–1941, doi:10.1126/science.1058913, 2001.

Semenov, V. S., Kubyshkin, I. V., Lebedeva, V. V., Rijnbeek, R. P., Heyn, M. F., Biernat, H. K., and Farrugia, C. J.: A comparison and review of steady-state and time-varying reconnection, Planet. Space Sci., 40, 63–87, doi:10.1016/0032-0633(92)90150-M, 1992.

Semenov, V. S., Penz, T., Ivanova, V. V., Sergeev, V. A., Biernat, H. K., Nakamura, R., Heyn, M. F., Kubyshkin, I. V., and Ivanov, I. B.: Reconstruction of the reconnection rate from Cluster measurements: First results, Journal of Geophysical Research (Space Physics), 110, 11 217–+, doi:10.1029/2005JA011181, 2005.

Shay, M. A., Drake, J. F., Rogers, B. N., and Denton, R. E.: Alfvénic collisionless magnetic reconnection and the Hall term, J. Geophys. Res., 106, 3759–3772, doi:10.1029/1999JA001007, 2001.

Smith, C. W., L'Heureux, J., Ness, N. F., Acuña, M. H., Burlaga, L. F., and Scheifele, J.: The ACE Magnetic Fields Experiment, Space Science Reviews, 86, 613–632, doi:10.1023/A:1005092216668, 1998.

Sonnerup, B. U. O., Paschmann, G., Papamastorakis, I., Sckopke, N., Haerendel, G., Bame, S. J., Asbridge, J. R., Gosling, J. T., and Russell, C. T.: Evidence for magnetic field reconnection at the earth's magnetopause, Journal of Geophysical Research, 86, 10 049–10 067, 1981.

Southwood, D. J., Farrugia, C. J., and Saunders, M. A.: What are flux transfer events?, Planet. Space Sci., 36, 503–508, doi:10.1016/0032-0633(88)90109-2, 1988.

Stasiewicz, K., Holmgren, G., and Zanetti, L.: Density depletions and current singularities observed by Freja, J. Geophys. Res., 103, 4251–4260, doi:10.1029/97JA02007, 1998.

Stasiewicz, K., Lundin, R., and Marklund, G.: Stochastic Ion Heating by Orbit Chaotization on Electrostatic Waves and Nonlinear Structures, Physica Scripta Volume T, 84, 60–63, doi:10.1238/Physica.Topical.084a00060, 2000.

Sweet, P. A.: The Neutral Point Theory of Solar Flares, in: Electromagnetic Phenomena in Cosmical Physics, edited by B. Lehnert, vol. 6 of *IAU Symposium*, pp. 123–+, 1958.

Topliss, S., Johnstone, A., Coates, A., Peterson, W. K., Kletzing, C. A., and Russell, C. T.: Charge neutrality and ion conic distributions at the equatorward electron edge of the midaltitude cusp, J. Geophys. Res., 106, 21 095–21 108, doi:10.1029/2000JA003032, 2001.

Trattner, K. J., Fuselier, S. A., and Petrinec, S. M.: Location of the reconnection line for northward interplanetary magnetic field, Journal of Geophysical Research (Space Physics), 109, 3219–+, doi: 10.1029/2003JA009975, 2004.

Trattner, K. J., Fuselier, S. A., Petrinec, S. M., Yeoman, T. K., Mouikis, C., Kucharek, H., and Reme, H.: Reconnection sites of spatial cusp structures, Journal of Geophysical Research (Space Physics), 110, 4207–+, doi:10.1029/2004JA010722, 2005.

Trattner, K. J., Mulcock, J. S., Petrinec, S. M., and Fuselier, S. A.: Probing the boundary between antiparallel and component reconnection during southward interplanetary magnetic field conditions, Journal of Geophysical Research (Space Physics), 112, 8210–+, doi:10.1029/2007JA012270, 2007.

Tsyganenko, N. A.: Modeling the Earth's magnetospheric magnetic field confined within a realistic magnetopause, J. Geophys. Res., 100, 5599–5612, doi:10.1029/94JA03193, 1995.

Vaivads, A., Khotyaintsev, Y., André, M., Retinò, A., Buchert, S. C., Rogers, B. N., Décréau, P., Paschmann, G., and Phan, T.: Structure of the Magnetic Reconnection Diffusion Region from Four-Spacecraft Observations, Phys. Rev. Lett., 93, 105 001–+, doi: 10.1103/PhysRevLett.93.105001, 2004.

Waara, M.: submitted, 2009.

Walker, R., Terasawa, T., Christon, S. P., Angelopoulos, V., Hoshino, M., Lennartsson, W., Maezawa, K., Sibeck, D. G., Treumann, R. A., Williams, D. J., and Zelenyi, L.: Chapter 6-Source and Loss Processes in the Magnetotail, Space Science Reviews, 88, 285–353, doi:10.1023/A:1005207918263, 1999.

Winglee, R. M., Chua, D., Brittnacher, M., Parks, G. K., and Lu, G.: Global impact of ionospheric outflows on the dynamics of the magnetosphere and cross-polar cap potential, Journal of Geophysical Research (Space Physics), 107, 1237–+, doi:10.1029/2001JA000214, 2002.

Wygant, J. R., Cattell, C. A., Lysak, R., Song, Y., Dombeck, J., McFadden, J., Mozer, F. S., Carlson, C. W., Parks, G., Lucek, E. A., Balogh, A., Andre, M., Reme, H., Hesse, M., and Mouikis, C.: Cluster observations of an intense normal component of the electric field at a thin reconnecting current sheet in the tail and its role in the shock-like acceleration of the ion

fluid into the separatrix region, Journal of Geophysical Research (Space Physics), 110, 9206–+, doi:10.1029/2004JA010708, 2005.

Yamada, M., Ji, H., Hsu, S., Carter, T., Kulsrud, R., Bretz, N., Jobes, F., Ono, Y., and Perkins, F.: Study of driven magnetic reconnection in a laboratory plasma, Physics of Plasmas, 4, 1936–1944, doi:10.1063/1.872336, 1997.

Paper 1

T. Lindstedt, Yu. V. Khotyaintsev, A. Vaivads, M. André, R. C. Fear, B. Lavraud, S. Haaland and C. J. Owen

Separatrix regions of magnetic reconnection at the magnetopause

Ann. Geophys., 27, 4039–4056, 2009

Ann. Geophys., 27, 4039–4056, 2009
www.ann-geophys.net/27/4039/2009/

Annales Geophysicae

Separatrix regions of magnetic reconnection at the magnetopause

T. Lindstedt[1,2], Yu. V. Khotyaintsev[1], A. Vaivads[1], M. André[1], R. C. Fear[3], B. Lavraud[4], S. Haaland[5,6], and C. J. Owen[7]

[1]Swedish Institute of Space Physics, P.O. Box 537, 751 21 Uppsala, Sweden
[2]Department of Physics and Astronomy, Space and Plasma Physics, P.O. Box 515, 751 20 Uppsala, Sweden
[3]Department of Physics and Astronomy, University of Leicester, Leicester LE1 7RH, UK
[4]Centre d'Etude Spatiale des Rayonnements, CNRS, Toulouse, France
[5]Department of Physics and Technology, University of Bergen, Bergen, Norway
[6]Max-Planck-Institut für Extraterrestrische Physik, Garching, Germany
[7]Mullard Space Science Laboratory, University College London, Dorking, UK

Received: 3 November 2008 – Revised: 7 October 2009 – Accepted: 7 October 2009 – Published: 26 October 2009

Abstract. Using data from the four Cluster spacecraft we study the separatrix regions of magnetic reconnection sites at the dayside magnetopause under conditions when reconnection is occurring in the magnetopause current layer which separates magnetosheath plasma from the hot magnetospheric plasma sheet. We define the separatrix region as the region between the separatrix – the first field line opened by reconnection – and the reconnection jet (outflow region). We analyze eight separatrix region crossings on the magnetospheric side of the magnetopause and present detailed data for two of the events. We show that characteristic widths of the separatrix regions are of the order of ten ion inertial lengths at the magnetopause. Narrow separatrix regions with widths comparable to a few ion inertial lengths are rare. We show that inside the separatrix region there is a density cavity which sometimes has complex internal structure with multiple density dips. Strong electric fields exist inside the separatrix regions and the electric potential drop across the regions can be up to several kV. On the magnetosheath side of the region there is a density gradient with strong field aligned currents. The observed strong electric fields and currents inside the separatrix region can be important for a local energization of ions and electrons, particularly of ionospheric origin, as well as for magnetosphere-ionosphere coupling.

Keywords. Magnetospheric physics (Magnetopause, cusp, and boundary layers) – Space plasma physics (Discontinuities; Magnetic reconnection)

Correspondence to: T. Lindstedt
(toli@irfu.se)

1 Introduction

Magnetic reconnection is an important process that occurs in different plasma environments: in the Earth's magnetosphere, at the Sun, in astrophysical plasmas as well as in laboratory plasmas (Biskamp, 2000). At the Earth's magnetopause, magnetic reconnection is the dominant process responsible for the entry of solar wind plasma into the magnetosphere, as well as for the transfer of energy across the magnetopause.

Reconnection geometry can be divided into two main regions: these are the inflow region where plasma is on a large scale drifting towards the current sheet, and the outflow region where accelerated plasma jets away from the X-line. The regions between outflow and inflow regions can have complicated structures that depends on the properties of the reconnecting plasmas. These regions can be described in different ways. In the MHD description of steady reconnection of two similar plasmas, outflow and inflow regions are separated by a pair of slow shocks originating in the diffusion region (Petschek, 1964). In the case of asymmetric reconnection, as at the magnetopause, the MHD description predicts an Alfvén wave (rotational discontinuity) on the magnetosheath side and a slow expansion fan on the magnetospheric side (Levy et al., 1964). Depending on the asymmetry the structure of discontinuities can be different (Lin and Lee, 1994). The simplified MHD description of discontinuities has been successful in explaining low altitude observations of ion and electron signatures (Lockwood et al., 1996). More complicated MHD discontinuities develop when plasmas are different on either side of the current sheet and/or the reconnection is time varying (Semenov et al., 1992; Biernat et al., 1998).

Published by Copernicus Publications on behalf of the European Geosciences Union.

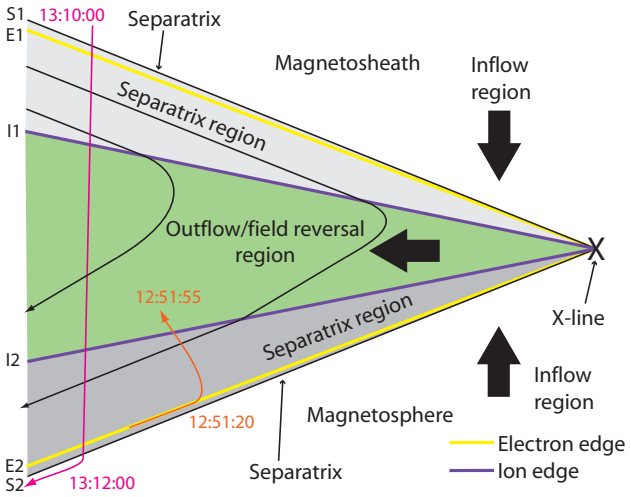

Fig. 1. Simplified sketch of a reconnection layer formed by an X-line at the magnetopause. The separatrices are the magnetic field lines connected to the reconnection X-line. Just inside the separatrix are the electron edges in yellow. The purple lines illustrate the ion edges that are closer together than the electron edges due to the time-of-flight effect. Between the separatrices and ion edges are the separatrix regions in grey. Between the ion edges is the outflow region. Spacecraft orbits for the two events that are discussed in detail are shown by orange (12:51 UT) and pink (13:11 UT) lines. This figure is similar to Fig. 5 in Gosling et al. (1990).

Detailed experimental studies reveal that it is usually difficult to identify fluid boundaries in the data, such as slow shocks. Instead, it is useful to introduce the separatrix region (see Fig. 1). The separatrix region is between the separatrix, the first field line opened by reconnection, and the reconnection jet (outflow/field reversal region, Fig. 1). To identify the separatrix region kinetic particle signatures are important (Gosling et al., 1990; Vaivads et al., 2006; Khotyaintsev et al., 2006). The separatrix regions are at one side bounded by the separatrices – the magnetic field lines connected to the reconnection X-line. The separatrices are located very close to the electron edges as electrons propagate relatively fast along the magnetic field. The magnetospheric electron edge (E2) is where (going from the magnetosphere to the magnetosheath) the first electrons originating in the magnetosheath are observed. Similarly, the magnetosheath electron edge (E1) is located where (going from the magnetosheath to the magnetosphere) the first magnetospheric electrons are observed. The separatrix regions contain a mixture of magnetospheric and magnetosheath electrons but not of ions. The ion edges are defined in a similar way (see also Gosling et al., 1990). In some studies a difference is made between the ion edge and the fluid boundary of the reconnection jet (Bogdanova et al., 2006). In particular, this is possible to do at lower altitudes. However, similar to Gosling et al. (1990), we do not make such a distinction because at the magnetopause it can be difficult to separate these boundaries. Thus, at the magnetospheric side the ion edge approximately coincides with the boundary of the reconnection jet (outflow/field reversal region in Fig. 1). Most of the magnetic field rotation from the magnetosheath to magnetospheric orientation happens inside the outflow/field reversal region bounded by the ion edges.

The separatrix region on the magnetospheric side of dayside magnetopause has been extensively studied at low altitudes (Lockwood et al., 1994, 1996; Sandholt et al., 1998, 2002) and mid (5–7 R_E) altitudes (Topliss et al., 2001; Bogdanova et al., 2004, 2006), as well as close to the magnetopause (Gosling et al., 1990; Khotyaintsev et al., 2006; Retinò et al., 2006). In some studies the separatrix region is referred to as the electron edge of the low latitude boundary layer (e.g. Bogdanova et al., 2006). On the basis of 8 events Bogdanova et al. (2004) discuss plasma and wave signatures characteristic for the separatrix regions (ULF waves, electron beams and outflow of ionospheric ions). Topliss et al. (2001) and Bogdanova et al. (2006) presented large statistical studies of this region. They found that the region can be up to 2° ILAT thick. The median thickness was estimated to ∼0.2° ILAT corresponding to roughly about 600 km at the magnetopause.

Separatrix regions are important for the coupling between the Earth's magnetosphere and the ionosphere, as they connect X-lines at the magnetopause to the ionosphere. It has been shown that separatrix regions can extend far from the X-line and still keep their narrow (ion inertial length scale) width as well as strong currents and electric fields (Khotyaintsev et al., 2006). Possible manifestations of the separatrix regions are strong auroras at the plasma sheet boundary layer (PSBL) for reconnection in the magnetotail and poleward moving auroral forms, PMAFs, (Sandholt et al., 1998, 2002) for reconnection at the dayside magnetopause.

Earlier studies of separatrix regions have led to a significant improvement in understanding of the basic structure of these regions. It has been shown that ions are not "frozen-in", $\boldsymbol{E}+\boldsymbol{v}_i\times\boldsymbol{B}\neq 0$, in the separatrix region (Khotyaintsev et al., 2006). The deviation from the "frozen-in" condition occurs on scales comparable to or smaller than the ion inertial length, $\lambda_i = c/\omega_{pi}$, and is mainly provided by the Hall term and electron pressure effects in the generalized Ohm's law (André et al., 2004; Vaivads et al., 2004b; Khotyaintsev et al., 2006). The separatrix regions are regions of strong electric fields, currents and wave activity. As in the case of the slow shock, plasma heating and energization takes place in the separatrix region (Wygant et al., 2005; Vaivads et al., 2006; Topliss et al., 2001; Bogdanova et al., 2004).

One characteristic feature of separatrix regions is the existence of a density cavity inside the region (Mozer et al., 2002; André et al., 2004; Wygant et al., 2005; Cattell et al., 2005; Retinò et al., 2006; Khotyaintsev et al., 2006). Numerical simulations also predict a density cavity as well as

strong currents and electric fields within the separatrix region (Shay et al., 2001; Pritchett and Coroniti, 2004). Several mechanisms have been suggested to explain the formation of the cavity: electron density decrease close to a separatrix can be caused by escape of energetic (hot) magnetospheric electrons to the magnetosheath along a newly opened field line (Khotyaintsev et al., 2006) and/or due to parallel electric fields at the separatrix (Cattell et al., 2005). At the same time, the decrease of ion density within the cavity can be due to the acceleration of ions by the strong electric fields in the normal direction as ions move from the magnetosphere into the outflow region (Shay et al., 2001; Khotyaintsev et al., 2006).

Systematic statistical studies addressing the internal structure and the electric and magnetic fields of the separatrix regions have so far been lacking. Here we present a study of multiple encounters of separatrix regions by the Cluster spacecraft during ongoing reconnection at the magnetopause. We investigate if the features of the separatrix region identified in single event studies (the density cavity, strong current and potential jump) are typical for most of the separatrix region crossings.

2 Data set

We analyze data from the four Cluster spacecraft during the time interval 12:30–14:30 UT on 4 January 2004. The spacecraft position is shown in Fig. 2 together with geomagnetic field lines obtained from the Tsyganenko T96 model (Tsyganenko, 1995). Cluster is located on the dusk side in the Northern Hemisphere sunward of the cusp. The separations between the spacecraft are small, about 300 km.

During the time interval we have studied, Cluster is in burst mode with high sampling rates on all instruments. We use data from all spacecraft. The electric field is obtained from the EFW instrument (Gustafsson et al., 2001). EFW measures two components of the electric field in the spacecraft spin plane low-pass filtered at 180 Hz and sampled at 450 Hz. We use plasma density derived from the spacecraft potential, available at a resolution of 5 Hz, using an empirical conversion law (Escoubet et al., 1997; Pedersen et al., 2008) and calibrated using electron density measured by PEACE. Thus we can obtain plasma density estimates at a higher temporal resolution than from particle instruments where the data must be integrated over the spin period of 4 s to obtain plasma density. The magnetic field data is from the fluxgate magnetometer (FGM) (Balogh et al., 2001). FGM has a sampling frequency of 67 Hz. The electron data is from the plasma electron and current experiment (PEACE) (Johnstone et al., 1997; Owen et al., 2001) on spacecraft C2. We have used the 3DXP product from the high energy electron analyzer (HEEA), which covers the energy range from 30 eV to 26 keV. The ion data is from the hot ion analyser part of the Cluster ion spectrometry experiment (CIS-HIA) (Rème et al., 2001) on C1, which measures the ion fluxes in the energy range from 5 to 32 000 eV/e. From the CIS-HIA instrument we also use the spin averaged ion velocity moment.

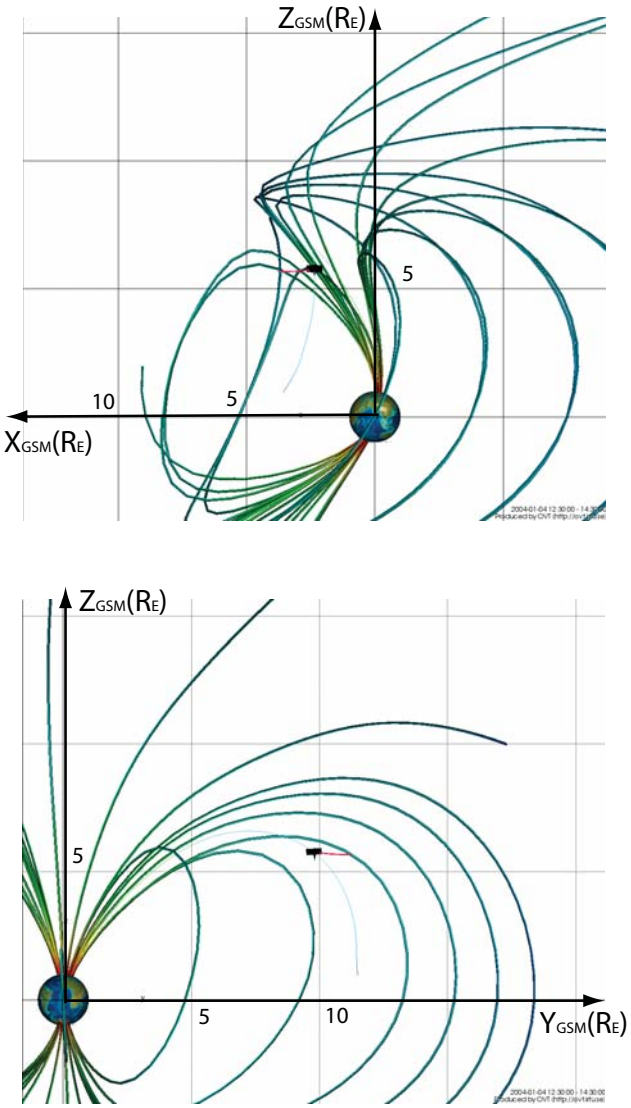

Fig. 2. Cluster orbit on 4 January 2004, 12:30–14:30 UT. During this time interval Cluster moved from [2.3 9.8 5.7] R_E (GSM) to [3.7 11.2 5.7] R_E (GSM). The maximum separation between the spacecraft is ∼300 km. The plot was created using OVT (http://ovt.irfu.se).

An overview of ACE (Smith et al., 1998; McComas et al., 1998) and Cluster data during the interval 12:30–14:30 UT on 4 January 2004 is presented in Fig. 3. The interplanetary magnetic field (IMF) z-component, measured by the MAG instrument on the ACE spacecraft, is shown in Fig. 3a together with the IMF clock angle $\theta = \arctan(B_y/B_z)$. This means that 0° and 360° correspond to positive B_z, 90° to positive B_y, 180° to negative B_z and 270° to negative B_y. The IMF is predominantly southward, with B_z (GSM) varying

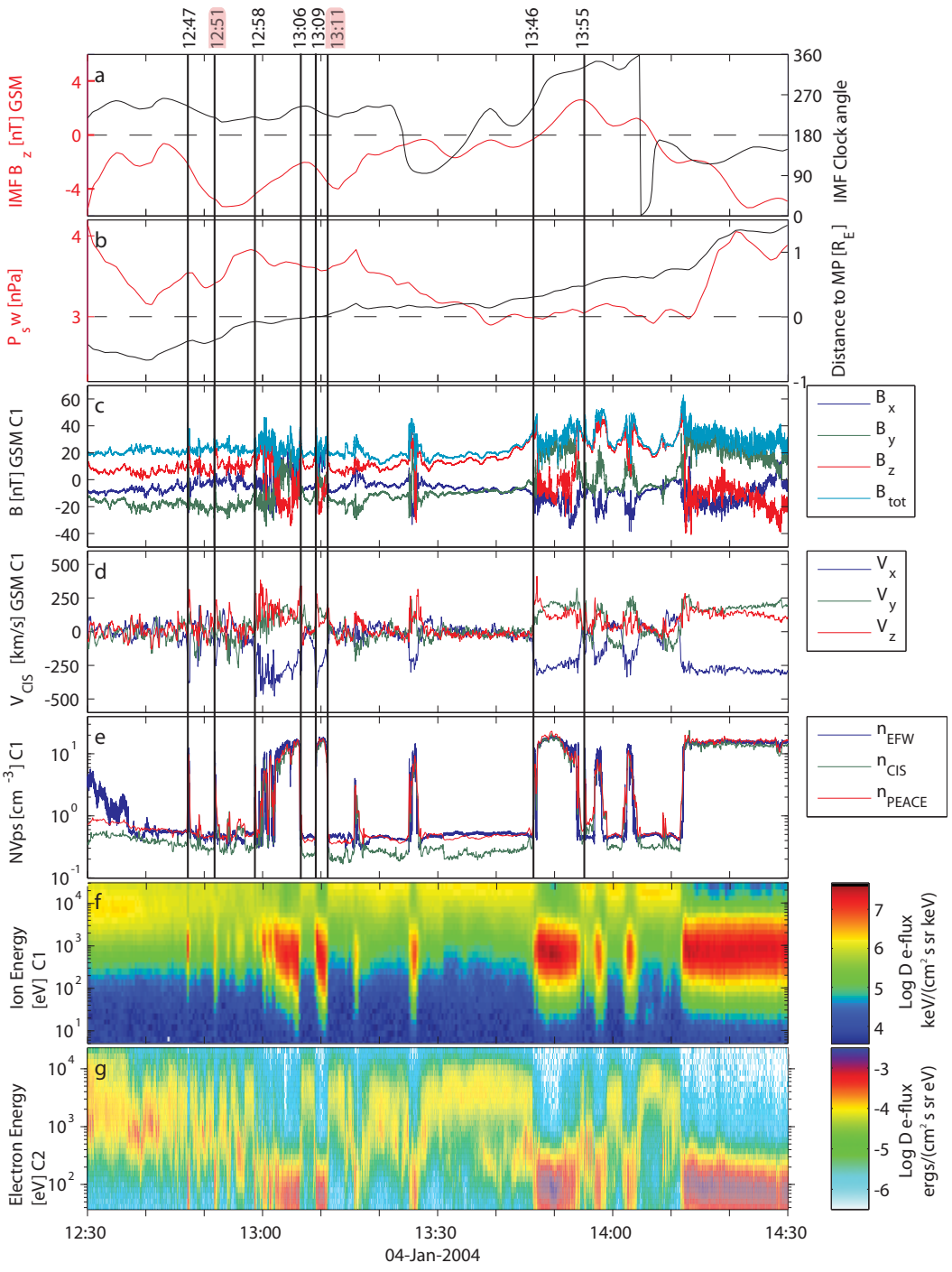

Fig. 3. Overview of the Cluster magnetopause crossing on 4 January 2004, 12:30–14:30 UT from SC1. Panel **(a)** shows the interplanetary magnetic field (IMF) B_z and the clock angle observed by the ACE spacecraft. Panel **(b)** shows the solar wind pressure and the estimated distance to the magnetopause. Panels (c–g) contain data from Cluster. Panel **(c)** shows the GSM components and magnitude of the magnetic field. Panel **(d)** shows the ion velocity in GSM coordinates. Panel **(e)** shows three different plasma density estimates based on the spacecraft potential, electron instrument PEACE and ion instrument CIS data. Panel **(f)** shows the ion differential energy flux spectrogram. Panel **(g)** shows the electron differential energy flux spectrogram. The vertical lines mark sub-intervals which are analyzed in detail and summarized in Table 1. Details for the sub-intervals marked in pink are shown in Figs. 8 and 9.

between −8 nT and 4 nT. In Fig. 3b we show the solar wind dynamic pressure together with the distance between the Cluster location and the model magnetopause calculated using the Shue model (Shue et al., 1997). The negative distance corresponds to locations inside the magnetosphere, as it is at the beginning of the interval, and the positive distance corresponds to the location inside the magnetosheath. ACE is located at the Lagrangian point L1 between the Sun and Earth. The time delay of the solar wind data is estimated with the method described by Weimer et al. (2003) with modifications by Haaland et al. (2006).

Figure 3c–g shows Cluster data during the same interval 12:30–14:30 UT. In the first half of the interval, between 12:30 and 13:45 UT, Cluster is located primarily inside the magnetosphere, and after a number of magnetopause crossings (change of sign of B_y and B_z between 12:45 and 14:15 UT, Fig. 3c) exits to the magnetosheath at 14:12 UT. At the magnetospheric side the magnetic field is directed primarily along the $+B_z$ and $-B_y$ GSM. The magnetospheric plasma is stagnant (flow velocity is close to zero) and has a relatively low density $\sim$0.5 cm^{-3} (Fig. 3d). The ion spectrogram at spin resolution in Fig. 3f show omni-directional ion energy fluxes. Magnetospheric ions (Fig. 3f) and electrons (Fig. 3g) are hot, their temperatures are a few keV and $\sim$10 keV respectively. In the magnetosheath the conditions are very different. The magnetic field is directed primarily along the $-B_z$ and $+B_y$ GSM. The plasma is relatively dense, $\sim$14 cm^{-3}, and flowing around the magnetopause (negative V_x, and positive V_y and V_z in Fig. 3d) at $\sim$350 km/s. The temperature of ions is $\sim$400 eV and electrons $\sim$100 eV.

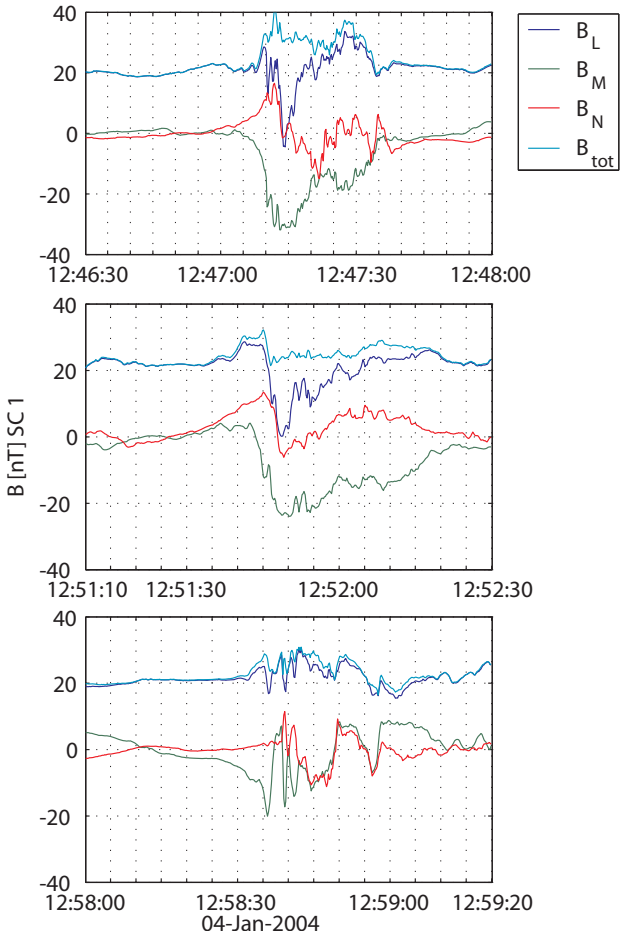

Fig. 4. The magnetic field in local *LMN*-coordinates from Cluster 1 for the events 12:47, 12:51 and 12:58, where B_L is dark blue, B_M is green, B_N is red and B_{TOT} is light blue. The N-direction here is the normal to the magnetopause for the entry into the magnetosheath at 14:10. This is direction is very similar to the local timing on the parallel current sheet used in the analysis. The L-direction is the local magnetospheric direction.

3 Reconnection evidence

In this section, we discuss large scale evidence of ongoing reconnection during the selected time interval when Cluster is located close to the magnetopause. Then we illustrate the motion of the flux tubes assuming reconnection is occurring. The kinetic evidence of reconnection based on the electron distribution properties is discussed in the next section where two crossings of separatrix region are presented in detail.

Earlier studies show that reconnection at the magnetopause can be associated with flux transfer events (FTEs), bulges due to varying magnetic reconnection rate propagating along the magnetopause (Russell and Elphic, 1978; Scholer, 1995; Khotyaintsev et al., 2004). The multiple crossings of the magnetopause we observe can also be caused by FTEs. Comparing magnetopause crossings with solar wind pressure variations in Fig. 3b we find no clear correlation and thus rule out solar wind pressure variations as a cause of most magnetopause crossings. During the first part of the interval Cluster is primarily located inside the magnetosphere, the FTEs can be identified in Fig. 3 as encounters of magnetosheath-like plasma on the magnetospheric field lines, e.g. at 12:47, 12:51, 12:58 UT. At these times the magnetic field increases in magnitude, however does not change to the magnetosheath direction. The ion velocity is sometimes as high as $\sim$500 km/s and the plasma density increases almost to the magnetosheath level. The plasma is a mixture of magnetospheric and magnetosheath populations. The magnetic field in local *LMN*-coordinates from Cluster 1 for the events 12:47, 12:51 and 12:58 are shown in Fig. 4. The normal component of the magnetic field B_N (red, normal direction is determined by inter-spacecraft timing on the full magnetopause crossing at 14:10) shows a bipolar signature characteristic for FTEs (Russell and Elphic, 1978; Owen et al., 2008). B_N changes from positive to negative, which is consistent with northward and tailward propagation of FTEs. The event at 12:51 UT shows a typical bipolar signature of

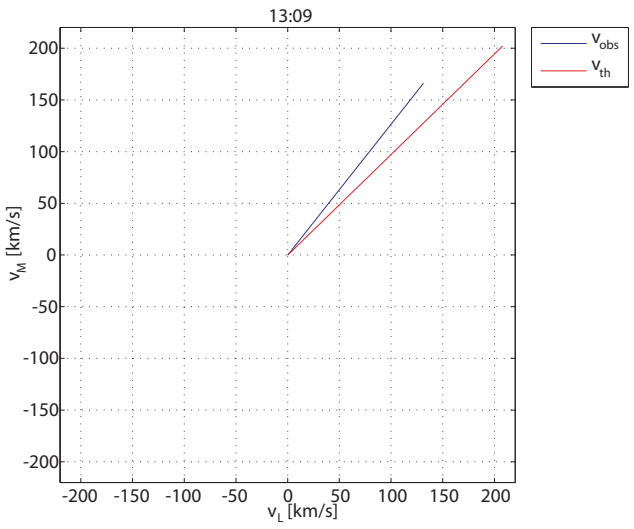

Fig. 5. Results of the Walén test for the event at 13:09 UT. The outflow region is observed for more than 10 s and the result indicate that reconnection is ongoing sunward of the spacecraft. The blue line corresponds to the observed velocity and the red line to the calculated velocity.

an FTE traveling tailward, and the event at 12:47 UT is very similar. The event at 12:58 UT has a more complicated structure of the normal magnetic field component; this structure, however, is likely to be produced by the same process as the FTE and can be interpreted as overlaid bipolar signatures.

To test for the presence of reconnection locally we have also carried out the Walén test (Sonnerup et al., 1981) for the events where there is data from both the outflow region and the magnetosheath, i.e. when the spacecraft cross the magnetopause. Figure 5 shows the Walén test for the magnetopause crossing at 13:09 UT. Figure 5 shows a comparison of the measured and estimated change of the velocity v_L and v_M components. The ratio between the absolute values of the predicted and the observed magnitudes of the velocity vectors is 0.73 and the angle between the vectors is 7°. The event at 13:09 UT shows a good agreement between the observed and predicted ion velocities and we conclude that within the magnetopause there is likely a rotational discontinuity with the reconnection X-line located sunward of the spacecraft. For the events 13:06 and 13:11 UT the crossings of the outflow region are very fast and ion moments are measured only in at most 1–2 points inside the outflow region. However, these few points cannot be fully trusted because the ion moments are computed from the data collected during one spin (∼4 s), and both the magnetic field and plasma density are highly variable at such time scales. Thus, we do not expect a good Walén test for these events. In summary, a reliable Walén test was only possible to perform on one crossing and this test suggest that the spacecraft are passing reconnecting flux tubes that has been reconnecting sunward from the spacecraft in all of the three analyzed crossings.

Both the polarity of the observed FTEs and the Walén test indicate that the reconnection site is located sunward from the spacecraft and this location is further supported by the Cooling model (Cooling et al., 2001). The Cooling model predicts the motion of reconnected flux tubes by calculating their velocity. This is the velocity of the de Hoffman-Teller frame calculated from the magnetosheath velocity, magnetic field and density. The magnetosheath magnetic field is from a model by Kobel and Fluckiger (1994) where characteristic solar wind magnetic field values for the time interval 12:50–13:10 UT is used. The geomagnetic field used by Cooling et al. (2001) to estimate the magnetopause current is very simple and the location of the anti-parallel X-line is approximate. We have made one run of the Cooling model for characteristic solar wind conditions during the interval (southward-duskward pointing IMF). In Fig. 6 we show the predictions of flux tube motion for the location of the reconnection X-line at the subsolar point (in Fig. 6a) and where the reconnecting fields are antiparallel (in Fig. 6b). In the first case, where we assume that the reconnection occurs near the subsolar point, see Fig. 6a, the flux tubes connected to the Northern Hemisphere move poleward and duskward (red paths) and pass the location of the spacecraft. In the second case, see Fig. 6b, we assume that reconnection sites are in the pre-noon sector of the Northern Hemisphere and post-noon sector of the Southern Hemisphere, as expected from anti-parallel reconnection (Crooker, 1979), and the model predicts that we should not expect reconnected flux tubes to pass the location of the spacecraft. Thus, we conclude that for characteristic IMF conditions during the interval the reconnection X-line is most probably located close to the subsolar point.

The FTE signatures and the Walén test show the presence of ongoing reconnection with an X-line located southward of the spacecraft during the major part of the studied interval with southward IMF. The Cooling model results indicate that for these IMF conditions the reconnection X-line is located near the sub-solar region. Note that there is additional evidence for Cluster crossing reconnected flux tubes related to the properties of the separatrix regions themselves and that is discussed in the next section, e.g. the mixture of magnetosheath and magnetospheric electrons.

4 Observations of separatrix regions

We have made a detailed analysis of the separatrix region on the magnetospheric side of the magnetopause reconnection layer (see Fig. 1). Eight crossings or partial entries into the magnetopause reconnection layer were selected and are marked by vertical lines in Fig. 3. The crossings were selected such that all four spacecraft observe similar signatures in magnetic field and density, thus making it possible to perform multi-spacecraft timing analysis (Schwartz, 2000). The events at 12:47, 12:51, 12:58, 13:46 and 13:55 UT are partial

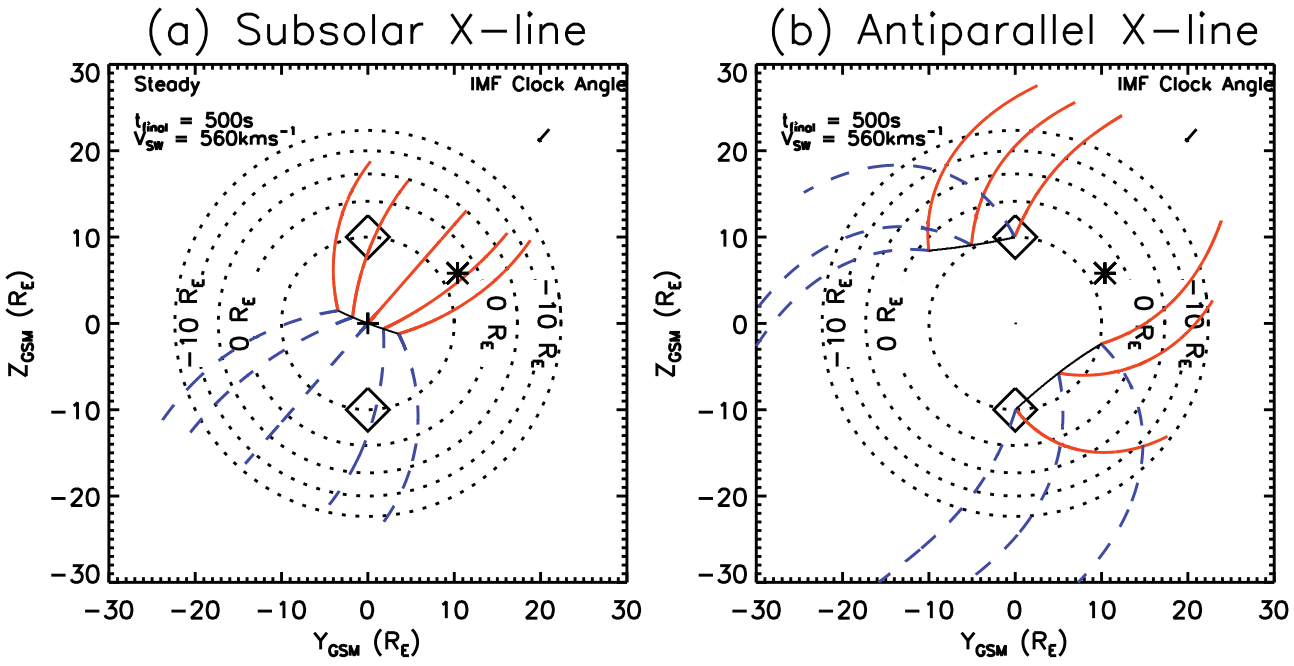

Fig. 6. Motion of the opened field lines predicted by the Cooling model. Field lines connected to the Northern Hemisphere are shown in red and field lines connected to the Southern Hemisphere are shown in blue. In **(a)** reconnection is initiated near the subsolar point. In **(b)** reconnection is initiated in region of highest shear in the Northern and Southern Hemisphere. The position of Cluster is shown with an asterisk. The diamond show the location of the cusp. The dotted lines are contours in X_{GSM}.

entries into regions with magnetosheath-like plasma located on magnetospheric field lines; the dominant magnetic field component B_z does not change sign throughout the crossing and thus the magnetic field preserves its magnetospheric orientation. The first event, at 12:47 UT, was analyzed in detail by Khotyaintsev et al. (2006). Note that some of these events may look like full crossings of the magnetopause reconnection layer in the overview plot (Fig. 3), e.g. 13:46 UT, but this is due to a short time delay between a partial and a full crossing. In the other events, at 13:06, 13:09 and 13:11 UT in Fig. 1, the spacecraft fully cross the main magnetopause current layer (identified by the change of B_z sign). We find similar characteristics for the eight events we have studied and present detailed data for the two sub-intervals (at 12:51 and 13:11 UT) marked with pink on top of Fig. 3. These two cases represent the two different situations: a partial (12:51 UT) and a full (13:11 UT) crossing of the magnetopause reconnection layer.

4.1 Full crossing of the magnetopause reconnection layer, 13:11 UT

The observations are presented in the local *LMN*-coordinate system of the magnetopause obtained from minimum variance analysis (MVA). The *N* direction given by MVA is consistent with normal direction obtained from timing analysis of the magnetopause crossing (both density and magnetic field). Observations of the magnetopause crossing at 13:11 UT are shown in Fig. 7. The panels from top to bottom show: plasma density from EFW spacecraft potential (Fig. 7a), *LMN*-components of the magnetic field from FGM (Fig. 7b), *N* (Fig. 7c) and *L* (Fig. 7d) components of plasma flow velocity, full (green) and perpendicular (red) from CIS-HIA and $\boldsymbol{E} \times \boldsymbol{B}$ from EFW, antiparallel (Fig. 7e) and parallel (Fig. 7f) to *B* electron fluxes from the PEACE 3DXP product (HEEA sensor) which has been rebinned using the actual magnetic field measured by the FGM.

Cluster is located in the magnetosheath (high density side) in the beginning of the interval and plasma flow is nearly parallel to *B*. Then plasma convection in the *N* direction increases (magnetopause moves outward) and Cluster crosses the main magnetopause current layer between 13:10:58 and 13:11:06 UT where B_L changes sign. On scales larger than ion inertial length $v_{\mathrm{EFW}} \sim v_{\mathrm{CIS}\perp}$ and this velocity reflects the overall motion of the magnetopause (marked by the green bar in Fig. 7) in the normal direction. Inside this current layer there is also an accelerated plasma flow in the *L* direction and we can identify the outflow/field reversal region (green bar marked OR in Fig. 7) bounded by the ion edges (purple bars). The ion edge on the magnetospheric side is identified at the main density gradient, that is the edge of the bulk flow of the reconnection jet. On the magnetosheath side the ion edge is located outside the field reversal region

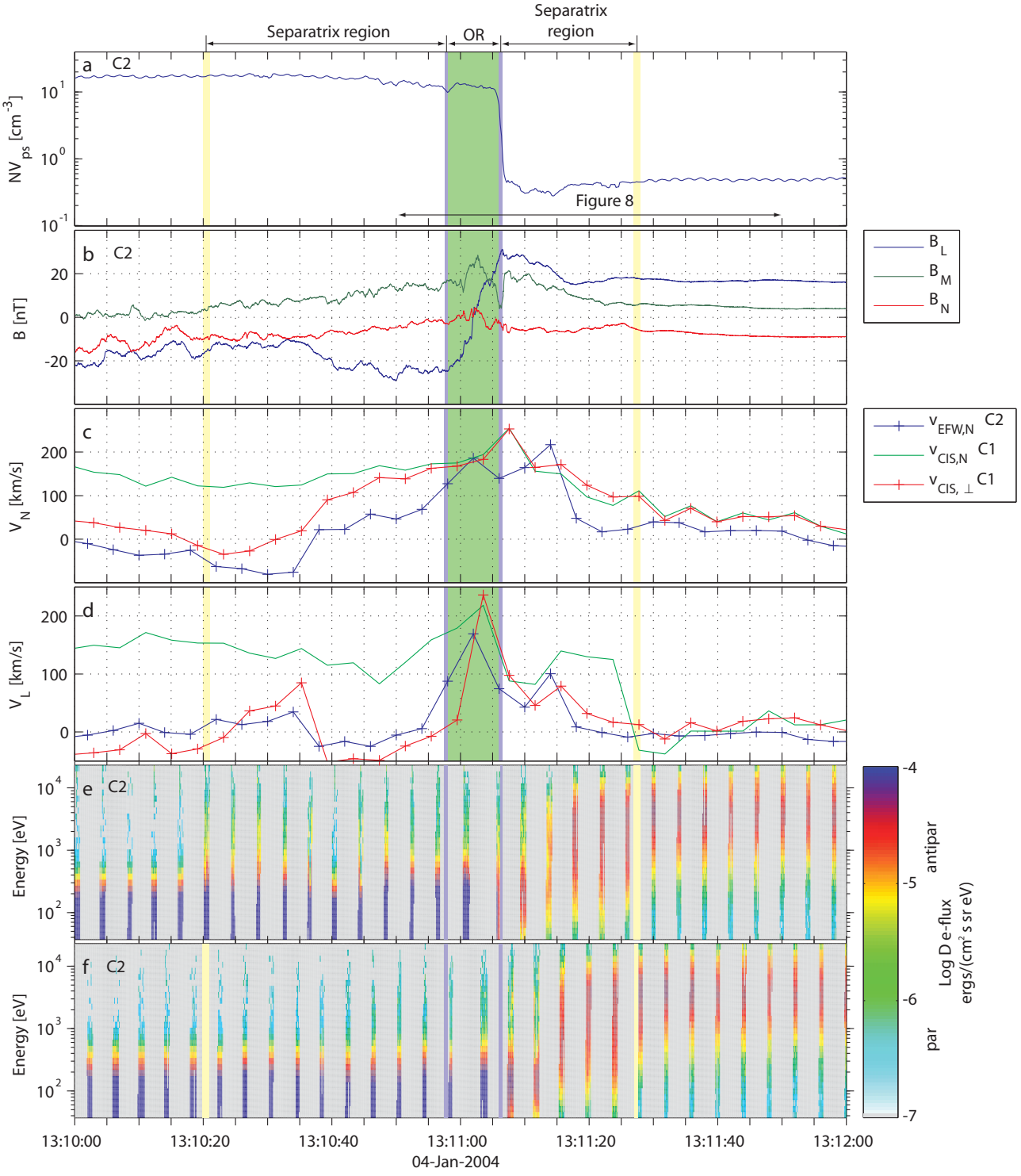

Fig. 7. Cluster crossing of the magnetopause reconnection layer on 4 January 2004, 13:11 UT. The panels from top to bottom show: **(a)** plasma density, **(b)** *LMN*-components of the magnetic field, **(c)** v_N normal plasma flow velocity, **(d)** v_L flow velocity components of plasma flow velocity (full and perpendicular), **(e)** electron flux anti-parallel to B and **(f)** electron flux parallel to B. The *LMN*-directions are: $\boldsymbol{L}$=[−0.73 −0.45 0.53], $\boldsymbol{M}$=[0.69 −0.48 0.55], $\boldsymbol{N}$=[0.01 0.76 0.65] in GSE. The velocity of the magnetopause is $\boldsymbol{v}_{\rm dis}$=210[−0.02 0.74 0.67] km/s GSE. Vertical green bar marks the outflow/field reversal region (OR), and yellow bars mark the outer and inner separatrices. Arrow in the top panel marks the time interval presented in detail in Fig. 8.

at the edge of the ion jet. B_N is negative, which is consistent with reconnection X-line being sunward from the spacecraft. While in the magnetosheath, at 13:10:20 UT Cluster detects a sharp increase in anti-parallel (away from the magnetopause) electron flux at energies above 400 eV, i.e. electrons of magnetospheric origin. At the same time there is no change in the parallel flux. We identify this point as the outer separatrix or magnetosheath electron edge (E1), see Fig. 1. In the separatrix region on the magnetospheric side of the magnetopause, 13:11:06–13:11:28 UT, we observe a mixture of magnetosheath-like electrons and electrons with energies 1–10 keV, similar to the magnetospheric electron population. The transition to purely magnetospheric populations happens at 13:11:28 UT. We identify this point as the inner separatrix or magnetospheric electron edge (E2).

We further investigate the details of the reconnection layer, particularly concentrating on its magnetospheric side. Figure 8 shows detailed observations. Figure 8a–d shows *LMN*-components and magnitude of the magnetic field. Figure 8e shows density derived from the EFW spacecraft potential. Figure 8f shows the ion energy spectrogram. Note that this ion spectrogram does not display the spin-averaged flux; it shows snapshots of the ion energy flux spectra for sub-spin accumulation periods of ∼0.25 s. The fact that ion energy fluxes vary in a periodic fashion simply reflects the presence of a bulk ion flow relative to the spacecraft which appears modulated due to the spacecraft spin. Figure 8g shows current parallel to the magnetic field. The observed localized current sheets are too narrow to use multi-spacecraft techniques such as the curlometer (Robert et al., 2000) to estimate their current density. Instead, we estimate the current using a single spacecraft method (Luhr et al., 1996): we assume that changes in the magnetic field are due to plane current sheets moving across the spacecraft with a velocity, $\boldsymbol{v}_{\rm dis}$, which is determined from timing analysis. Figure 8h shows the N-component of the electric field from EFW. Figure 8i shows the electric potential which is obtained by integrating the N-component of the electric field across the boundary. The full E-field vector is computed from the 2-D electric field measured by EFW using the zero parallel electric field assumption. Figure 8j–k show the electron differential energy flux in two directions. The flux is obtained from the PEACE 3DXP product (HEEA sensor) which has been rebinned using the actual magnetic field measured by the FGM. Then we select the sectors being perpendicular (Fig. 8j) and with the smallest measured angle relative to the magnetic field (the most parallel direction, Fig. 8k). The observed angle between the selected sector with the smallest pitch angle and the magnetic field is shown in Fig. 8l (blue line). The sector with the smallest pitch angle is often rather far from being parallel to the magnetic field (up to 60°) and the direction parallel to B is generally sampled only once per spin (angle ∼ 0°). Since the electron distribution is anisotropic, the changing pitch angle of the parallel sector recorded in Fig. 8k produces a characteristic periodic pattern. Figure 8m shows distance to the magnetopause obtained by integration of the N-component of the plasma convection velocity, $(\boldsymbol{E}\times\boldsymbol{B})_N$, shown in Fig. 7c. The time axes of spacecraft SC1, SC3 and SC4 have been time shifted so that the different spacecraft data can be compared in the boundary reference frame.

The magnetopause current layer is identified by a change of B_L from negative in the magnetosheath to positive in the magnetosphere. Inside this current layer B_M makes a bipolar change (Fig. 8b). Such bipolar signatures are usually attributed to Hall magnetic fields (Vaivads et al., 2004b). The magnetospheric edge of the B_M variation coincides with the main magnetopause density gradient, at which the density drops from the magnetosheath to magnetospheric level, and this is also the location of the ion edge (marked by the purple bar). At the density gradient there is a strong current parallel to the magnetic field (Fig. 8g); the current density is 0.2 $\mu A/m^2$. The parallel current is produced by Hall currents flowing towards and away from the X-line, in this case the strongest parallel current is flowing towards the X-line.

The high energy magnetospheric ion population is present on both sides of the magnetopause current layer (Fig. 8f). The magnetospheric population starts at several keV and goes outside the CIS-HIA energy range. The magnetospheric edge of the ion jet is located at 13:11:06 UT, at the main density gradient. At the high density side the plasma is dominated by the magnetosheath population with a typical energy of several hundred eV. As the spacecraft cross the density gradient it moves into a region populated mainly by plasma of dayside plasma sheet origin. At the same time (13:11:06 UT) the L-component of the plasma flow velocity decreases (Fig. 7d). The ion jet (V_L∼200 km/s), accelerated by the $\boldsymbol{J}\times\boldsymbol{B}$ force, is localized inside the magnetopause current layer and is directed mostly perpendicular to B. On the magnetospheric side the main density gradient bounds the ion jet and we identify it as the "ion edge" (I2), see Fig. 1. Some magnetosheath ions with flux lower than in the magnetosheath are still seen within the gyroradius distance from the density gradient, ρ_i∼230 km, and even deeper inside the magnetosphere (seen around 13:11:22 UT in Fig. 8f, and a corresponding secondary velocity peak in V_L in Fig. 7d). The ion edges bound the outflow region observed between 13:10:58–13:11:06 UT where the plasma flow L-component increases in Fig. 7. On the magnetosheath side the ion edge cannot be well defined due to the data resolution and the larger gyroradius of magnetospheric ions. A good estimation of the position of the ion edge on the magnetosheath side is at the start of the accelerated ion flow, i.e. where the longitudinal plasma flow, V_L, in Fig. 7 increases as the spacecraft enter the outflow region from the magnetosheath.

Prior to the magnetopause current layer crossing we observe mainly the magnetosheath electron population in Fig. 8j and Fig. 8k, with electron energies up to 200 eV (T_e∼40 eV). On the magnetospheric side of the magnetopause current layer (on the low density side) the magnetosheath population is of much lower density, and it is mixed

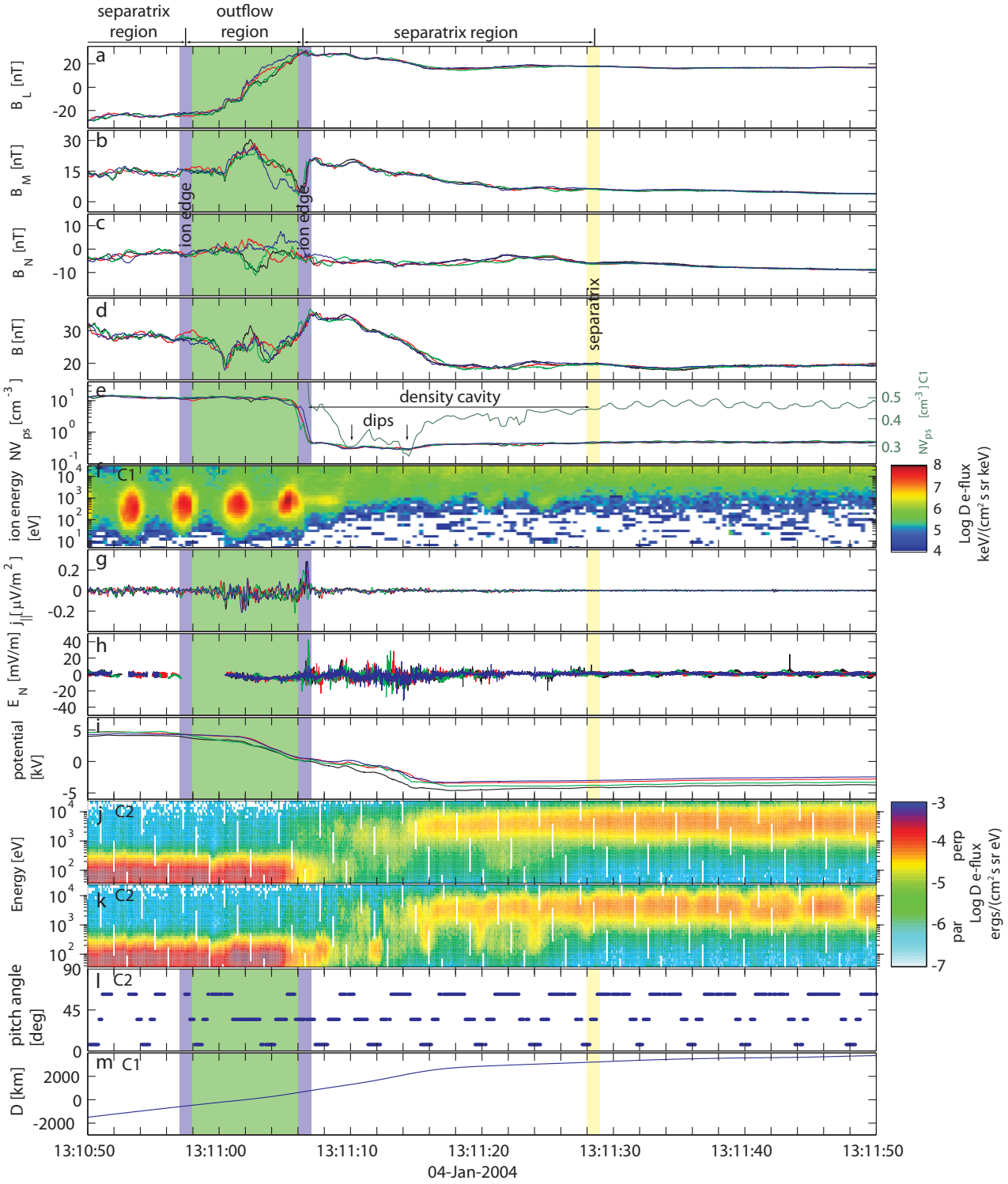

Fig. 8. Cluster crossing of the magnetopause reconnection layer on 4 January 2004, 13:11 UT. Panels **(a–d)** show the magnetic field *LMN*-components and magnitude of the magnetic field for all four spacecraft. Panel **(e)** shows the density and the density on a different scale from C1, **(f)** the energy spectrogram of ions over all angles from C1, **(g)** the current density parallel to the magnetic field, **(h)** the normal electric field, **(i)** the electric potential, **(j)** the energy spectrogram of electrons perpendicular to the magnetic field from C2, **(k)** the energy spectrogram of electrons with the smallest measured pitch angle, from C2 and **(l)** the pitch angle of electrons in panel **(k)**, **(m)** the distance to the magnetopause. The black, red, green and blue lines represent spacecraft 1, 2, 3 and 4, respectively. The *LMN*-directions are the same as in Fig. 7. The time axes for spacecraft 1–4 are shifted by [1.0 0 0.5 −0.3] s.

with the magnetospheric population (energies above 2 keV, $T_e \sim 2$ keV). Alongside with high energy (above 2 keV) magnetospheric electrons, electrons in the intermediate energy range 0.2–2 keV (above typical magnetosheath energy and below the magnetospheric) are observed between 13:11:06 (magnetospheric ion edge) and 13:11:28 UT, which we have identified as "magnetospheric separatrix". The region between the separatrix and the ion jet, is the "separatrix region". At the magnetospheric side of the separatrix (after 13:11:28 UT) electrons have a typical distribution with a narrow loss cone, calculated to be $\sim 2°$. The loss cone appears as periodic pattern in the parallel electrons (Fig. 8k) observed after 13:11:28 UT; the pattern is created due to a variation of the detector angle with respect to $\boldsymbol{B}$: minima are seen when the angle (Fig. 8l) is close to zero. When plasma crosses the separatrix from the closed magnetic field lines of the magnetosphere to the open field lines of the separatrix region, parallel magnetospheric electrons start to escape to the magnetosheath creating a wider loss cone. At the same time also the magnetosheath electrons enter the separatrix region along the open field lines. During the magnetopause current layer crossing these electrons can be further accelerated into the intermediate energy range 0.2–2 keV that is higher than typical electron energies in the magnetosheath. Such electrons with parallel energies less than 2 keV are observed at 13.11:28, 24, 20 UT, e.g. at times when PEACE samples the most field aligned population (pitch angle $\sim 0°$ in Fig. 8l). We locate the separatrix around 13:11:28 UT where the most energetic parallel electrons start to disappear and the accelerated magnetosheath electrons appear.

The separatrix region is 2400 km wide (Fig. 8m) and it coincides with a region of increased magnetic field magnitude and decreased plasma density (cavity, Fig. 8e). However, it is important to notice that the density is derived from the spacecraft potential and changes in the spacecraft potential are mainly related to variations in electron density, but also depend slightly on variations in electron temperature. Therefore on boundaries separating plasmas of different temperatures and densities, as in our case the separatrix region, the estimation of the density from the spacecraft potential is more complicated and the absolute depth of the density cavities needs to be further investigated. The density/spacecraft potential cavities are characteristic for separatrix regions on the magnetospheric side and they can even be useful in the identification of separatrix regions. In the cavity there are at least two individual density dips (Fig. 8e), each a few seconds long. Multi-spacecraft data allow us to see that the observations of the individual density dips are time lagged among the spacecraft in such a way that we can conclude that the spacecraft cross multiple density dips and do not make multiple encounters of the same density dip.

Inside the separatrix region there are strong normal electric fields (E_N, Fig. 8h) up to 30 mV/m. The estimated change of the electric potential across separatrix region is 4 kV between 13:11:05–13:11:16 UT. The small distance between 13:11:16–13:11:28 UT does not affect the electric potential considerably.

4.2 Partial crossing of the magnetopause reconnection layer, 12:51 UT

The event at 12:51 UT (partial BL crossing, FTE) is presented in Fig. 9 (the format is the same as for Fig. 8). In this case the reference system based on the minimum variance analysis is not appropriate because the spacecraft does not cross the main magnetopause current, but the parallel current sheets within the boundary layer, where the minimum variance analysis does not gives reliable results. Instead we use $\boldsymbol{N}=\boldsymbol{L}\times(\boldsymbol{n}\times\boldsymbol{L})$, where $\boldsymbol{n}$ is the boundary normal given by the boundary velocity $\boldsymbol{v}_{\rm dis}=v_{\rm dis}\boldsymbol{n}$ which is determined from the time delays between observations of the boundary by different spacecraft. The timing analysis is made on both the parallel current sheet and the density gradient to give the best fit over the boundary. Note that this parallel current sheet is not the main magnetopause current layer, but a local current sheet located on the magnetospheric side from the magnetopause current layer on the border between the magnetosphere (separatrix region) and the outflow region. The L-direction is the direction of the magnetic field inside the magnetosphere. M completes the orthogonal system $\boldsymbol{M}=\boldsymbol{N}\times\boldsymbol{L}$.

In the event at 12:51 UT the longitudinal component of the magnetic field (B_L in Fig. 9a) decreases to almost zero but does not change sign. It means that the spacecraft does not cross the main magnetopause current layer but enters into it and then return back to the magnetosphere. At 12:51:46 UT perpendicular electrons in Fig. 9j show a characteristic transition from the hot magnetospheric plasma (electron temperature $T_e \sim 3$ keV) to the colder magnetosheath-like plasma ($T_e \sim 80$ eV). Low energy perpendicular electrons are not present prior to the transition. The flux of high energy magnetospheric perpendicular electrons drastically decreases at the transition; however, some of these electrons are still present after the transition. The first magnetosheath ions (energies between 100 eV–3 keV) are observed at the transition corresponding to the ion edge (purple bar), as seen in the high resolution time-energy ion spectrogram (Fig. 9f). Magnetospheric ions (~ 10 keV) are still present after the ion edge. After 12:51:46 UT there are mixed ions and electrons from the magnetosheath and the magnetosphere. At the same time the ion velocity (not shown) increases to about 300 km/s which means that the spacecraft enters the ion jet (reconnection outflow/field reversal region). The density in the outflow region ($n \sim 6\ {\rm cm}^{-3}$) is significantly higher than the magnetospheric density ($n \sim 0.5\ {\rm cm}^{-3}$).

The region prior to 12:51:33 UT we identify as the separatrix (marked with a yellow bar in Fig. 9). The identification of this region as the separatrix is based on observing the electrons parallel to the magnetic field in Fig. 9k (at times when the parallel sector is aligned with B, i.e. the angle in Fig. 9l is close to zero). Parallel electrons are observed at energies

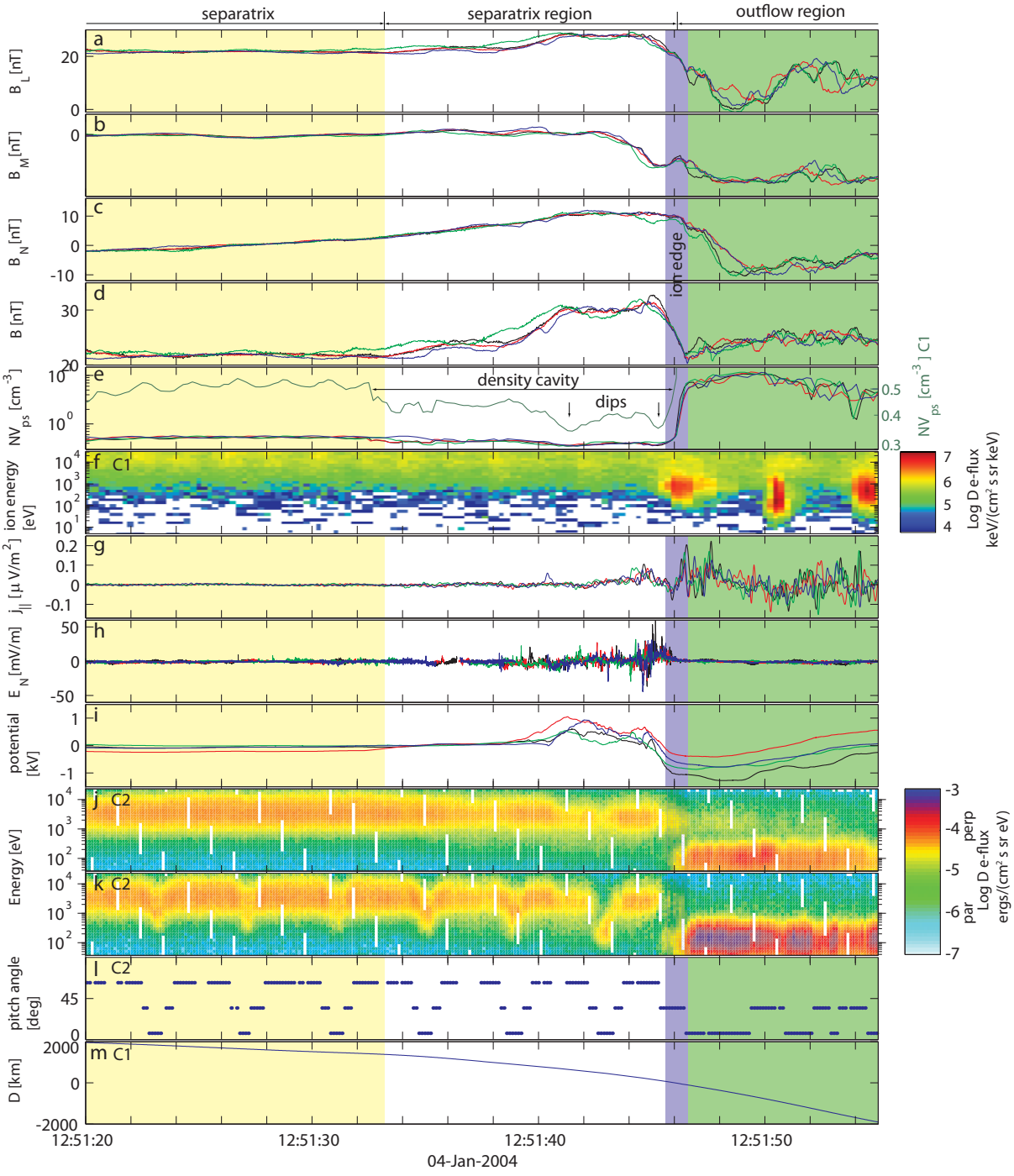

Fig. 9. Cluster crossing from the magnetosphere into the reconnection layer on 4 January 2004, 12:51 UT. Format of the figure is the same as for Fig. 8. The *LMN*-directions are : $\boldsymbol{L}$=[−0.21 −0.95 0.25], $\boldsymbol{M}$=[−0.08 0.27 0.96], $\boldsymbol{N}$=[0.92 0.40 −0.04] in GSE. The velocity of the discontinuity is $\boldsymbol{v}_{\rm dis}$=176[−0.92 −0.40 0.04] km/s GSE. The time axes for spacecraft 1–4 are shifted by [−0.42 0 −1.40 0.03] s.

∼0.5–1 keV which is lower than the plasma sheet energies and, thus, originate from the magnetosheath, i.e. being the most energetic part of the magnetosheath population. We expect to observe such magnetosheath electrons only very close to the first opened field line. A similar distribution with parallel magnetosheath ∼1 keV electrons is observed at the separatrix during the first event (see Fig. 8, 13:11:28 UT). In contrast to the first event, where such a distribution is observed

only during one spacecraft spin and the separatrix can be located very precisely, such a distribution is observed for many spins in this second event and the separatrix is observed for a longer time interval in Fig. 9. However, this interval still corresponds to a very narrow region in space. For this event we calculate the distance in the same way as for the previous event. Prior to 12:51:33 UT the spacecraft move very slowly and efficiently stay at the same position relative to the magnetopause (Fig. 9m).

At 12:51:33 UT the normal velocity increases to ∼180 km/s (corresponding to the slope of the distance D in Fig. 9m) and the spacecraft cross the separatrix region reaching the ion edge at ∼12:51:46 UT. The width of the separatrix region is ∼2100 km. Similar to the first event, the separatrix region coincides with the density cavity and the increased total magnetic field. As the spacecraft cross the separatrix region and get closer to the ion edge the characteristic energy of parallel electrons continuously decreases (Fig. 9k); the energy of the parallel electrons is changing more gradually than the rapid change in the perpendicular electrons at 12:51:46 UT in Fig. 9j. After the ion edge (12:51:47 UT) magnetosheath electrons are the dominant population.

Strong electric fields normal to the boundary (E_N, Fig. 9h) with amplitude up to 50 mV/m are observed inside the separatrix region. By integrating the normal electric field we get the electric potential which will affect ions crossing the separatrix region (Fig. 9i). Inside the separatrix region the potential first increases and then decreases and in total the electric potential changes by 1.4 kV across the region. The steady potential increase inside the outflow region (after 12:51:47 UT) is due to the large plasma convection there. The strongest electric fields are localized on the low density side of the main density gradient. In Fig. 9g there is a current parallel to the magnetic field with a magnitude of 0.2 $\mu A/m^2$ at 12:51:47 UT. The parallel current is coinciding with the density gradient located on the ion edge (I2) in Fig. 1. The magnitude of this parallel current and its location is the same as for the first event. The calculation of the current depends on the timing analysis which is valid up to only 12:51:47 UT for this event so the current estimation is no longer valid.

5 Discussion

We have analyzed in detail eight crossings of the magnetopause reconnection layer (marked by vertical lines in Fig. 3) which are consistent with the spacecraft crossing separatrix regions of reconnection sites during ongoing reconnection. Evidence for ongoing reconnection are based on the properties of the observed reconnection ion jets and observations of FTEs as well as observations of separatrix regions. The Cooling model shows that the observations are consistent with a reconnection site located sunward of the spacecraft.

All the events we analyzed show a very similar boundary structure to the ones presented in detail in Fig. 8 and 9. Table 1 presents a summary of the main characteristics for all these events: the boundary velocity, the width of the separatrix region (distance between the separatrix and the main density gradient), potential variation inside the separatrix region and the maximum parallel current. For all of our events summarized in Table 1 we observe a density cavity between the magnetosphere and the outflow region (ion jet). The cavities contain a density decrease down to about half of the magnetospheric density and have a width ranging from 300 km ($\sim 1c/\omega_{pi(MS)} \sim 4c/\omega_{pi(SH)}$) to 2500 km ($\sim 9c/\omega_{pi(MS)} \sim 34c/\omega_{pi(SH)}$). We find cavities which are on average much wider than the one found by André et al. (2004) that is about 300 km, and by Retinò et al. (2006) which is only 100 km wide. A discussion on how the density cavity is created can be found in Khotyaintsev et al. (2006). We could not identify the cause of different cavity widths. Our typical values of the width of the separatrix region can be compared with the separatrix region width estimates at much lower altitude in the mid altitude cusp region by Bogdanova et al. (2006). They find the separatrix region to have widths up to 2° ILAT with 0.2° ILAT being characteristic value. This width corresponds to a width of ∼600 km near the magnetopause when mapped along the magnetic field and thus falls within the range of our estimates.

Almost all the magnetopause reconnection layer crossings show similar characteristic properties of the separatrix region. The main density gradient defines the edge of the ion jet and the ion boundary to the the separatrix region. The outflow region is dominated by plasma of magnetosheath origin. In the data we see that the outflow region and the magnetopause current layer, identified as the time interval when the B_L-component rotate from positive to negative values, at least sometimes overlap (see Fig. 7 and Fig. 8). When the spacecraft is crossing from the magnetosheath to the magnetosphere, there is a sharp change in the ion distribution at the ion edge; the magnetospheric population becomes dominant, and a rather sharp change in the perpendicular electrons is observed. The parallel electrons, on the other hand, are changing more gradually and represent a mixture of the magnetosheath and magnetospheric populations throughout the separatrix region. Observations of this mixing of magnetosheath and magnetospheric electron populations inside the separatrix region provide additional (kinetic) evidence for ongoing reconnection. Closer to the main density gradient we observe mostly the low energy magnetosheath electrons transmitted through the magnetopause. The flux of such electrons decreases as we move deeper into the magnetosphere. Further away from the magnetopause in the magnetosphere we observe a loss cone distribution in high energy magnetospheric electrons created due to escape of energetic electrons with small pitch angles along the open field lines. At lower energies magnetosheath electrons are entering along the opened field lines. The magnetospheric edge

Table 1. Summary of parameters of the observed separatrix regions on 4 January 2004. The table shows (1) the time of the event, (2) the velocity of the discontinuity, (3) the width of the separatrix region, (4) the potential change over the separatrix region with the starting point on the magnetospheric side of the separatrix region, (5) the potential dip with respect to the magnetospheric level and positive sign corresponds to diverging electric fields and (6) the magnitude of the parallel current. The potential dip is a potential change over a region smaller than the width of the separatrix region.

Time	v_{dis} (km/h)	width (km)	potential change (kV)	potential dip (kV)	current ($\mu A/m^2$)
12:47	270	300	-2.6 ± 1.3	–	0.3
12:51	180	1400	-0.7 ± 0.3	0.8 ± 0.3	0.2
12:58	250	1500	1.1 ± 0.6	-1.0 ± 0.4	0.5
13:06	60	1500	5.4 ± 0.9	–	0.6
13:09	150	1500	5.4 ± 1.6	–	0.3
13:11	210	2300	3.8 ± 0.7	–	0.2
13:46	180	2500	0.8 ± 0.8	-1.5 ± 0.5	0.1
13:55	140	300	0.75 ± 0.3	–	0.2

of the separatrix region is the separatrix, a transition from the open to closed magnetospheric field lines. Low energy (below the typical plasma sheet energies) field aligned electrons are no longer observed on the magnetospheric side of the separatrix. This point also coincides with the magnetospheric edge of the density cavity.

On the main density gradient which is located on the ion boundary of the magnetospheric separatrix region we observe a thin parallel current sheet with typical current densities between 0.1 $\mu A/m^2$ and 0.6 $\mu A/m^2$. Presumably, these field-aligned currents are at one end closed by the Hall currents in the ion diffusion region (Vaivads et al., 2004b), and at the other end most probably closed through the currents in the ionosphere. Mapping the field aligned current densities to the ionosphere results in expected field aligned current densities at the top of the ionosphere of 200 $\mu A/m^2$–1200 $\mu A/m^2$. For the mapping we use that $B \sim 1/R^2$ and $J \sim 1/R^2$ so $B \sim J$ and a typical magnetic field value of 20 nT in the magnetosphere and 4×10^4 nT in the ionosphere. Large field aligned currents of hundreds $\mu A/m^2$ have previously been observed by the low altitude satellites such as Freja and Astrid-II on similar magnetospheric flux tubes (Stasiewicz et al., 1998; Ivchenko and Marklund, 2002). In the ionosphere the manifestation of field-aligned currents originating in the magnetosheath have been observed, e.g. in the form of poleward moving auroral forms (PMAFs) (Sandholt et al., 1998).

All observed separatrix regions are associated with strong electric fields. The strongest electric field component is in the direction normal to the boundary and the values that we have observed (e.g. in Fig. 8 and Fig. 9) are of the same magnitude as previously observed by André et al. (2004) and Retinò et al. (2006). Note that it is the tangential electric field and not the normal electric field that corresponds to the plasma motion across the boundary. The normal electric field has a fast fluctuating component with frequency above a few Hz, that is most probably related to electrostatic lower hybrid drift waves that propagate along the cavity (Vaivads et al., 2004a). The normal electric field can be integrated to obtain the electric potential structure across the separatrix region. The studied separatrix regions show that there exists a potential jump across the separatrix region varying between 0.3 kV and 5.5 kV (Table 1). The electric fields observed locally close to the magnetopause will map along the magnetic field lines into the ionosphere. Thus the local potential drops that are observed across the separatrix region at the magnetopause can be expected to lead to similar potential drops down in the ionosphere. The observed values are of the same magnitude as the ones observed across the dayside auroral region at low altitudes supporting the idea that such potential jumps can map down into the ionosphere (Lundin et al., 1995). The shape of the electric potential across the separatrix regions is different for the different events; for example, in the event of 12:51 in Fig. 9i the electric potential first increased and then decreased, which corresponds to diverging electric fields, i.e. pointing outwards from the separatrix region. For another event at 13:11 in Fig. 8i the potential monotonically decreases over the separatrix region and the corresponding electric field is directed from the magnetosphere to the magnetosheath, similar to the event of Khotyaintsev et al. (2006). It is important to notice that when the normal electric field extension in the normal direction is sufficiently small (in comparison to the ion gyro-radius) ions entering the separatrix region are accelerated by the normal electric field and in this way obtain energy comparable to the potential jump within the separatrix region. This can be particularly important for cold ionospheric ions that in this way can increase their energy hundredfold. There are no ionospheric ions detected for the current event, however, preliminary studies of other events show that energization of ionospheric ions within the separatrix region can be significant. Also Topliss et al. (2001), Bogdanova et al. (2004) and Bogdanova et al. (2006) observed energized ionospheric ions in

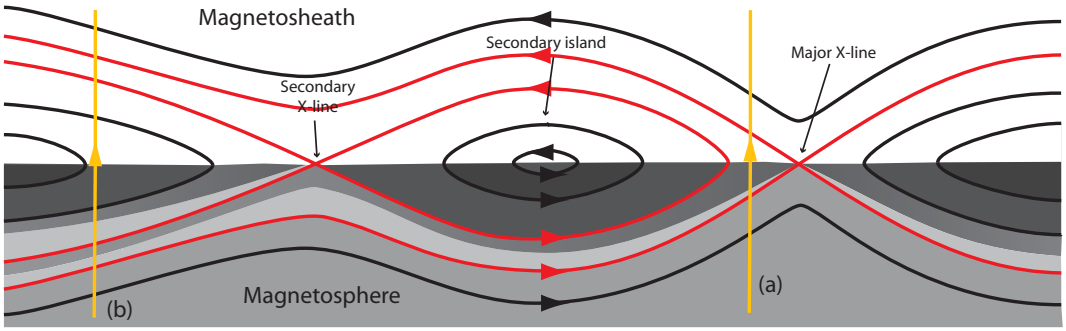

Fig. 10. Illustration of the spacecraft crossings of the magnetopause during reconnection due to multiple X-lines. The major X-line is on the right and the secondary X-line is on the left. Separatrices associated with the X-lines are marked in red and plasma density is shaded in grey, density cavities associated with the X-lines can be seen as light grey bands next to the separatrices. Two example crossings by spacecraft are marked in yellow. The spacecraft on the left crosses a wide cavity with multiple dips due to multiple X-lines, the spacecraft on the right crosses closer to the major X-line and sees only one narrow cavity.

the separatrix region. Earlier studies show that the strong normal electric fields are mainly Hall fields, $\boldsymbol{E} \sim \boldsymbol{j} \times \boldsymbol{B}/ne$, and do not correspond to the large scale motion of the plasma (Khotyaintsev et al., 2006).

In 7 out of 8 events we observe a complex internal structure of the separatrix region with multiple density dips inside the cavities. The origin of the dips is not fully understood. One possibility involves existence of multiple X-lines (and multiple separatrices) due to formation of secondary magnetic islands at the reconnection site. The existence of such islands has been confirmed both using numerical simulations (Daughton et al., 2006) and spacecraft observations (Eastwood et al., 2007; Chen et al., 2008). If the formation of a density cavity is characteristic for every active X-line we could use this to monitor whether reconnection is ongoing at a single or multiple X-lines. Figure 10 illustrates spacecraft crossings of the magnetopause with two X-lines. The yellow line shows the spacecraft orbit. In the crossing (a) to the right in Fig. 10 the spacecraft is crossing the magnetopause near the major X-line and only observe a single separatrix on the magnetospheric side. The density in Fig. 10 is illustrated by the grey background color. Light grey color corresponds to low density and darker to high density. The single separatrix crossing then corresponds to the crossing of a single density cavity. In the crossing (b) to the left in Fig. 10 there is another X-line present between the spacecraft and the major X-line. In this case we observe a density cavity with two density dips corresponding to crossing two separatrices, one from the major X-line and one from the secondary X-line. In the future it is necessary to test if similar wide density cavities with multiple dips can be produced in numerical simulations and whether multiple dips are correlated with the presence of multiple X-lines.

6 Conclusions

We have studied Cluster spacecraft observations in the vicinity of the dayside magnetopause on 4 January 2004, between 12:30 and 14:30 UT. During this time the IMF was varying but mainly directed southward and we find signatures of ongoing reconnection. We analyze in detail eight encounters of the separatrix region of magnetic reconnection on the magnetospheric side of the magnetopause current layer, i.e. the region located between the inner (magnetospheric) separatrix and the reconnection jet.

We find a similar structure of the separatrix region in all our events: (1) a density cavity, (2) strong parallel currents which coincide with the ion boundary, (3) strong electric fields and (4) large potential variations across the region. In most events there are multiple density dips inside the cavities. The total width of the cavities varies between 300 km and 2500 km which is from a few to a few tens of the ion inertial length and consistent with observations at much lower altitudes (Bogdanova et al., 2006). The electron distributions observed inside the separatrix regions show a gradual change in the parallel energy due to transition from the magnetospheric to magnetosheath electron population that is consistent with expected signatures when magnetospheric and magnetosheath electrons mix on newly opened field lines.

The strong parallel currents are concentrated on the main density gradient on the magnetosheath side of the cavity. Only in one earlier case study by André et al. (2004) the strong parallel current has been found to be located on the magnetospheric side of the cavity. The observed strong currents on the ion boundary of the separatrix region, when mapped into the ionosphere would correspond to very strong ionospheric currents, more than 200 $\mu A/m^2$, which can be important for formation of the aurora and global magnetosphere-ionosphere coupling.

Inside the density cavity we find strong electric fields directed normal to the boundary. We integrate this electric field to obtain the electric potential structure across the separatrix region. The electric potential shows potential jumps of several kV across the separatrix region. In some cases there can be internal structure of the electric potential showing diverging electric fields but in most cases the potential changes monotonically across the separatrix region. The strong electric fields within the separatrix region can contribute to the energization (by a few keV), of the ions crossing this region. This can be particularly important for cold ionospheric ions.

Acknowledgements. We Would like to thank CIS, FGM and PEACE teams as well as the ESA Cluster Active Archive for providing the data.

Topical Editor I. A. Daglis thanks two anonymous referees for their help in evaluating this paper.

References

André, M., Vaivads, A., Buchert, S. C., Fazakerley, A. N., and Lahiff, A.: Thin electron-scale layers at the magnetopause, Geophys. Res. Lett., 31, 3803, doi:10.1029/2003GL018137, 2004.

Balogh, A., Carr, C. M., Acuña, M. H., Dunlop, M. W., Beek, T. J., Brown, P., Fornacon, K.-H., Georgescu, E., Glassmeier, K.-H., Harris, J., Musmann, G., Oddy, T., and Schwingenschuh, K.: The Cluster Magnetic Field Investigation: overview of in-flight performance and initial results, Ann. Geophys., 19, 1207–1217, 2001, http://www.ann-geophys.net/19/1207/2001/.

Biernat, H. K., Semenov, V. S., Drobysh, O. A., and Heyn, M. F.: Magnetic reconnection: Observations on October 29, 1979, and model results, J. Geophys. Res., 103, 11919–11928, doi:10.1029/98JA00587, 1998.

Biskamp, D.: Magnetic reconnection in Plasmas, Cambridge University Press, iSBN 0 521 58288 1, 2000.

Bogdanova, Y. V., Fazakerley, A. N., Owen, C. J., Klecker, B., Cornilleau-Wehrlin, N., Grison, B., André, M., Cargill, P., Rème, H., Bosqued, J. M., Kistler, L. M., and Balogh, A.: Correlation between suprathermal electron bursts, broadband extremely low frequency waves, and local ion heating in the midaltitude cleft/low-latitude boundary layer observed by Cluster, J. Geophys. Res. (Space Physics), 109, 12226, doi:10.1029/2004JA010554, 2004.

Bogdanova, Y. V., Owen, C. J., Fazakerley, A. N., Klecker, B., and Rème, H.: Statistical study of the location and size of the electron edge of the Low-Latitude Boundary Layer as observed by Cluster at mid-altitudes, Ann. Geophys., 24, 2645–2665, 2006, http://www.ann-geophys.net/24/2645/2006/.

Cattell, C., Dombeck, J., Wygant, J., Drake, J. F., Swisdak, M., Goldstein, M. L., Keith, W., Fazakerley, A., André, M., Lucek, E., and Balogh, A.: Cluster observations of electron holes in association with magnetotail reconnection and comparison to simulations, J. Geophys. Res. (Space Physics), 110, 1211, doi:10.1029/2004JA010519, 2005.

Chen, L.-J., Bhattacharjee, A., Puhl-Quinn, P. A., Yang, H., Bessho, N., Imada, S., Mühlbachler, S., Daly, P. W., Lefebvre, B., Khotyaintsev, Y., Vaivads, A., Fazakerley, A., and Georgescu, E.: Observation of energetic electrons within magnetic islands, Nature Physics, 4, 19–23, doi:10.1038/nphys777, 2008.

Cooling, B. M. A., Owen, C. J., and Schwartz, S. J.: Role of the magnetosheath flow in determining the motion of open flux tubes, J. Geophys. Res., 106, 18763–18776, doi:10.1029/2000JA000455, 2001.

Crooker, N. U.: Dayside merging and cusp geometry, J. Geophys. Res., 84, 951–959, doi:10.1029/JA084iA03p00951, 1979.

Daughton, W., Scudder, J., and Karimabadi, H.: Fully kinetic simulations of undriven magnetic reconnection with open boundary conditions, Phys. Plasmas, 13, 2101, doi:10.1063/1.2218817, 2006.

Eastwood, J. P., Phan, T.-D., Mozer, F. S., Shay, M. A., Fujimoto, M., Retinò, A., Hesse, M., Balogh, A., Lucek, E. A., and Dandouras, I.: Multi-point observations of the Hall electromagnetic field and secondary island formation during magnetic reconnection, J. Geophys. Res. (Space Physics), 112, 6235, doi:10.1029/2006JA012158, 2007.

Escoubet, C. P., Pedersen, A., Schmidt, R., and Lindqvist, P. A.: Density in the magnetosphere inferred from ISEE 1 spacecraft potential, J. Geophys. Res., 102, 17595–17610, doi:10.1029/97JA00290, 1997.

Gosling, J. T., Thomsen, M. F., Bame, S. J., Onsager, T. G., and Russell, C. T.: The electron edge of the low latitude boundary layer during accelerated flow events, Geophys. Res. Lett., 17, 1833–1836, 1990.

Gustafsson, G., André, M., Carozzi, T., Eriksson, A. I., Fälthammar, C.-G., Grard, R., Holmgren, G., Holtet, J. A., Ivchenko, N., Karlsson, T., Khotyaintsev, Y., Klimov, S., Laakso, H., Lindqvist, P.-A., Lybekk, B., Marklund, G., Mozer, F., Mursula, K., Pedersen, A., Popielawska, B., Savin, S., Stasiewicz, K., Tanskanen, P., Vaivads, A., and Wahlund, J.-E.: First results of electric field and density observations by Cluster EFW based on initial months of operation, Ann. Geophys., 19, 1219–1240, 2001, http://www.ann-geophys.net/19/1219/2001/.

Haaland, S., Paschmann, G., and Sonnerup, B. U. Ö.: Comment on "A new interpretation of Weimer et al.'s solar wind propagation delay technique" by Bargatze et al., J. Geophys. Res. (Space Physics), 111, 6102, doi:10.1029/2005JA011376, 2006.

Ivchenko, N. and Marklund, G.: "Current singularities" observed on Astrid-2, Adv. Space Res., 30, 1779–1782, 2002.

Johnstone, A. D., Alsop, C., Burge, S., Carter, P. J., Coates, A. J., Coker, A. J., Fazakerley, A. N., Grande, M., Gowen, R. A., Gurgiolo, C., Hancock, B. K., Narheim, B., Preece, A., Sheather, P. H., Winningham, J. D., and Woodliffe, R. D.: Peace: a Plasma Electron and Current Experiment, Space Sci. Rev., 79, 351–398, doi:10.1023/A:1004938001388, 1997.

Khotyaintsev, Y., Buchert, S., Stasiewicz, K., Vaivads, A., Savin, S., Papitashvili, V. O., Farrugia, C. J., Popielawska, B., and Tung, Y.-K.: Transient reconnection in the cusp during strongly negative IMF By, J. Geophys. Res. (Space Physics), 109, 4204, doi:10.1029/2003JA009908, 2004.

Khotyaintsev, Y. V., Vaivads, A., Retinò, A., André, M., Owen, C. J., and Nilsson, H.: Formation of Inner Structure of a Reconnection Separatrix Region, Phys. Rev. Lett., 97, 205003, doi:10.1103/PhysRevLett.97.205003, 2006.

Kobel, E. and Fluckiger, E. O.: A model of the steady state magnetic field in the magnetosheath, J. Geophys. Res., 99, 23617,

doi:10.1029/94JA01778, 1994.

Levy, R. H., Petschek, H. E., and Siscoe, G. L.: Aerodynamic aspects of the magnetospheric flow, AIAA, 2, 2065–2076, 1964.

Lin, Y. and Lee, L. C.: Reconnection layer at the flank magnetopause in the presence of shear flow, Geophys. Res. Lett., 21, 855–858, doi:10.1029/94GL00704, 1994.

Lockwood, M., Onsager, T. G., Davis, C. J., Smith, M. F., and Denig, W. F.: The characteristic of the magnetopause reconnection X-line deduced from low-altitude satellite observations of cusp ions, Geophys. Res. Lett., 21, 2757–2760, doi:10.1029/94GL02696, 1994.

Lockwood, M., Cowley, S. W. H., and Onsager, T. G.: Ion acceleration at both the interior and exterior Alfvén waves associated with the magnetopause reconnection site: Signatures in cusp precipitation, J. Geophys. Res., 101, 21501–21514, doi:10.1029/96JA01948, 1996.

Luhr, H., Warnecke, J. F., and Rother, M. K. A.: An algorithm for estimating field-aligned currents from single spacecraft magnetic field measurements: a diagnostic tool applied to Freja satellite data, IEEE Transactions on Geoscience and Remote Sensing, 34, 1369–1376, doi:10.1109/36.544560, 1996.

Lundin, R., Yamauchi, M., Woch, J., and Marklund, G.: Boundary layer polarization and voltage in the 14 MLT region, J. Geophys. Res., 100, 7587–7597, 1995.

McComas, D. J., Bame, S. J., Barker, P., Feldman, W. C., Phillips, J. L., Riley, P., and Griffee, J. W.: Solar Wind Electron Proton Alpha Monitor (SWEPAM) for the Advanced Composition Explorer, Space Sci. Rev., 86, 563–612, doi:10.1023/A:1005040232597, 1998.

Mozer, F. S., Bale, S. D., and Phan, T. D.: Evidence of Diffusion Regions at a Subsolar Magnetopause Crossing, Phys. Rev. Lett., 89, 015002, doi:10.1103/PhysRevLett.89.015002, 2002.

Owen, C. J., Fazakerley, A. N., Carter, P. J., Coates, A. J., Krauklis, I. C., Szita, S., Taylor, M. G. G. T., Travnicek, P., Watson, G., Wilson, R. J., Balogh, A., and Dunlop, M. W.: Cluster PEACE observations of electrons during magnetospheric flux transfer events, Ann. Geophys., 19, 1509–1522, 2001, http://www.ann-geophys.net/19/1509/2001/.

Owen, C. J., Marchaudon, A., Dunlop, M. W., Fazakerley, A. N., Bosqued, J.-M., Dewhurst, J. P., Fear, R. C., Fuselier, S. A., Balogh, A., and Rème, H.: Cluster observations of "crater" flux transfer events at the dayside high-latitude magnetopause, J. Geophys. Res. (Space Physics), 113, 7, doi:10.1029/2007JA012701, 2008.

Pedersen, A., Lybekk, B., André, M., Eriksson, A., Masson, A., Mozer, F. S., Lindqvist, P.-A., Décréau, P. M. E., Dandouras, I., Sauvaud, J.-A., Fazakerley, A., Taylor, M., Paschmann, G., Svenes, K. R., Torkar, K., and Whipple, E.: Electron density estimations derived from spacecraft potential measurements on Cluster in tenuous plasma regions, J. Geophys. Res. (Space Physics), 113, 7, doi:10.1029/2007JA012636, 2008.

Petschek, H. E.: Magnetic Field Annihilation, pp. 425–+, 1964.

Pritchett, P. L. and Coroniti, F. V.: Three-dimensional collisionless magnetic reconnection in the presence of a guide field, J. Geophys. Res. (Space Physics), 109, 1220, doi:10.1029/2003JA009999, 2004.

Rème, H., Aoustin, C., Bosqued, J. M., Dandouras, I., Lavraud, B., Sauvaud, J. A., Barthe, A., Bouyssou, J., Camus, Th., Coeur-Joly, O., Cros, A., Cuvilo, J., Ducay, F., Garbarowitz, Y., Medale, J. L., Penou, E., Perrier, H., Romefort, D., Rouzaud, J., Vallat, C., Alcaydé, D., Jacquey, C., Mazelle, C., d'Uston, C., Möbius, E., Kistler, L. M., Crocker, K., Granoff, M., Mouikis, C., Popecki, M., Vosbury, M., Klecker, B., Hovestadt, D., Kucharek, H., Kuenneth, E., Paschmann, G., Scholer, M., Sckopke, N., Seidenschwang, E., Carlson, C. W., Curtis, D. W., Ingraham, C., Lin, R. P., McFadden, J. P., Parks, G. K., Phan, T., Formisano, V., Amata, E., Bavassano-Cattaneo, M. B., Baldetti, P., Bruno, R., Chionchio, G., Di Lellis, A., Marcucci, M. F., Pallocchia, G., Korth, A., Daly, P. W., Graeve, B., Rosenbauer, H., Vasyliunas, V., McCarthy, M., Wilber, M., Eliasson, L., Lundin, R., Olsen, S., Shelley, E. G., Fuselier, S., Ghielmetti, A. G., Lennartsson, W., Escoubet, C. P., Balsiger, H., Friedel, R., Cao, J.-B., Kovrazhkin, R. A., Papamastorakis, I., Pellat, R., Scudder, J., and Sonnerup, B.: First multispacecraft ion measurements in and near the Earth's magnetosphere with the identical Cluster ion spectrometry (CIS) experiment, Ann. Geophys., 19, 1303–1354, 2001, http://www.ann-geophys.net/19/1303/2001/.

Retinò, A., Vaivads, A., André, M., Sahraoui, F., Khotyaintsev, Y., Pickett, J. S., Bavassano Cattaneo, M. B., Marcucci, M. F., Morooka, M., Owen, C. J., Buchert, S. C., and Cornilleau-Wehrlin, N.: Structure of the separatrix region close to a magnetic reconnection X-line: Cluster observations, Geophys. Res. Lett., 33, 6101, doi:10.1029/2005GL024650, 2006.

Robert, P., Dunlop, M. W., Roux, A., and Chanteur, G.: Accuracy of Current Density Determination, in: Analysis Methods for Multi-Spacecraft Data, edited by Paschmann, G. and Daly, P. W., chap. 16, pp. 395–418, Int. Space Sci. Inst., Bern., 2000.

Russell, C. T. and Elphic, R. C.: Initial ISEE magnetometer results - Magnetopause observations, Space Sci. Rev., 22, 681–715, doi:10.1007/BF00212619, 1978.

Sandholt, P. E., Farrugia, C. J., Moen, J., Noraberg, Ø., Lybekk, B., Sten, T., and Hansen, T.: A classification of dayside auroral forms and activities as a function of interplanetary magnetic field orientation, J. Geophys. Res., 103, 23325–23346, doi:10.1029/98JA02156, 1998.

Sandholt, P. E., Denig, W. F., Farrugia, C. J., Lybekk, B., and Trondsen, E.: Auroral structure at the cusp equatorward boundary: Relationship with the electron edge of low-latitude boundary layer precipitation, J. Geophys. Res. (Space Physics), 107, 1235, doi:10.1029/2001JA005081, 2002.

Scholer, M.: Models of Flux Transfer Events, pp. 235, Physics of the Magnetopause, 1995.

Schwartz, S. J.: Shock and Discontinuity Normals, Mach Numbers, and Related Parameters, in: Analysis Methods for Multi-Spacecraft Data, edited by: Paschmann, G. and Daly, P. W., chap. 10, pp. 249–270, Int. Space Sci. Inst., Bern., 2000.

Semenov, V. S., Kubyshkin, I. V., Lebedeva, V. V., Rijnbeek, R. P., Heyn, M. F., Biernat, H. K., and Farrugia, C. J.: A comparison and review of steady-state and time-varying reconnection, Planet. Space Sci., 40, 63–87, doi:10.1016/0032-0633(92)90150-M, 1992.

Shay, M. A., Drake, J. F., Rogers, B. N., and Denton, R. E.: Alfvénic collisionless magnetic reconnection and the Hall term, J. Geophys. Res., 106, 3759–3772, doi:10.1029/1999JA001007, 2001.

Shue, J.-H., Chao, J. K., Fu, H. C., Russell, C. T., Song, P., Khurana, K. K., and Singer, H. J.: A new functional form to study the solar wind control of the magnetopause size and shape, J. Geophys.

Res., 102, 9497–9512, doi:10.1029/97JA00196, 1997.

Smith, C. W., L'Heureux, J., Ness, N. F., Acuña, M. H., Burlaga, L. F., and Scheifele, J.: The ACE Magnetic Fields Experiment, Space Sci. Rev., 86, 613–632, doi:10.1023/A:1005092216668, 1998.

Sonnerup, B. U. O., Paschmann, G., Papamastorakis, I., Sckopke, N., Haerendel, G., Bame, S. J., Asbridge, J. R., Gosling, J. T., and Russell, C. T.: Evidence for magnetic field reconnection at the earth's magnetopause, J. Geophys. Res., 86, 10049–10067, 1981.

Stasiewicz, K., Holmgren, G., and Zanetti, L.: Density depletions and current singularities observed by Freja, J. Geophys. Res., 103, 4251–4260, doi:10.1029/97JA02007, 1998.

Topliss, S., Johnstone, A., Coates, A., Peterson, W. K., Kletzing, C. A., and Russell, C. T.: Charge neutrality and ion conic distributions at the equatorward electron edge of the midaltitude cusp, J. Geophys. Res., 106, 21095–21108, doi:10.1029/2000JA003032, 2001.

Tsyganenko, N. A.: Modeling the Earth's magnetospheric magnetic field confined within a realistic magnetopause, J. Geophys. Res., 100, 5599–5612, doi:10.1029/94JA03193, 1995.

Vaivads, A., André, M., Buchert, S. C., Wahlund, J.-E., Fazakerley, A. N., and Cornilleau-Wehrlin, N.: Cluster observations of lower hybrid turbulence within thin layers at the magnetopause, Geophys. Res. Lett., 31, 3804, doi:10.1029/2003GL018142, 2004a.

Vaivads, A., Khotyaintsev, Y., André, M., Retinò, A., Buchert, S. C., Rogers, B. N., Décréau, P., Paschmann, G., and Phan, T.: Structure of the Magnetic Reconnection Diffusion Region from Four-Spacecraft Observations, Phys. Rev. Lett., 93, 105001, doi:10.1103/PhysRevLett.93.105001, 2004b.

Vaivads, A., Retinò, A., and André, M.: Microphysics of Magnetic Reconnection, Space Sci. Rev., 122, 19–27, doi:10.1007/s11214-006-7019-3, 2006.

Weimer, D. R., Ober, D. M., Maynard, N. C., Collier, M. R., McComas, D. J., Ness, N. F., Smith, C. W., and Watermann, J.: Predicting interplanetary magnetic field (IMF) propagation delay times using the minimum variance technique, J. Geophys. Res. (Space Physics), 108, 1026, doi:10.1029/2002JA009405, 2003.

Wygant, J. R., Cattell, C. A., Lysak, R., Song, Y., Dombeck, J., McFadden, J., Mozer, F. S., Carlson, C. W., Parks, G., Lucek, E. A., Balogh, A., Andre, M., Reme, H., Hesse, M., and Mouikis, C.: Cluster observations of an intense normal component of the electric field at a thin reconnecting current sheet in the tail and its role in the shock-like acceleration of the ion fluid into the separatrix region, J. Geophys. Res. (Space Physics), 110, 9206, doi:10.1029/2004JA010708, 2005.

Paper 2

T. Lindstedt, Yu. V. Khotyaintsev, A. Vaivads, M. André, H. Nilsson, and M. Waara

Oxygen Energization by Localized Perpendicular Electric Fields at the Cusp Boundary

Manuscript

Oxygen Energization by Localized Perpendicular Electric Fields at the Cusp Boundary

T. Lindstedt,[1] Yu. V. Khotyaintsev,[1] A. Vaivads,[1] M. André,[1] H. Nilsson,[2] and M. Waara[2]

Here we report Cluster observations of oxygen energization by several keV at a boundary between the high latitude cusp and lobe. We find that a localized electric potential at the cusp/lobe boundary is responsible for a significant part of the observed energization. Ions become non-adiabatic in a spatially inhomogeneous electric field and get accelerated by the field. Additional heating may be provided by low frequency waves around the oxygen gyro-frequency.

1. Introduction

It is well known that plasma density and composition to a large extent affect dynamics of the magnetosphere. Ion populations from the solar wind and the ionosphere are mixed in the magnetosphere. Ionospheric ions are accelerated by a number of different processes to well above the escape velocity [*Chappell*, 1988]. These ionospheric ions constitute an essential part of the magnetospheric plasma. Even though the oxygen ions are only a small part of the plasma number density, their large mass make them important [*Winglee et al.*, 2002]. The outflowing ions can be further energized to several keV [*Seki et al.*, 2001].

Transverse wave heating is the most important mechanism for ion acceleration at altitudes below a few R_E [*André and Yau*, 1997; *Norqvist et al.*, 1998]. Ions are energized transversally to the magnetic field being in resonance with the left-hand polarized waves at the ion cyclotron frequency [*Chang et al.*, 1986]. The mirror force then transfers the transverse velocity into parallel and folds the velocity distribution. Local transverse acceleration is observed as a velocity distribution with a component perpendicular to the magnetic field – this is called ion conics. Close to the heating region the ion conics are observed with the small folding and pitch angle close to 90 degrees [*André and Yau*, 1997; *Moore et al.*, 1999].

At mid altitudes it was also found that regions with outflowing ions are correlated with low frequency waves [*Bogdanova et al.*, 2004]. *Topliss et al.* [2001] similarly observed ion conics at higher altitudes. However, above 4.5 R_E the wave heating becomes less important [*Bouhram et al.*, 2004]. Still, locally energized oxygen ions are observed at high altitudes [*Arvelius et al.*, 2005; *Nilsson et al.*, 2006; *Waara et al.*, 2009]. *Nilsson et al.* [2004] have shown that the acceleration mechanism at high altitudes prefers heavy ions (O^+) before light ions (H^+).

In addition to the wave heating mechanism mentioned above ions can gain energy in the perpendicular electric field if their motion is non-adiabatic [*Cole*, 1976]. Assume an ion is moving in crossed magnetic and electric fields, where the electric field is along the x-axis and has a constant gradient along $\mathbf{E}$, $\mathbf{E}_\perp = \mathbf{E}_{0\perp} + \nabla E_\perp \mathbf{x}$. The ion motion becomes non-adiabatic for significantly large value of the electric field gradient:

$$\frac{m_i \nabla E_\perp}{eB^2} > 1, \tag{1}$$

and the ion is constantly gaining energy in the electric field. The total energy change over scale L is then given by

$$e\Delta\Phi = \frac{eL^2 \nabla E_\perp}{2}. \tag{2}$$

This mechanism was for example employed to explain ion heating by low frequency waves ($\omega \ll \omega_{ci} = eB/m_i$) [*Lundin and Hultqvist*, 1989; *Stasiewicz et al.*, 2000]. One can see that condition (1) is sensitive to the ion mass, and relatively weaker electric field gradients are necessary to make motion of heavier ions non-adiabatic.

In this letter we present a high latitude oxygen energization event and study possible mechanisms responsible for energization of oxygen ions.

2. Observations

We analyze Cluster [*Escoubet et al.*, 1997] observations of oxygen energization at a lobe/cusp boundary on March 13, 2002. The interplanetary magnetic field (IMF) is dominated by a strong y-component as seen by ACE (panel a in Figure 1). Cluster is located close to the southern cusp at [3, -2, -9] R_E GSM, on the side of the cusp where one expects reconnection jets for positive IMF B_y. A summary of Cluster data is presented in panels (b) to (i) in Figure 1. Panel (b) shows magnetic field GSE components and magnitude on C4 measured by FGM [*Balogh et al.*, 2001]. Panel (c) shows plasma density measured by PEACE on C2 [*Johnstone et al.*, 1997], CIS-CODIF on C4 [*Rème et al.*, 2001], and density estimated from the spacecraft potential [*Pedersen et al.*, 2008] measured by EFW on C4 [*Gustafsson et al.*, 2001]. Densities measured by different instruments are very similar, except for the low density region around 10:30 UT; CIS-CODIF data is not shown (panels c and d) in the low density due to low number of counts. Panels (d) and (e) show velocity in GSE and time-energy spectrogram of protons measured on C4 by CIS-CODIF. Panels (f) to (i) show time-energy spectrogram and pitch angle of oxygen (O^+) in three energy ranges (0–0.5, 0.5–3 and 3–6 keV) measured on C4 by CIS-CODIF.

In the beginning of the interval shown in Figure 1 Cluster is located in the cusp identified by high density and decreased magnetic field. Between 10:25 and 10:27 UT there is an increase in proton flow speed; the flow is downward and primarily anti-parallel to B. The highest proton energies are observed closer to the lobe, which is consistent with

[1]Swedish Institute of Space Physics, Uppsala, Sweden
[2]Swedish Institute of Space Physics, Kiruna, Sweden

0094-8276/09/$5.00

energy-latitude dispersion expected for reconnection at high latitudes. At 10:27:45 UT the plasma density drops below $\sim$0.1 cm^{-3} and Cluster enters a boundary layer populated by low density solar wind ions. The lobe is observed between 10:29 and 10:31 UT, identified by low proton counts (white area in panel e). Then, Cluster again observes the low density boundary layer between 10:31 and 10:32:40 UT. A new proton injection/cusp entry is observed at 10:32:40 UT (marked by vertical lines). So, to summarize the large scale picture, Cluster moved from the cusp to lobe and then back to the cusp.

Next we examine the oxygen data shown in panels (f) to (i) of Figure 1. Between the cusp edges (marked by vertical lines) we see cold oxygen with energies ranging from $\sim$100 eV in the lobe and up to 1 keV in the boundary layer, and pitch-angles close to 90 degrees. The observed oxygen energy is by order of magnitude consistent with being due to $\mathbf{E} \times \mathbf{B}$-drift. The largest change of the oxygen characteristics is happening at the cusp boundaries (at 10:27:45 and 10:32:40 UT). Inside the cusp oxygen is much more energetic and observed at energies ranging from $\sim$1 keV up to the upper energy limit of CODIF. The process of oxygen energization is best illustrated in panels (g) to (i) showing the pitch-angle distribution, where areas of interest are marked by boxes. In the lobe oxygen is detected only at energies below 0.5 keV (panel g). In the boundary layer oxygen appears between 0.5 and 3 keV (panel h), and only after passing the cusp boundary we detect oxygen above 3 keV (panel i). The observed pitch angles are close to 90 degrees which suggests local oxygen energization. It must be noted that the oxygen close to the cusp boundary is clearly distinguishable from the protons, which have pitch angle close to 180 degrees (earthward, mostly field-aligned injections).

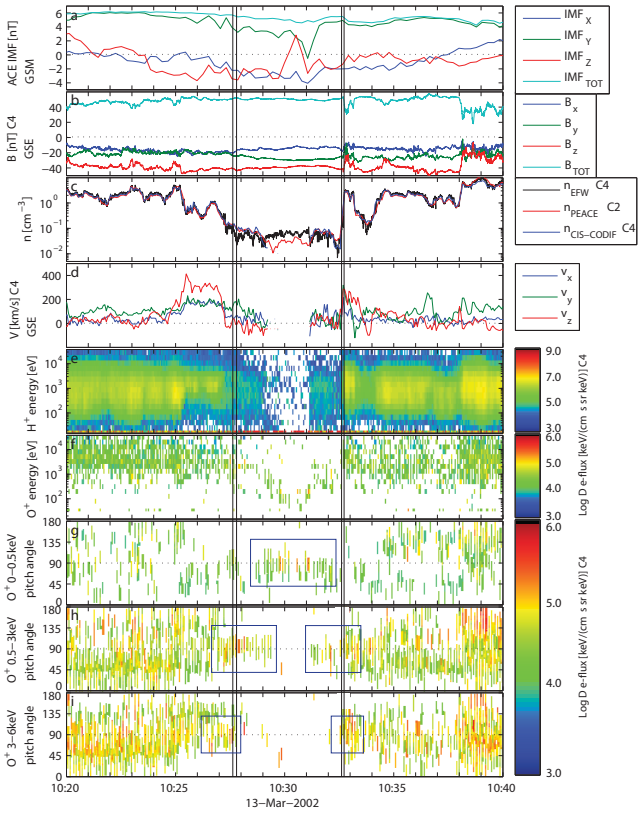

Figure 1. Observation of oxygen heating. Panel (a) shows ACE IMF data time shifted to the Earth. Panels below show measurements by Cluster 4: (b) magnetic field, (c) density from EFW, CIS-CODIF and PEACE (Cluster 2), (d) plasma velocity from CIS-CODIF, (e,f) flux integrated over all directions for H^+ and O^+ respectively, (g,h,i) O^+ pitch angle in energy ranges 0-0.5 keV(g), 0.5-3 keV (h) and 3-6 keV (i).

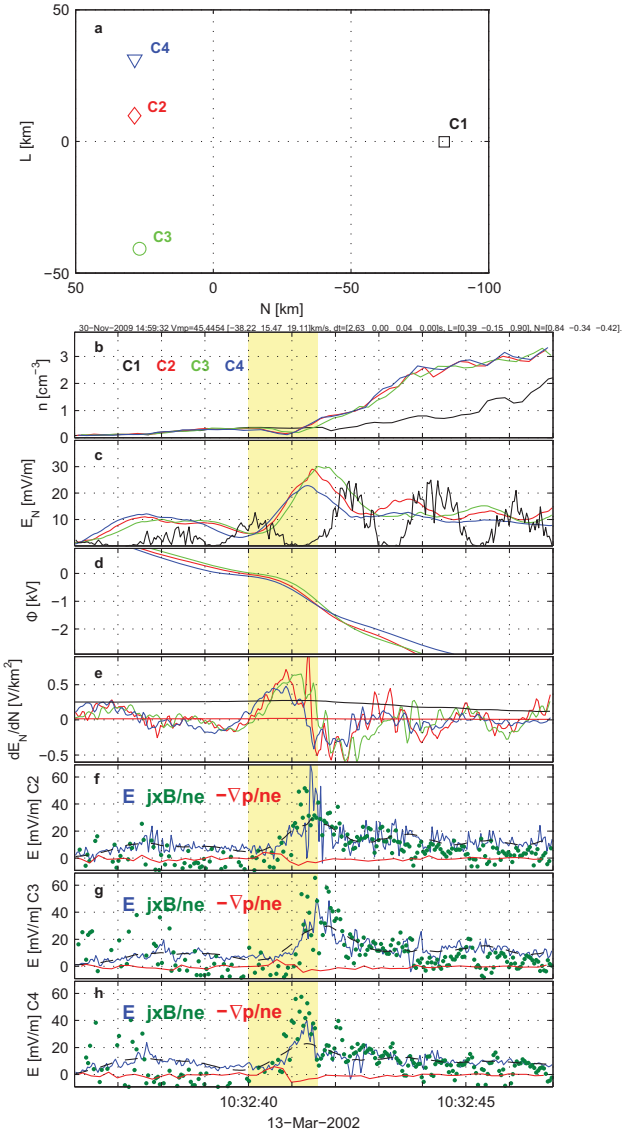

Figure 2. Observation electric field on the cusp boundary. The top panel shows orientation of Cluster spacecraft in the LN plane, where L=[0.39 -0.15 0.90] GSE is along the average magnetic filed direction, and N=[0.84 -0.34 -0.42] GSE is deduced from timing. Panels (b) – (h) show the following parameters measured by Cluster: (b) plasma density, (c) normal electric filed measured by EFW, full resolution for C1 and lowpass filtered at 0.5 Hz for C2, C3 and C4, (d) electric potential across the boundary, (e) condition given by Eq. 1, (f–h) normal components of the electric field, $\mathbf{J} \times \mathbf{B}/ne$ and $-\nabla p_e/ne$ from C2, C3 and C4 respectively; dashed lines show the lowpass filtered electric filed, the same as in panel (c).

To investigate the possible mechanism responsible for oxygen energization at the cusp boundary we examine the electric field at the boundary. We are able to analyze only the second crossing, i.e. crossing from the lobe to cusp at 10:32:40 UT, as here the crossing is fast enough to make timing analysis using the 4 spacecraft data possible. From timing of the magnetic field and density we determine the normal velocity of the boundary, $V_N \approx -45$ [0.84 −0.34 −0.42] km/s GSE, which corresponds to tailward motion of the cusp. Panel (b) in Figure 2 shows the plasma density as measured by the four Cluster spacecraft. C2, C3 and C4 cross the density gradient and reach the cusp density level of $\sim$3 cm^{-3} between 10:32:41 and 10:32:44 UT. C1, which is separated by $\sim$100 km in N direction from the rest of the spacecraft (panel a), is crossing the cusp boundary (density gradient) at a later time (panel a) and at a slower speed as the density gradient is smoother comparing to the other spacecraft. Panel (c) shows the normal to the boundary component of the electric field. Note, that probe 1 is not functioning on C1, and thus the electric field is measured only on one EFW probe pair [*Khotyaintsev et al.*, 2009]. This means that only one component of the E-field is measured in the spinning frame, producing the oscillating waveform seen in panel (c). Thus one only the peak values of the C1 measurements represent real electric field values. Assuming that the electric field is spatial and using $dN = V_N * dt$ we can compute the electric potential across the boundary and spatial gradient of the normal electric filed along the normal, dE_N/dN, which are shown in panels (d) and (e). Support for electric field being spatial comes from C1 observations. The boundary width observed by C2,3,4 is $\sim$2 seconds (both density and E-field peak), corresponding to 90 km, which is about the separation between the spacecraft. C1 is located inside the boundary for a longer period of time and at a later time, and sees the same magnitude of the normal electric field ($\sim E_x$) meaning the field is spatial.

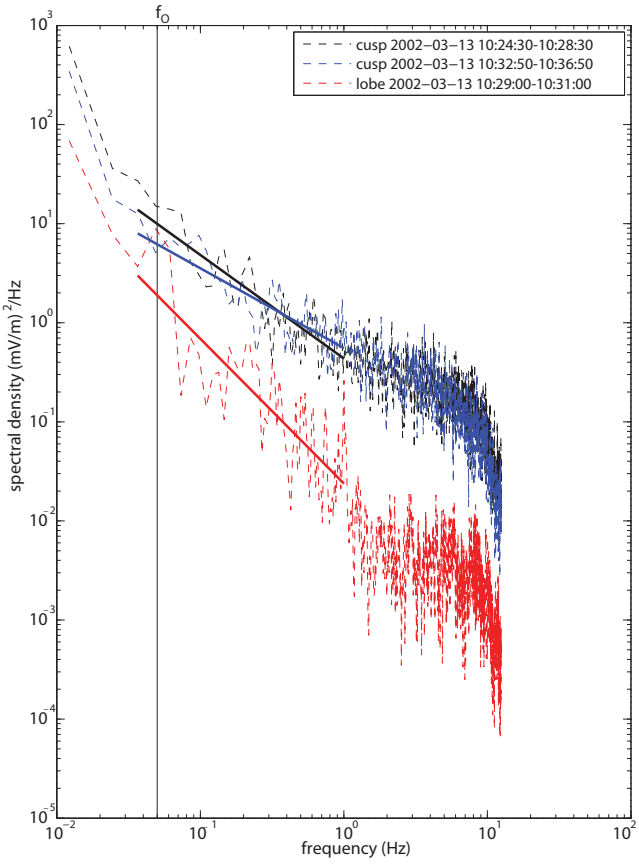

Figure 3. The power spectral density in the cusp (black and blue) is $\sim$10 (mV/m)^2/Hz and in the lobe (red) $\sim$1 (mV/m)^2. The straight lines are made by linear fitting. The vertical line corresponds to the oxygen gyro frequency $\sim$50 mHz. The frequency resolution is $\sim$10 mHz.

Panel (e) in Figure 2 shows the spatial gradient of the electric field across the boundary, where red and black horizontal lines indicate the critical value of the gradient for which the condition (1) is satisfied for oxygen (O^+) and hydrogen (H^+) ions respectively. The time interval during which the condition is satisfied is shaded by a yellow bar; both oxygen and hydrogen are non-adiabatic at this time. Alternative support for the ions being non-adiabatic comes from the fact that the large electric field observed is balanced by the Hall term, $E_n \approx (\mathbf{J} \times \mathbf{B})_n/en$ (panels f–h) in the generalized Ohm's law [*Khotyaintsev et al.*, 2006, e.g.]. The electron pressure term makes a relatively small contribution, $\nabla p_e/ne \approx 0$, implying that $\mathbf{v_i} \times \mathbf{B} \approx 0$ and $\mathbf{E} \approx \mathbf{v_e} \times \mathbf{B} \approx (\mathbf{J} \times \mathbf{B})/en$, i.e. that ions do not $\mathbf{E} \times \mathbf{B}$-drift in this region, but instead get accelerated by the electric field. The current $\mathbf{J}$ in panels (f)–(h) is computed using the single spacecraft method; the pressure gradient is computed as $\nabla p_e \approx T_e \nabla n$, with T_e=100 eV. Panel (d) shows the integrated electric field across the boundary; the ions get an energy of $\sim$1 keV when crossing the narrow region of strong E. The ion data shows that after crossing this region (cusp boundary) oxygen is detected in the energy range 3–6 keV, while before the crossing is was seen only below 3 keV, which is consistent will energization by several keV at the boundary.

3. Discussion

Magnetic reconnection is known to produce strong localized regions of Hall electric fields $\mathbf{E} \sim (\mathbf{J} \times \mathbf{B})/en$ located along the separatrices [*Khotyaintsev et al.*, 2006]. Such regions have a transversal scale comparable to ion inertial length $L \sim c/\omega_{pi}$ and contain a change of electric potential of several kilo volts [*Lindstedt et al.*, 2009]. As the separatrix regions extend over large distances away from the X-line, this potential can be used to energize the ions inside the magnetosphere. For this it is necessary that the potential change over scale $L \approx c/\omega_{pi}$ ($\omega_{pi} = \omega_{pp}$ for proton dominated plasma) is large enough to make ion motion non-adiabatic (substituting Eq. 2 into Eq. 1)

$$e\Delta\Phi > \frac{m_p}{m_i}\frac{m_p V_A^2}{2}, \tag{3}$$

where $V_A = B(\mu_0 m_p n)^{-1/2}$ is the Alfvén velocity in plasma dominated by protons. As a typical potential applied across the separatrix region at the X-line is $m_p V_A^2/2$, condition (1) is satisfied for protons only marginally, however for oxygen it is well satisfied due to the m_p/m_O factor. Both ion species are non-adiabatic in the ion diffusion region. With increasing distance from the X-line the potential can become smaller and/or extended over larger scale and condition (1) can be no longer satisfied for protons, however it will be still valid for oxygen, making oxygen energization possible at large distances away from the reconnection X-line.

It is likely that the observed boundary is a separatrix region, i.e. is mapping to the reconnection X-line at the magnetopause. The spacecraft are located on the dawn side from the cusp. Here one expects reconnection jets for IMF

dominated by positive B_y. The observed direction of ion flows (positive Y, and negative Z, Figure 1) is consistent with reconnection with X-line located dawnward from the spacecraft. In such a case the poleward boundary of the cusp (cusp-lobe) boundary is mapping to the X-line.

In addition to the localized electric fields ion energization can be provided by the wave heating mechanism, i.e. heating by waves near the oxygen cyclotron frequency [*André and Yau*, 1997]. Figure 3 shows power spectral density of the electric field measured by C4 in different parts of the cusp and lobe. The vertical line marks the oxygen gyro-frequency f_{O^+}=50 mHz. From Figure 1 it can be seen that the heated oxygen has pitch angles between 60 and 100 degrees, which corresponds to a rather wide range of distances to the heating region. As the resolution of the ion data does not allow us to determine pitch angle with better accuracy, we make a rough estimate of the heating produced by waves assuming the pitch angle of 80 degrees. For spectral power density W=10 $(\mathrm{mV/m})^2$/Hz (maximum observed), where 20% goes to heating the ions (on lower altitudes $\leq$10% of the spectral density is needed to explain transversal heating of ions [*André et al.*, 1998]), and assuming the oxygen ions spend 125 seconds in the heating region (which corresponds to the heating region located 600 km below the spacecraft), we get heating by 0.8 keV. This suggests that the wave mechanism can produce energization comparable to the localized electric fields, however it requires that the O^+ ions spend a sufficiently long time in the heating region.

4. Conclusions

We have presented observations of oxygen energization by strong localized electric fields located at the boundary between cusp and lobe. The electric field represent a spatial structure with a transverse size of $\sim$100 km. We show that the oxygen ions are non-adiabatic in the region of strong electric field and that they can get accelerated by the electric field gaining energy of several keV. Additional heating can be provided by waves at the oxygen cyclotron frequency. Our observations demonstrate that perpendicular electric fields in localized structures are one of the mechanisms providing keV O^+ ions in the magnetosphere.

Acknowledgments. We thank the ESA Cluster Active Archive for proving the data for this study.

References

André, M., and A. Yau, Theories and Observations of Ion Energization and Outflow in the High Latitude Magnetosphere, *Space Science Reviews*, *80*, 27–48, doi: 10.1023/A:1004921619885, 1997.

André, M., P. Norqvist, L. Andersson, L. Eliasson, A. I. Eriksson, L. Blomberg, R. E. Erlandson, and J. Waldemark, Ion energization mechanisms at 1700 km in the auroral region, *J. Geophys. Res.,* , *103*, 4199–4222, doi:10.1029/97JA00855, 1998.

Arvelius, S., et al., Statistics of high-altitude and high-latitude O^+ ion outflows observed by Cluster/CIS, *Annales Geophysicae*, *23*, 1909–1916, 2005.

Balogh, A., et al., The Cluster Magnetic Field Investigation: overview of in-flight performance and initial results, *Annales Geophysicae*, *19*, 1207–1217, 2001.

Bogdanova, Y. V., et al., Correlation between suprathermal electron bursts, broadband extremely low frequency waves, and local ion heating in the midaltitude cleft/low-latitude boundary layer observed by Cluster, *J. Geophys. Res.*, *109*, 12,226–+, doi:10.1029/2004JA010554, 2004.

Bouhram, M., B. Klecker, G. Paschmann, H. Rème, A. Blagau, L. Kistler, P. Puhl-Quinn, and J. Sauvaud, Multipoint analysis of the spatio-temporal coherence of dayside O+ outflows with Cluster, *Annales Geophysicae*, *22*, 2507–2514, 2004.

Chang, T., G. B. Crew, N. Hershkowitz, J. R. Jasperse, and J. M. Retterer, Transverse acceleration of oxygen ions by electromagnetic ion cyclotron resonance with broad band left-hand polarized waves, *Geophys. Res. Lett.,* , *13*, 636–639, doi: 10.1029/GL013i007p00636, 1986.

Chappell, C. R., The terrestrial plasma source - A new perspective in solar-terrestrial processes from Dynamics Explorer, *Reviews of Geophysics*, *26*, 229–248, doi: 10.1029/RG026i002p00229, 1988.

Cole, K. D., Effects of crossed magnetic and /spatially dependent/ electric fields on charged particle motion, *Planetary Space Sci.*, *24*, 515–518, doi:10.1016/0032-0633(76)90096-9, 1976.

Escoubet, C. P., C. T. Russell, and R. Schmidt, *The Cluster and PHOENIX missions*, Dordrecht: Kluwer, 1997, edited by Escoubet, C.P.; Russell, C.T.; Schmidt, R., 1997.

Gustafsson, G., et al., First results of electric field and density observations by Cluster EFW based on initial months of operation, *Annales Geophysicae*, *19*, 1219–1240, 2001.

Johnstone, A. D., et al., Peace: a Plasma Electron and Current Experiment, *Space Science Reviews*, *79*, 351–398, doi: 10.1023/A:1004938001388, 1997.

Khotyaintsev, Y. V., A. Vaivads, A. Retinò, M. André, C. J. Owen, and H. Nilsson, Formation of Inner Structure of a Reconnection Separatrix Region, *Physical Review Letters*, *97*(20), 205,003–+, doi:10.1103/PhysRevLett.97.205003, 2006.

Khotyaintsev, Y. V., P.-A. Lindqvist, A. Eriksson, and M. André, The EFW Data in the CAA, in *The Cluster Active Archive*, edited by H. Laakso, pp. 95–+, 2009.

Lindstedt, T., Y. V. Khotyaintsev, A. Vaivads, M. André, R. C. Fear, B. Lavraud, S. Haaland, and C. J. Owen, Separatrix regions of magnetic reconnection at the magnetopause, *Annales Geophysicae*, *27*, 4039–4056, 2009.

Lundin, R., and B. Hultqvist, Ionospheric plasma escape by high-altitude electric fields - Magnetic moment 'pumping', *J. Geophys. Res.,* , *94*, 6665–6680, doi:10.1029/JA094iA06p06665, 1989.

Moore, T. E., R. Lundin, D. Alcayde, M. André, S. B. Ganguli, M. Temerin, and A. Yau, Chapter 2-Source Processes in the High-Latitude Ionosphere, *Space Science Reviews*, *88*, 7–84, doi:10.1023/A:1005299616446, 1999.

Nilsson, H., et al., The structure of high altitude O+ energization and outflow: a case study, *Annales Geophysicae*, *22*, 2497–2506, 2004.

Nilsson, H., et al., Characteristics of high altitude oxygen ion energization and outflow as observed by Cluster: a statistical study, *Annales Geophysicae*, *24*, 1099–1112, 2006.

Norqvist, P., M. André, and M. Tyrland, A statistical study of ion energization mechanisms in the auroral region, *J. geophys. Res.*, *103*, 23,459–23,474, doi:10.1029/98JA02076, 1998.

Pedersen, A., et al., Electron density estimations derived from spacecraft potential measurements on Cluster in tenuous plasma regions, *Journal of Geophysical Research (Space Physics)*, *113*, 7–+, doi:10.1029/2007JA012636, 2008.

Rème, H., et al., First multispacecraft ion measurements in and near the Earth's magnetosphere with the identical Cluster ion spectrometry (CIS) experiment, *Annales Geophysicae*, *19*, 1303–1354, 2001.

Seki, K., R. C. Elphic, M. Hirahara, T. Terasawa, and T. Mukai, On Atmospheric Loss of Oxygen Ions from Earth Through Magnetospheric Processes, *Science*, *291*, 1939–1941, doi: 10.1126/science.1058913, 2001.

Stasiewicz, K., R. Lundin, and G. Marklund, Stochastic Ion Heating by Orbit Chaotization on Electrostatic Waves and Nonlinear Structures, *Physica Scripta Volume T*, *84*, 60–63, doi: 10.1238/Physica.Topical.084a00060, 2000.

Topliss, S., A. Johnstone, A. Coates, W. K. Peterson, C. A. Kletzing, and C. T. Russell, Charge neutrality and ion conic distributions at the equatorward electron edge of the midaltitude cusp, *J. Geophys. Res.*, *106*, 21,095–21,108, doi: 10.1029/2000JA003032, 2001.

Waara, M., H. Nilsson, G. Stenberg, M. André, H. Gunell, and H. Rème, Oxygen ion energization observed at high altitudes, Annales Geophysicae (submitted), 2009.

Winglee, R. M., D. Chua, M. Brittnacher, G. K. Parks, and G. Lu, Global impact of ionospheric outflows on the dynamics of the magnetosphere and cross-polar cap potential, *Journal of Geophysical Research (Space Physics)*, *107*, 1237–+, doi: 10.1029/2001JA000214, 2002.

T. Lindstedt, Swedish Institute of Space Physics, Box 537, Uppsala, SE-75121, Sweden. (toli@irfu.se)